

Superconducting phenomena in systems with unconventional magnets

Yuri Fukaya,^{1,*} Bo Lu,^{2,†} Keiji Yada,^{3,‡} Yukio Tanaka,^{3,4,§} and Jorge Cayao^{5,¶}

¹*Faculty of Environmental Life, Natural Science and Technology, Okayama University, 700-8530 Okayama, Japan*

²*Center for Joint Quantum Studies, Tianjin Key Laboratory of Low Dimensional Materials Physics and Preparing Technology, Department of Physics, Tianjin University, Tianjin 300354, China*

³*Department of Applied Physics, Nagoya University, 464-8603 Nagoya, Japan*

⁴*Research Center for Crystalline Materials Engineering, Nagoya University, 464-8603 Nagoya, Japan*

⁵*Department of Physics and Astronomy, Uppsala University, Box 516, S-751 20 Uppsala, Sweden*

(Dated: February 24, 2025)

In this work we review the recent advances on superconducting phenomena in junctions formed by superconductors and unconventional magnets. Conventional magnets, such as ferromagnets and antiferromagnets, are characterized by broken time-reversal symmetry but only ferromagnets produce a finite net magnetization due to parallel spin alignment and spin-split bands in momentum. Very recently, a new type of magnets have been reported and here we refer to them as *unconventional magnets* because they exhibit special properties of both ferromagnets and antiferromagnets: they exhibit zero net magnetization (like antiferromagnets) and a nonrelativistic spin splitting of energy bands (like ferromagnets), both leading to anisotropic spin-polarized Fermi surfaces. An interesting property of unconventional magnets is that their magnetic order can be even or odd with respect to momentum, where *d-wave altermagnets* and *p-wave magnets* are the most representative examples. In this regard, *d-wave altermagnetism* and *p-wave magnets* are seen as counterparts in magnetism of the unconventional *d-wave* and *p-wave* superconducting states, respectively. While the impact of conventional magnetism on superconductivity has been largely studied, the combination of unconventional magnets and superconductivity has only lately attracted considerably attention. This work provides a comprehensive review of the recent progress on the interplay between superconductivity and unconventional magnets. In particular, we focus on the fundamental emerging superconducting phenomena and also discuss the potential implications towards quantum applications.

I. INTRODUCTION

Superconductivity and magnetism were initially saw to be incompatible due to the destruction of spin-singlet Cooper pairs by the exchange field but their combination was later shown to be the key for novel superconducting phenomena and quantum applications [1–8]. One salient example is the realization of spin-triplet Cooper pairs [1], which not only characterize an emergent spin-triplet superconducting phase but also represent the key for superconducting spintronics [3–8], topological superconductivity and Majorana zero modes [9–17], and superconducting qubits [18–24]. The role of magnetism for converting spin-singlet Cooper pairs into spin-triplet ones is crucial, an aspect that has been mostly studied in superconducting systems formed by ferromagnets (FMs) and antiferromagnets (AFMs), see e. g., Refs. [4, 5, 8, 25–30]. FMs and AFMs are examples of collinear magnetism arising from the spontaneous arrangements of magnetic moments oriented parallel and antiparallel to each other, respectively [31–34]; whenever necessary, FMs and AFMs will be referred to as conventional magnets. In both types of these conventional magnets, time reversal symmetry

is broken, but only FMs exhibit a finite net magnetization and spin-split electronic bands [35–38]. While both FMs and AFMs have been shown to promote novel superconducting phases, in terms of applications both poses considerable challenges. For instance, the finite net magnetization of FMs, useful in some situations [39], is detrimental for scalability and stability of superconductor-FM devices [40–42]; moreover, AFMs are excellent in terms of scalability due to zero net magnetization [38, 39, 43], they do not host the useful spin-dependent effects of FMs which difficulties reading data stored in AFMs [40–42]. It would be therefore desirable to realize magnetic phases containing the positive properties of both AFMs and FMs, such that, when combining with superconductivity, the emergent superconducting phase can be useful for realistic applications.

Recently, a new family of magnetic materials with properties akin to both FMs and AFMs has been predicted [44–51]. These new magnets have been shown to have zero net magnetization (like AFMs) and a spin-splitting of electronic bands (like FMs) that depends on momentum but of nonrelativistic origin [52–56] and hence distinct from common spin-orbit coupling [57, 58]. For these reasons, the new magnets are known as *unconventional magnets (UMs)* [50, 51, 59–61]. A particular consequence of the momentum dependent spin-split energy bands in UMs is that they exhibit anisotropic spin-polarized Fermi surfaces in momentum space as well as a momentum dependent magnetic order that can have even- [52, 53] and odd-parity [54–56], akin to what happens in unconventional superconductors [62, 63]. The

* yuri.fukaya@ec.okayama-u.ac.jp

† billmarx@tju.edu.cn

‡ yada.keiji.b8@mail.nagoya-u.ac.jp

§ ytanaka@nuap.nagoya-u.ac.jp

¶ jorge.cayao@physics.uu.se

even-parity magnetic order can have s -, d -, g -, or i -wave symmetries, corresponding to the degree 0, 2, 4, or 6 of the exchange magnetic field polynomials with momenta space as variables. Similarly, the odd-parity magnetic order can have p - or f -wave symmetries, corresponding to the degree 1 or 3 of the exchange magnetic field in momentum. The simplest UMs, where the even- and odd-parity exchange fields are quadratic and linear in momenta, have so far attracted an enormous attention and were coined d -wave altermagnets (AMs) [52, 53] and p -wave UMs (PUMs) [54–56], respectively. In what follows we will refer to all the even-parity UMs as to AMs, while to all the odd-parity UMs simply as to UMs, of course indicating always the type of parity symmetry. Even though the intriguing spin-momentum locking and spin splitting in both types of UMs have a nonrelativistic origin, they originate from distinct symmetries that is different for even- and odd-parity UMs. For instance, AMs are collinear-compensated magnets in real space where time-reversal symmetry is broken but inversion symmetry is preserved [52, 53]; atoms in AMs exhibit an alternating spin direction and spatial orientation on the neighbouring sites. Moreover, AMs break time-reversal symmetry but preserve inversion symmetry, while opposite spins are connected by crystal rotation or mirror symmetries [52, 53]. A recent study suggested that the concept of AMs can be extended to non-collinear spins as well [64], which certainly expands the materials search of altermagnetism. On the other hand, PUMs are noncollinear and noncoplanar magnets, protected by the combination of time-reversal and a translation of a half the unit cell, where time-reversal symmetry is preserved but inversion symmetry is broken [54–56].

All these intriguing properties of UMs have inspired a large number of theoretical and experimental studies in the normal state, although mostly in AMs, see Refs. [44–51]. At the moment, there already are around 60 materials predicted to host altermagnetism [52, 53, 65]; among the predicted materials, CrSb and MnTe are believed to be g -wave AMs, while RuO₂, Mn₅Si₃, MnF₂ and MnO₂ are expected to be d -wave AMs. Several of these materials have already been measured to be altermagnetic, such as V₂Se₂O and V₂Te₂O [49, 66–68], RuO₂ [69–71], Mn₅Si₃ [72, 73], La₂CuO₄ [74], MnTe [75–77], MnTe₂ [78], Weyl semimetal CrSb [79, 80]. In this regard, multiple experiments have reported band splitting in AMs [70, 71, 75–77, 79, 81–83] as well as anomalous and spin transport effects [48, 72, 75, 84–89], spin currents [83, 90–98], magnetooptical effects [99–104], among other phenomena [60, 61]; see also theoretical studies on the said topics in the normal state of AMs [105–124]. In relation to UMs with odd-parity, some materials have been proposed, such as Mn₃GaN and CeNiAsO [55] for p -wave UMs, and, given the ongoing activities [125], experiments are very likely to be reported in the near future; see also [56, 116, 126, 127] for recent theoretical activity in the normal state of PUMs. It is thus evident that the peculiar nonrelativistic spin splitting and spin-momentum

locking in UMs make them promising for spin-dependent effects, with strong implications towards scalable spintronic devices in the normal state [60].

The properties of UMs have also triggered a great deal of attention in the superconducting state, placing unconventional magnetism as the key mechanism to engineer novel superconducting phenomena while maintaining zero net magnetization. In this regard, emergent superconducting states have been explored as intrinsic effects and also as induced phenomena at interfaces of hybrid junctions when coupling UMs and superconductors. The first study on the intrinsic coexistence of altermagnetism and superconductivity as well as the possibility of superconductivity due to AM spin fluctuations was theoretically carried out in 2022 [128], almost immediately after the prediction of AMs in the normal state. Later, it was shown that such intrinsic coexistence of altermagnetism and superconductivity can promote finite momentum superconductivity without any net magnetization [129–134], and, to date, there exist signs of this coexistence effect in strained RuO₂ [135–137] and in monolayer FeSe [138]; see also Ref. [139]. As an intrinsic effect, altermagnetism was also predicted to appear in the parent cuprate La₂CuO₄ of a high-temperature superconductor [53] and recently also suggested to appear in the strongly correlated CuAg(SO₄)₂ [140], see also [141]. As an intrinsic effect, altermagnetism was also shown to be useful for topological superconductivity [142] and for spin-polarized with a p -wave superconductivity [143], while its emergence was recently also shown to be possible in Sr₂RuO₄ [144].

On a parallel front, hybrid systems formed by coupling UMs and superconductors have also received an enormous interest, originating a plethora of novel phenomena with fundamental and applied prospects. For instance, under generic grounds, it was shown that UMs not only induce a spin-singlet to spin-triplet conversion but also transfer their parity, generating superconducting correlations with spin-triplet symmetry and higher angular momentum [145, 146]; this unveils the fundamental role of unconventional magnetism in superconductors; see also Refs. [147–149]. Moreover, in the simplest superconducting junction, when an AM is coupled to a superconductor, the reflection of an incident electron into a hole known as Andreev reflection (AR) was shown to strongly depend on the crystal orientation and the spin-splitting [150–156]; crossed ARs have also been studied in AM-superconductor-AM junctions [157, 158]. There also exist preliminary theoretical work on ARs in PUM-superconductor junctions [152], with predictions of even zero-bias peaks [146]. We note that the dependence of ARs on the transverse momentum originates the appearance of Andreev bound states (ABSs) that strongly disperse with such momentum, shown for superconducting junctions with d -wave AMs and p_y -wave UMs [146]. Very recently, it was reported a single experimental study on the AR in AMs, which involved a planar junction between an indium electrode and MnTe altermagnetic

candidate [159]. Since a finite AR in the UM of a UM-superconductor junction is directly related to the induced superconducting correlations in the UMs [15, 146], we conclude that unconventional magnetism strongly affects the proximity effect [160]. The role of potential impurities in AMs was recently also studied [161], reporting impurity-induced local sign change of the order parameter and highly tunable spin-dependent tunneling that can be useful for quantum information processing.

The impact of unconventional magnetism was also investigated in junctions formed by two superconductors coupled via an UM in the form of superconductor-UM-superconductor Josephson junctions (JJs), thus allowing to explore the Josephson effect [162]. In JJs, ARs at both interfaces lead to the formation of ABSs, which become dependent on the superconducting phase difference that allows them to carry a dissipationless supercurrent and determine the Josephson effect [163–170]; see also Refs. [171–180]. In Josephson junctions based on d -wave AMs and spin-singlet s -wave superconductors, it was shown that altermagnetism induces in the free energy $0 - \pi$ oscillations [146, 156, 181–185] and oscillations away from $0, \pi$ with double degeneracy [146, 184], which result from the strong influence of altermagnetism on the emergent ABSs. The $0-\pi$ transitions were also predicted in altermagnet-based Josephson junctions formed by spin-singlet and spin-triplet superconductors [186]. For $0-\pi$ transitions in Josephson junctions without AMs, see Refs. [165, 187–190]. The nontrivial features induced by altermagnetism in the free energy and ABSs induce anomalous features in the current-phase curves, involving the contribution from multiple harmonics of the superconducting phase difference [146, 184], presence of multiple nodes [184], tunable skewness [185], and unconventional Fraunhofer patterns [183].

Besides the intriguing Josephson phenomena, altermagnetism was also shown to be useful for realizing other emergent superconducting phenomena. For instance, it was predicted that altermagnetism can be used to engineer topological superconductivity [142, 149, 191–193], where Majorana states are found to appear with a zero net magnetization; similarly, Ref. [194] recently reported the realization of topological superconductivity by using p -wave magnetism, while Ref. [195] suggested the design of Majorana flat bands. As in regular semiconductor-superconductor Majorana devices, altermagnet-based heterostructures might be also susceptible to the formation to topologically trivial zero-energy ABSs [196], which can, however, be distinguished e. g., by Josephson measurements [197–200]. For trivial ABSs in superconducting junctions, including Josephson junctions, we refer to Refs. [201] and also to Refs. [197–199, 202–219]. Altermagnetism was also proposed as a key ingredient for the superconducting diode effect [220–222], where it can even promote perfect efficiencies due to finite momentum states [222]. It was also uncovered that the perfect diode effect in [222] is related to topology, opening the possibility for realizing topologically

protected superconducting diodes, before suggested in superconductor-semiconductor Majorana systems [223]; see also [224–226] for the diode effect in topological insulators and Refs. [227–237] for other studies on superconducting diodes. It is worth noting that the peculiar spin-momentum locking of UMs allows a nontrivial light-matter coupling that is able to induce spin-triplet states e.g., by means of Floquet engineering [238]. We lastly note that AMs have recently been explored for realizing the magnetoelectric effect [239, 240], where a spin response is generated by an applied current and is relevant for superconducting spintronics. Thus, despite the recent studies on the interplay between UMs and superconductivity, the field has already seen an enormous and rapid progress, which reflects the importance of the field and believe that the advances will motivate experiments soon.

In this work, we aim at reviewing the recent progress on superconducting phenomena in systems formed by UMs and superconductors, with a particular attention on the low-energy models and their theoretical predictions. We first in Section II introduce unconventional magnetism, including even- and odd-parity magnets, how they are often modelled using minimal models, and their main properties. We then in Section III discuss the impact of superconductivity and unconventional magnetism, highlighting the possible superconducting symmetries that can emerge due to their combination in a hybrid system. In this part, we also address the Andreev reflection, proximity effect, and inverse proximity effect. In Section IV, we focus on the Josephson effect and comment on how to model Josephson junctions, the formation of ABSs, the current-phase curves, induced correlations, and Josephson diode effects. In Section V, we discuss the recent experimental advanced in UMs in the normal state and the single experiment involving superconductors. Our conclusions are presented in VI, where we also remark possible future research directions driven by the interplay between unconventional magnetism and superconductivity.

This review does not intend to cover all the important advances in the field of unconventional magnetism and superconductivity. There are excellent reviews addressing distinct aspects of these areas and we therefore refer to those works. For reviews on altermagnetism in the normal state, we refer to Refs. [60, 61], while for readers interested in ferromagnets and antiferromagnets we refer to Ref. [1, 2, 37]. Moreover, for reviews on anomalous Hall antiferromagnets, we refer to Ref. [241], for antiferromagnetic spintronics to Refs. [38, 41–43, 242, 243], and for spintronics to Refs. [39, 40, 244–247]. Furthermore, for readers interested in superconductor-ferromagnet heterostructures, superconducting spintronics, and topological superconductivity, we refer to Refs. [1, 2], Refs. [3–8], and Refs. [9–17, 21, 22, 24, 201, 248], respectively.

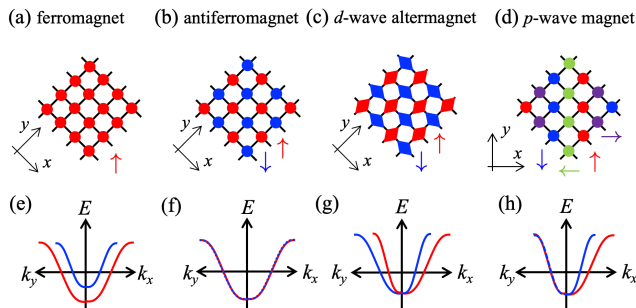


Figure 1. (a-d) Schematic illustration of the lattices in a ferromagnet (a), antiferromagnet (b), altermagnet (c) [53], and unconventional p -wave magnet (d) [55, 56]. Up and down arrows colored with blue and red represent spin down and up, respectively. In panel (d), blue, red, green and purple arrows represent the noncollinear spin structure. (e-h) Energy dispersions along k_x and k_y directions for the corresponding magnetic order of panels (a-d), where the blue and red curves indicate opposite spins. Panels (g,h) show the momentum dependent spin splitting in d -wave AMs and p -wave UMs.

II. UNCONVENTIONAL MAGNETISM IN THE NORMAL STATE

We start by discussing unconventional magnetism with even- and odd-parity magnetic orders which characterize e.g., d -wave altermagnets (AMs) and p -wave unconventional magnets (PUMs). Altermagnetism is believed to be a third class of collinear magnetic phases, in addition to the well-known ferromagnets and antiferromagnets [45–48, 50, 52, 53, 60, 61, 64, 68, 105, 110, 249–251]. The term ‘altermagnet’ was named after the anisotropic magnetization that ‘alternates’ direction in momentum space. The study on this state can be traced back to a series of discoveries of unconventional magnetism before the name was given, such as in the momentum-dependent spin split bands with antiferromagnetic order [46, 47, 91, 105, 110], the crystal Hall effect [48], the C -paired spin-valley locking in antiferromagnets [49], or in the ferromagnetic response in antiferromagnets [250].

To understand the properties of AMs, we first review some characteristics of ferromagnets and antiferromagnets since AMs share common features with them. For ferromagnets, the exchange field induces a majority spin state and a minority spin state for all lattice sites [Fig. 1 (a)], making the majority spin state more populated at the Fermi surface [Fig. 1 (e) and Fig. 2 (a)]. In some half-metal materials, the minority spin state can disappear at the Fermi surface which results in full polarization. Thus, ferromagnets possess a non-vanishing net macroscopic magnet moment [32, 34]. In Landau’s broken symmetry theory, ferromagnets can be described by a ferromagnetic order parameter: the exchange field [32]. Such an exchange field is isotropic in ferromagnets since the ferromagnetic state is invariant under a unitary lattice symmetry. Another type of collinear magnets are antiferromagnets, which has an alternating spin polar-

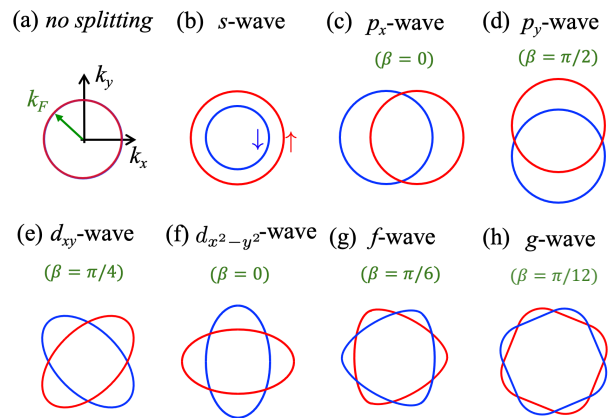


Figure 2. Sketch of the Fermi surfaces for up (red circle) and down (blue circle) spins in distinct normal state systems, including (a) a normal metal, (b) a ferromagnet (s -wave magnetic order), (c) a p_x -wave UM, (d) a p_y -wave UM, (e) a d_{xy} -wave AM, (f) a $d_{x^2-y^2}$ -wave AM, (g) a f -wave UM, and (h) g -wave AM. The yellow arrow in (a) indicates the Fermi wavevector and β indicates the direction of the nodes where the exchange field becomes zero.

ization in real space with neighboring sites possessing different spin Fig. 1 (b). Thus, antiferromagnets are invariant under a unitary lattice translation or inversion symmetries [31–34]. The spin degeneracy of an antiferromagnet is not lifted as dictated by parity-time-inversion (\mathcal{PT}) symmetry [Fig. 1 (f)].

Based on the above discussion, AMs are similar to ferromagnets [Fig. 2 (a)] because both of them have a spin splitting of energy bands and spin-polarized Fermi surfaces. However, the spin states of AMs compensate each other and result in zero net magnetization, akin to what occurs in antiferromagnets but distinct from ferromagnets. As already pointed out, AMs exhibit an exchange field that is even in momentum (even-parity), which can possess d -, g -, i -wave symmetries. Unlike antiferromagnets, the Kramers degeneracy in AMs is lifted in because the opposite-spin sublattices can not map onto each other by a translation or inversion, but are connected by a real-space rotation transformation, as shown in Fig. 1 (c)(g). In AMs, \mathcal{PT} is broken by the combined lattice geometry and spin ordering. Furthermore, an important property of AMs is that the spin-splitting field does not originate from relativistic effects, which is distinct from relativistically spin-orbit coupling [57, 58]. Due to that reason, the spin-splitting field can be much larger in AM, e.g., reaching the order of 1 eV [52]. In relativistically spin-orbit coupling systems, such as semiconductors with Rashba spin-orbit couplings, it requires heavy element to produce large spin-splitting but their values are not very large. In contrast, AMs have advantages in providing significant spin-splitting field in lighter compounds based on e.g., Fe and Mn. Even though the field is still developing, there have already been a large number of theoretical and experimental

studies addressing AMs and their properties; see e. g., Refs. [45, 48, 53, 66, 67, 70, 77, 105, 110] for some previous experiments and Section V for more details on the experimental advances. In terms of theoretical developments in the normal state, AMs have been proposed to realize ultrafast THz switching devices with no stray fields and with low damping spin currents [252–254] and they have also been suggested to generate a giant tunneling magnetoresistance effect [255]. Moreover, AMs were shown to be useful for anomalous Hall effects [48, 75, 85, 91, 106], including a skyrmion Hall effect [256], as well as for promoting high harmonic generation [257]. Other studies of AMs involved impurity-induced Friedel oscillations in the local density of states [126], strain spin splitting [258], spin splitting Nernst effect [119], higher-order topological state [122], field-sensitive dislocation bound states [259], parity anomaly in weak topological insulators [260], bilayer stacking ferromagnets with antiferromagnet coupling [261], in heavy fermions systems [262], a Landau theory of altermagnetism [120], and nonlinear spin currents [116]; see also Refs. [50, 51, 60, 61] for a more detailed discussion of the advances on AMs in the normal state. It is clear that the number of candidate altermagnetic materials is now rapidly growing [52, 53, 60, 61, 66, 68, 80, 263–265], and all the advances support the benefits of AMs for potential spintronic applications.

After the prediction and discovery of altermagnetism, the field moved quickly to the study of odd-parity unconventional magnets, which can exhibit a magnetic order with p and f -wave symmetries. The Fermi surfaces of these odd-parity magnets are shown in Fig. 2 (c,d,g). In the case of p -wave unconventional magnets, they are both noncollinear and noncoplanar magnets with preserved time-reversal symmetry and broken inversion symmetry. Then, p -wave unconventional magnets are protected by the combination of the time-reversal operation (\mathcal{T}) and a translation of half the unit cell (τ) [55]. Ref. [55] predicted Mn_3GaN and CeNiAsO as candidate materials for p -wave magnetism but their experimental verification is still an open task. In Fig. (d,h), we show the lattice and the energy dispersion in a p -wave magnet, induced by the spin-rotational structure along one direction. Studies on PUMs have addressed Friedel oscillations in the local density of states [126], transverse spin currents [266], linear and nonlinear conductivities [127], and a spin-current diode effect [116], and highly efficient non-relativistic Edelstein effect [267].

Most of the theoretical advances on both AMs and PUMs have employed minimal models that capture the main properties of both UMs. Due to the relevance of these models for the advance of the field and for understanding most of the phenomena in UMs, we discuss them in the next subsection.

A. Minimal models for understanding unconventional magnetism

In this part, we discuss the minimal models to describe unconventional magnetism, with a particular focus on d -wave AMs and p -wave UMs. Within a simple, but proven useful, description of the itinerant electrons in UMs is given by the phenomenological exchange field with momentum dependence $M_{\mathbf{k}}$ [52]. From a microscopic point of view, the tight-binding models for UMs are proposed based on fundamental symmetries [55, 56, 121, 143]. In what follows, we summarize the minimal models for UMs and their consequent electronic band structures.

To model UMs, effective two-band models describing momentum-dependent spin-splitting bands in the continuum model were adopted and they are given by [52]

$$\hat{H}(\mathbf{k}) = \frac{\hbar^2 \mathbf{k}^2}{2m} - \mu - M_{\mathbf{k}} \mathbf{n}_{\mathbf{k}} \cdot \boldsymbol{\sigma}, \quad (1)$$

where μ is the chemical potential, $M_{\mathbf{k}}$ is the momentum-dependent exchange field characterizing the unconventional magnetic order, $\mathbf{n}_{\mathbf{k}}$ a unit vector that dictates the direction of the spin polarization and $\boldsymbol{\sigma} = [\sigma_x, \sigma_y, \sigma_z]$ is the vector of Pauli matrices in spin space. The energy dispersion of Eq. (1) is given by

$$\varepsilon_{\mathbf{k}}^{\pm} = \hbar^2 \mathbf{k}^2 / 2m - \mu \pm M_{\mathbf{k}}, \quad (2)$$

which clearly reveals that $M_{\mathbf{k}} \neq 0$ induces a momentum-dependent splitting of spin bands. One of the simplest situations of the above Hamiltonian is a two-dimensional model with a collinear spin configuration along the direction $\mathbf{n}_{\mathbf{k}} = (0, 0, 1)$, which is the focus of our discussion in what follows.

The symmetry of $M_{\mathbf{k}}$ can be classified in the same way as that of the superconducting pair potential. Thus, the conventional ferromagnetic state is classified as s -wave magnetic order with $M_{\mathbf{k}}^s = J$, which does not exhibit any momentum dependence. Similarly, the magnetic order of p -wave magnets can be modelled by [55, 56]

$$M_{\mathbf{k}}^p = \frac{J}{k_{\text{F}}} [k_x \cos \beta + k_y \sin \beta], \quad (3)$$

while the magnetic order of d -wave AMs by [52]

$$M_{\mathbf{k}}^d = \frac{J}{k_{\text{F}}^2} [2k_x k_y \sin 2\beta + (k_x^2 - k_y^2) \cos 2\beta], \quad (4)$$

where $k_{\text{F}} = \sqrt{2m\mu/\hbar^2}$ is the Fermi wavevector as shown in Fig. 2, while β represents the angle between the x -axis and the nodes where the exchange field becomes zero. By setting $\beta = 0$ or $\beta = \pi/2$, $M_{\mathbf{k}}^p$ models a p_x - or a p_y -wave UM. Also, for AMs, $M_{\mathbf{k}}^p$ at $\beta = 0$ models a $d_{x^2-y^2}$ -wave AM, while $M_{\mathbf{k}}^p$ at $\beta = \pi/4$ models a d_{xy} -wave AM. Note that we use J to label the strength of magnetic order, irrespective of the type of magnet. Following a

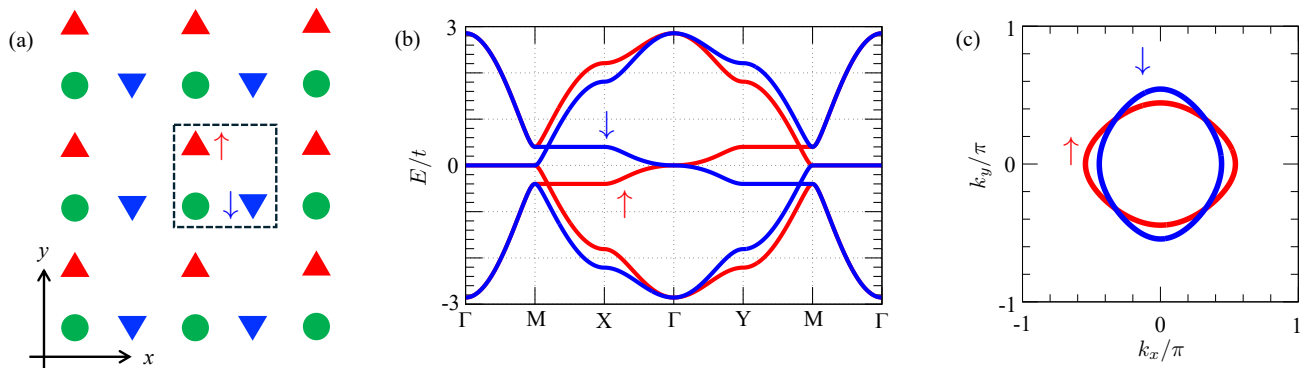


Figure 3. (a) Schematic illustration of the d -wave altermagnet in Ref. [143]. Red and blue triangles indicate the magnetic sites with spin-up and down, respectively. A green circle is a nonmagnetic site. The black-dotted line means the unit cell. (b) Energy dispersion and (c) Fermi surface of (a). The red and blue lines correspond to the up and down-spin, respectively. We set the magnetic order as $M = 0.4t$. In (c), we choose the chemical potential as $\mu = 2.5t$.

similar discussion, the magnetic order of f -, g -, and i -wave magnets [116, 145]

$$\begin{aligned}
 M_{\mathbf{k}}^f &= \frac{J}{k_F^3} [k_x(k_x^2 - 3k_y^2) \cos 3\beta \\
 &\quad + k_y(3k_x^2 - k_y^2) \sin 3\beta], \\
 M_{\mathbf{k}}^g &= \frac{J}{k_F^4} [(k_x^4 - 6k_x^2k_y^2 + k_y^4) \cos 4\beta \\
 &\quad + 4k_xk_y(k_x^2 - k_y^2) \sin 4\beta], \\
 M_{\mathbf{k}}^i &= \frac{J}{k_F^6} [(k_x^6 - 15k_x^4k_y^2 + 15k_x^2k_y^4 - k_y^6) \cos 6\beta \\
 &\quad + 2k_xk_y(3k_x^2 - k_y^2)(k_x^2 - 3k_y^2) \sin 6\beta].
 \end{aligned} \tag{5}$$

These continuum models can be generalized to three dimensions as well, see Ref. [116]; and also Ref. [121] for higher order even-parity UMs. Note that the symmetry of the Hamiltonian in Eq. (1) for the even-parity UMs (s -wave, d -wave, g -wave, i -wave) and odd-parity UMs (p -wave, f -wave) are completely different in terms of the time-reversal symmetry. While the odd-parity UMs have time-reversal symmetry as given by

$$\mathcal{T} \hat{H}(\mathbf{k}) \mathcal{T}^{-1} = \hat{H}(-\mathbf{k}), \tag{6}$$

the even-parity UMs breaks this symmetry, where $\mathcal{T} = -i\sigma_y \mathcal{K}$ is the time-reversal operator. Thus, according to the common view that a magnet should break time-reversal symmetry [32–34], p -wave magnets cannot be regarded as magnets but instead as another kind of magnetic phase. However, we will not discuss these points here and will always refer to them as p -wave magnets as already adopted in the literature, see e. g., Ref. [55, 56, 116, 145].

Before going further, we note that, under certain circumstances, it is also important to consider the lattice models of UMs, where one can also incorporate point group symmetries and other properties of actual crystals.

Broadly speaking, when considering a Hamiltonian in a crystal, e.g. given by Eq.(1), a lattice regularization is performed on said Hamiltonian. Then, the Hamiltonian must have the property that $\hat{H}(\mathbf{k}) = \hat{H}(\mathbf{k} + \mathbf{G})$, where \mathbf{G} is the reciprocal lattice vector. In the case of a tetragonal crystal system, $\mathbf{G} = (2\pi/a, 0)$ and $(0, 2\pi/a)$. Thus, $\hat{H}(\mathbf{k})$ is expressed by sine and cosine functions, $\sin(nk_{x,y}a)$ and $\cos(nk_{x,y}a)$, and their products, where n and a are arbitrary integer and the lattice constant; we set $a = 1$ unless otherwise specified. Here, we can simply do the following replacements: $k_{x,y} \rightarrow \sin k_{x,y}$ and $k_{x,y}^2 \rightarrow 2 - 2 \cos k_{x,y}$. Then, Eq.(1) for an UM in a square lattice is given by

$$\hat{H}_1(\mathbf{k}) = -2t(\cos k_x + \cos k_y) - \mu + \hat{H}_M^j(\mathbf{k}), \tag{7}$$

where the first term is the kinetic energy with t being the hopping parameter, while the second term is the exchange field $\hat{H}_M^j(\mathbf{k})$ describing the type of magnetic order in a lattice. For s -wave magnets (ferromagnet), p -wave UMs, and d -wave AMs, $\hat{H}_M^j(\mathbf{k})$ are given by

$$\begin{aligned}
 \hat{H}_M^s(\mathbf{k}) &= m_z \sigma_z, \\
 \hat{H}_M^p(\mathbf{k}) &= [t_x \sin k_x + t_y \sin k_y] \sigma_z, \\
 \hat{H}_M^d(\mathbf{k}) &= [2t_{xy} \sin k_x \sin k_y \\
 &\quad + t_{x^2-y^2} (\cos k_x - \cos k_y)] \sigma_z,
 \end{aligned} \tag{8}$$

where m_z is the amplitude of the ferromagnetic order, t_x and t_y are the strength of unconventional p_x and p_y -wave magnetic order, while t_{xy} and $t_{x^2-y^2}$ are strengths of d_{xy} and $d_{x^2-y^2}$ -wave altermagnetic order. The second and third expressions of Eqs. (8) characterize spin-dependent hopping integrals in UMs, incorporated here within a two-band model description although their origin requires a more elaborated microscopic modelling, as discussed below.

To understand the microscopic origin of the spin-dependent hopping integrals in UMs beyond two-band models, minimal models that incorporate the sublattice degree of freedom and local magnetic spins have been

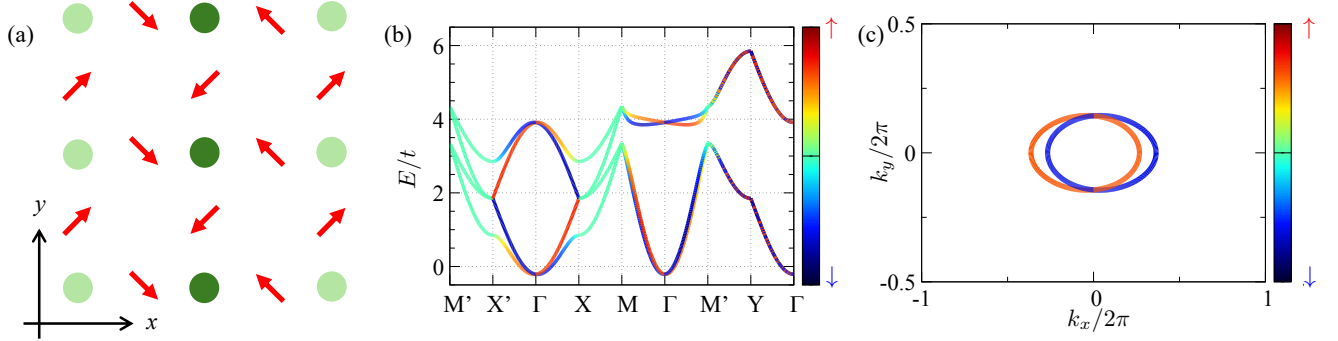


Figure 4. (a) Schematic illustration of the p -wave magnet in Ref. [55]. Dark and light green colors denotes nonmagnetic atoms and red color denotes the spins of magnetic atoms in the xy -plane. This sketch corresponds to Eq. (10). (b) Energy dispersion and (c) Fermi surface of (a) with $t_J = 0.25t$ and the chemical potential $\mu = -3.85t$.

proposed for UMs [52, 55, 56]. To be more precise, in the case of d -wave AMs [52], the minimal model consists of two magnetic sites with distinct spin and one nonmagnetic site, as schematically shown in Fig. 3(a). Now, to comprehend the spin dependent hopping integrals, it is important to consider the hopping processes between the neighboring nonmagnetic sites, denoted by green filled circles in the Fig. 3(a). The first process is the direct hopping terms, which is included in the first term of Eq. (7) and characterized by t . Moreover, in addition to the direct hopping, there are also virtual processes through the magnetic sites, denoted by blue (and red) triangles in Fig. 3(a). These virtual processes cause the spin-dependent hopping integrals in the third term of Eq. (7), see also second and third expressions of Eqs. (8). Thus, in the case when the magnetic moment between the nearest neighbor magnetic sites along the x -direction and the y -direction are opposite, the correspondent effective hopping integrals become those given by the third expression of the Hamiltonian in Eq. (7) for d -wave AMs. The minimal model discussed here can be reformulated in terms of a Hamiltonian by considering a sublattice structure composed of a nonmagnetic site and two magnetic sites with positive and negative magnetic moments shown in Fig. 3(a) [143]. Thus, the minimal model Hamiltonian for d -wave AMs can be written as

$$\hat{H}_2(\mathbf{k}) = \begin{pmatrix} -\mu & -2t \cos k_x/2 & -2t \cos k_y/2 \\ -2t \cos k_x/2 & M\sigma_z + V - \mu & 0 \\ -2t \cos k_y/2 & 0 & -M\sigma_z + V - \mu \end{pmatrix} \quad (9)$$

where t is the hopping between the non-magnetic and two magnetic sites, while M and V are the magnetic moments and the on-site potential of the magnetic sites, respectively. When the Fermi energy is close to the energy levels of the magnetic sites, we can trace out the nonmagnetic site and an effective 4×4 Hamiltonian in Ref. [147] can be obtained. This two-dimensional tight-binding Hamiltonian can capture the characteristics of AMs where the opposite-spin arrangement can not be obtained from the lattice translation but from the four-

fold rotation of the system. In Fig. 3(b,c), the energy dispersion at $M = 0.4t$ and the Fermi surface at $\mu = 2.5t$ for the $d_{x^2-y^2}$ -wave alternating order are obtained by solving the tight-binding Hamiltonian.

Having understood the spin-dependent hopping integrals in AMs in terms of a minimal model, we now focus on p -wave UMs. As we already know, p -wave UMs do not break time-reversal symmetry because $M_{\mathbf{k}}$ is an odd function in \mathbf{k} -space and Eq. (6) is satisfied. The minimal model for the p -wave magnet consists of two nonmagnetic sites and four magnetic sites with noncollinear spins [55], see Fig. 4; see also Refs. [56, 126]. In this case, the spin-dependent hopping integrals arise from the noncollinear magnetic structure between nonmagnetic sites [55]. Following the spirit of one of the initial works, an effective minimal Hamiltonian for a p -wave UM can be written as [55]

$$\hat{H}_3(\mathbf{k}) = -\{2t[\cos(k_x/2)\tau_x + \cos(k_y)] + \mu\}\sigma_0 + 2t_J[\sin(k_x/2)\sigma_x\tau_y + \cos(k_y)\sigma_y\tau_z], \quad (10)$$

where σ_i and τ_i are the i -th Pauli matrix in spin and sublattice spaces, respectively. In this model, the real-space magnetic structure is noncollinear [Fig. 4 (a)], and the spin along the $(x+y)$ - and $(x-y)$ - direction couples to σ_y and σ_x , respectively. Intuitively, the direction of the spin corresponds to the direction of the couplings, while there is a mismatch between the spin-directions of Fig. 4(a) and the coupling in Eq. (10). In the proposed material in Ref. [55], the z -components of atomic coordinates of magnetic sites and non-magnetic sites are different, which could be the cause for this mismatch between models. The spin expectation values in this model have S_x and S_y parts and also a S_z term [55]. In Fig. 4(b), the energy dispersion is shown from the tight-binding Hamiltonian in Eq. (10), color coded by the the spin expectation values along z . We see that there is a splitting of momentum dependent bands having opposite values of S_z at low energies around the Γ point. This spin-splitting is further confirmed by looking at the two spin-split Fermi surfaces shown in Fig. 4(c). Having a

spin polarization that is opposite for positive and negative momenta unveils its odd-parity nature, which can be also proved to be linear in momentum, and hence of p -wave nature. The minimal model discussed here is similar to the models discussed in Refs. [56, 126] for noncollinear spin structures along one direction in the real space. In particular, Refs. [56] suggest a minimal model for a p -wave UM given by $\hat{H}_4(\mathbf{k}) = -\{2t[\cos(k_x a) + \cos(k_y a) + \mu]\sigma_0\tau_0 + [t_x \sin(k_x a) + t_y \sin(k_y a)]\sigma_{z'}\tau_0 + J_{sd}\sigma_{x'}\tau_z\}$, where the prime spin coordinates in $\sigma_{i'}$ indicate that they are in principle decoupled from the crystal coordinates; in the simplest case, the spin coordinates are the same as the crystal coordinates, but distinct magnetic textures require appropriate rotation of the primed spin coordinates, see Ref. [56]. Moreover, in the model of [56], the J_{sd} characterizes the sd coupling which arises due to the interaction between itinerant electrons and a localized spin with a noncollinear magnetic structure. Thus, p -wave UMs can be modelled by either $\hat{H}_3(\mathbf{k})$ or $\hat{H}_4(\mathbf{k})$. Furthermore, it is worth noting that the momentum dependence of the exchange field in unconventional p -wave UMs is equivalent to the momentum configuration in a persistent helix, see e. g., Refs. [55, 268–274]. This spin-helix phase is accidentally realized by the combination of Rashba- and Dresselhaus-type spin-orbit coupling when their strength are of the same order [268, 275–277] and therefore, it is of a relativistic origin.

At this point, we comment on the proper use of these Hamiltonians to model UMs. For d -wave AMs, the Hamiltonians given in Eq.(7) and (9) provide similar bulk information, such as the dispersion and their magnetic splitting near the Fermi level. On the other hand, the momentum dependent spin-splitting may affect transport in junctions or systems with edge states, and in this case one has to be careful when using the real space or continuum descriptions of UMs. This problem becomes important when addressing magnetic properties of the edge states or the spin-transport in junctions because local spin structure at the edge/interface may affect them. For instance, this is relevant when considering the particular [100] edge, the magnetic moments at the edge depend on the termination of the system. To consider the local spin-structure in continuum model, magnetic boundary conditions are required, which in principle involve distinct conditions for up- and the down-spins. A similar discussion applies to the use of p -wave UMs. To summarize, we have reviewed the minimal models of UMs. The effective Hamiltonians in the continuum are given by Eqs. (1) while in the tight-binding description is given by Eqs. (8). While these models have been broadly used for investigating superconductivity involving unconventional magnets, discussed in Sections III and IV, we note that it would be interesting to adopt the microscopic models in the form of Eqs. (9) and (10) in future studies of transport phenomena.

B. Topological phases in unconventional magnets

The past two decades have witnessed significant progress in topological materials, with an enormous focus on systems with spin-orbit coupling. In this regard, UMs provide an alternative ground to realize functional topological materials. Since the field is still developing [52, 192], most of the studies are theoretical but experimental activity will very likely be reported soon. By now, it has already been predicted that it is possible to realize topological nontrivial UMs [50, 56, 192, 259, 278–285], efforts that also suggest to engineer topological states by combing UMs with topological materials.

For intrinsic altermagnetic materials, relativistic spin-orbit coupling, which generally exists in actual crystal environment or induced by external inversion symmetry breaking [57, 58], are crucial for producing topological phases. Several examples are related to the spin-degenerate nodal lines in the Brillouin zone. In Ref. [50, 283], the authors showed that the nodal lines enabled by spin-orbit coupling give rise to pinch points in altermagnetic metals. Such pinch points behave as single or double type-II Weyl nodes due to a nontrivial Berry curvature around them and thus can be viewed as topological objects. Consequently, a topological transition occurs from altermagnetic to ferromagnetic phases driven by an external field. Another representative example is the altermagnetic Weyl semimetal CrSb [284], where the splitting of the non-relativistic nodal plane by the relativistic spin-orbit coupling leads to the emergence of pairs of Weyl points. For a two-dimensional AM, the band structure normally has spin-polarized Dirac points but the presence of spin-orbit coupling can gap out the Dirac points, resulting in the formation of the first-order topological insulator [279, 280]. The topological phases in AMs can even be tuned by the strength and directions of an applied external magnetic field combined with spin-orbit coupling, see Ref. [286]. Moreover, when AMs are combined with first-order topological insulators, Refs. [122, 192] showed that it is possible to induce high-order topological insulator phases. Apart from these studies, it is important to remark that among the most interesting phenomena associated with the topological nature of AMs are the anomalous Hall effect and its thermal counterpart (known as anomalous Nernst effect) reported in Refs. [48, 85, 87, 287]. The authors showed that these Hall phases occur due to nontrivial berry curvatures induced by broken $\mathcal{T}\tau$ and \mathcal{PT} symmetries in AMs; here, \mathcal{T} , \mathcal{P} and τ represent the time-reversal, space inversion, and translation symmetries. The intriguing role of the Berry curvature was recently taken further in Ref. [288] which showed that quantum geometry, involving the Berry curvature and quantum metric [289], can induce a nonlinear third-order response in planar AMs.

In relation to topological phases based on p -wave UMs, less number of works have been reported in the normal state [56, 290] since the field is still in its infancy. Ref. [290] shows that the one-dimensional hybrid system

made of a p -wave magnet and a metal possessing the orbital degree of freedom can realize a topological insulator without the spin-orbit interaction. By considering momentum-dependent sd -coupling in p -wave UMs, Ref. [56] showed that nontrivial topology can be generated.

By now, it is perhaps well accepted that UMs provide promising opportunities to realize topological phases without relying on relativistic spin-orbit coupling in contrast to the arena offered by semiconductors [57, 58]. Of interest is also that unconventional magnetism can also enhance the often small relativistic spin-orbit coupling, thus allowing the possibility to boost topological order. Another important route is to combine the characteristic magnetic order of UMs with other topological phases, e.g., in the form of heterostructures, a situation that can lead to induced emergent phases with entirely new functionalities. Motivated by these opportunities, in the next section, we focus on the interplay between unconventional magnetism and superconductivity, with a broader goal to identify novel emergent phenomena.

III. SUPERCONDUCTIVITY AND UNCONVENTIONAL MAGNETISM

After discussing the properties of UMs in the normal state, here we focus on their interplay with superconductivity. As we have already pointed out in the introduction, superconductivity in UMs has been studied as an intrinsic effect in AMs [128–134, 139, 142, 143, 147, 222, 291, 292] and PUMs [148] but also as a proximity-induced effect in hybrid junctions formed by superconductors and AMs [115, 145, 146, 149–151, 153–157, 183–186, 192, 196, 220, 221, 238–240, 293–295] and PUMs [145, 146, 148, 152, 238, 266, 296]. As we can indeed see, superconductivity in AMs and in hybrid junctions has attracted the majority of the attention.

To understand how superconductivity has been addressed in the systems mentioned above, we start by providing a basic introduction to the topic. Since superconductivity is an ordered state, it is characterized by an order parameter often known as pair potential. This pair potential represents the macroscopic wavefunction of Cooper pairs and its functionalities determine the type of superconducting state. Under generic circumstances, the pair potential is obtained by a mean-field decomposition of an interacting Hamiltonian and taking into account anomalous averages of two annihilation (or creation) operators. Thus, for an homogeneous system in space, the pair potential can be written as

$$\Delta_{\sigma\sigma'}(\mathbf{k}) = \frac{1}{\beta N} \sum_{\mathbf{k}'} \sum_n V_{\mathbf{k},\mathbf{k}'}^{\sigma\sigma'} F_{\sigma\sigma'}(\mathbf{k},\mathbf{k}',\omega_n), \quad (11)$$

where N is the volume of the system, $\beta = 1/(\kappa_B T)$, with κ_B being the Boltzmann constant, T the temperature, $(\mathbf{k}, \mathbf{k}')$ denotes the momenta, and (σ, σ') represents the

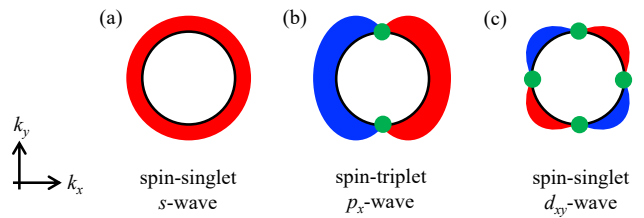


Figure 5. (a-c) Schematic representation of the pair potentials with spin-singlet s -wave, spin-triplet p_x -wave, and spin-singlet d_{xy} -wave symmetries. The red and blue colors denote the sign of the pair potentials, while the green circle indicates their nodes.

spins, while $V_{\mathbf{k},\mathbf{k}'}^{\sigma\sigma'}$ is an attractive electron interaction and $F_{\sigma\sigma'}(\mathbf{k},\mathbf{k}',\omega_n)$ is the anomalous Green's function defined as

$$F_{\sigma\sigma'}(\mathbf{k},\mathbf{k}',\omega_n) = - \int_0^\beta d\tau e^{i\omega_n\tau} \langle c_{\mathbf{k}\sigma}(\tau) c_{\mathbf{k}'\sigma'}(0) \rangle. \quad (12)$$

Here, $\omega_n = \pi\kappa_B(2n+1)T$ is the Matsubara frequency, with T being the temperature, $c_{\mathbf{k}\sigma}(\tau) = e^{\tau H_{\text{MF}}} c_{\mathbf{k}\sigma} e^{-\tau H_{\text{MF}}}$, with H_{MF} the mean field Hamiltonian describing the system under study. It is worth noting that $F_{\sigma\sigma'}(\mathbf{k},\mathbf{k}',\omega_n)$ represents the thermodynamic expectation value of two annihilation operators, sometimes referred to as Cooper pair wavefunction or simply as *pair amplitude* [62]. Since to find $c_{\mathbf{k}\sigma}(\tau)$ one needs the mean field Hamiltonian H_{MF} , to determine the pair potential $\Delta_{\sigma\sigma'}(\mathbf{k})$, Eq. (11) needs to be solved within a self-consistent approach. In this case, it is common to write the mean field Hamiltonian in Nambu space where electrons and holes are taken at the same footing, which gives us the so-called Bogolyubov-de Gennes (BdG) Hamiltonian [297, 298]

$$H_{\text{BdG}}(\mathbf{k}) = \begin{pmatrix} \hat{H}(\mathbf{k}) & \hat{\Delta}(\mathbf{k}) \\ \hat{\Delta}^\dagger(\mathbf{k}) & -\hat{H}^*(-\mathbf{k}) \end{pmatrix}, \quad (13)$$

where $\hat{H}(\mathbf{k})$ and $-\hat{H}^*(-\mathbf{k})$ are matrices in spin space describing electrons and holes, respectively, while $\hat{\Delta}(\mathbf{k})$ is a matrix containing all the pair potential elements given by Eq. (11). Thus, the pair potential, being a function of momentum \mathbf{k} and spins (σ, σ') , are written as a matrix in spin space

$$\hat{\Delta}(\mathbf{k}) = \begin{pmatrix} \Delta_{\uparrow\uparrow}(\mathbf{k}) & \Delta_{\uparrow\downarrow}(\mathbf{k}) \\ \Delta_{\downarrow\uparrow}(\mathbf{k}) & \Delta_{\downarrow\downarrow}(\mathbf{k}) \end{pmatrix}, \quad (14)$$

where $\Delta_{\sigma\sigma'}(\mathbf{k})$ is given by Eq. (11).

To further understand the type of pair potential, and hence of superconducting state, the symmetries of $\Delta_{\uparrow\uparrow}(\mathbf{k})$ need to be inspected. For this purpose, we note that the pair potential is composed of an orbital part and a spin part, with the former determined by the momentum dependence. Since $\Delta_{\sigma\sigma'}(\mathbf{k})$ describes the Cooper pair wavefunction, the orbital and spin dependences are linked

Type of superconductor	Pair potential
spin-singlet s -wave	$d_0^s(\mathbf{k}) = \Delta$
spin-singlet d -wave	$d_0^d(\mathbf{k}) = \Delta[(k_x^2 - k_y^2) \cos 2\beta + 2k_x k_y \sin 2\beta]/k_F^2$
spin-triplet chiral p -wave	$\mathbf{d}(\mathbf{k}) = \Delta(k_x + ik_y)\hat{\mathbf{z}}/k_F$
spin-triplet helical p -wave	$\mathbf{d}(\mathbf{k}) = i\Delta(k_x\hat{\mathbf{y}} + k_y\hat{\mathbf{x}})/k_F$

Table I. Expressions of the d vectors for distinct types of superconductors. Here, $d_0(\mathbf{k})$ describes the spin-singlet s - and d -wave superconductors, while $\mathbf{d}(\mathbf{k})$ describes the spin-triplet chiral and helical p -wave superconductors. The spin-triplet chiral (helical) p -wave pair potential corresponds to the mixed spin-triplet (equal spin-triplet) superconductor [299]. Here, Δ is a constant quantity representing the amplitude of the pair potential, while β depicts the angle between the x -axis and the lobe of the d -wave superconductor [164, 188, 300–302], see Fig. 5. Moreover, k_F is the Fermi wavevector and $(\hat{x}, \hat{y}, \hat{z})$ is a unit vector in 3D.

by the antisymmetry condition imposed by the fermionic nature of the paired electrons. In a two-electron system, the possible spin states are spin singlet and three spin triplet states, which are *odd* and *even* functions under the exchange of spins, respectively. Thus, a spin singlet pair potential must be even in momentum (also known as parity) which leads to $\hat{\Delta}^s(\mathbf{k}) = i\sigma_y d_0(\mathbf{k})$: here $d_0(\mathbf{k}) = [\Delta_{\uparrow\downarrow}(\mathbf{k}) - \Delta_{\downarrow\uparrow}(\mathbf{k})]/2$, $d_0(\mathbf{k}) = d_0(-\mathbf{k})$, $\Delta_{\uparrow\downarrow}(\mathbf{k}) = -\Delta_{\downarrow\uparrow}(\mathbf{k})$, $\Delta_{\sigma\sigma}(\mathbf{k}) = 0$. In Fig. 5(a,c), we schematically show two examples of spin-singlet even-parity pair potentials, which include isotropic s -wave and anisotropic d -wave symmetries; these two cases are examples of conventional and unconventional superconducting states respectively, and can be described by the following pair potentials: $d_0^s(\mathbf{k}) = \Delta$ and $d_0^d(\mathbf{k}) = k_x k_y \Delta/k_F^2$ or $d_0^d(\mathbf{k}) = \Delta(k_x^2 - k_y^2)/k_F^2$, with k_F the Fermi wavevector and the $s(d)$ superscript symbol denoting the $s(d)$ -wave parity, see also Tab. III. Similarly, a spin triplet pair potential must be an *odd* function of momentum and can be written as $\hat{\Delta}^t(\mathbf{k}) = [\mathbf{d}(\mathbf{k}) \cdot \boldsymbol{\sigma}](i\sigma_y)$, where $\mathbf{d}(\mathbf{k}) = (d_x(\mathbf{k}), d_y(\mathbf{k}), d_z(\mathbf{k}))$ with $\mathbf{d}(\mathbf{k}) = -\mathbf{d}(-\mathbf{k})$, $d_x(\mathbf{k}) = [\Delta_{\downarrow\downarrow}(\mathbf{k}) - \Delta_{\uparrow\uparrow}(\mathbf{k})]/2$, $d_y(\mathbf{k}) = [\Delta_{\downarrow\downarrow}(\mathbf{k}) + \Delta_{\uparrow\uparrow}(\mathbf{k})]/(2i)$, and $d_z(\mathbf{k}) = [\Delta_{\uparrow\downarrow}(\mathbf{k}) + \Delta_{\downarrow\uparrow}(\mathbf{k})]/2$. In Fig. 5(b), we schematically show an example of spin-triplet odd-parity pair potential with a p -wave symmetry; this is also an example of unconventional superconductivity and with a pair potential $\mathbf{d}(\mathbf{k}) = \Delta(k_x + ik_y)\hat{\mathbf{z}}/k_F$, see also Tab. III. It is well-understood in the community that, while the isotropic spin-singlet s -wave pair potential describes conventional superconductors, the anisotropic spin-singlet d -wave and spin-triplet p -wave pair potentials describe unconventional superconductors [62].

Taking into account the previous discussion, the pair potential given by Eq. (14) can be parametrized as

$$\hat{\Delta}(\mathbf{k}) = [d_0(\mathbf{k}) + \mathbf{d}(\mathbf{k}) \cdot \boldsymbol{\sigma}](i\sigma_y) \quad (15)$$

An interesting point about the matrix representation of the pair potential is that it becomes simpler to identify

which ones are unitary and nonunitary, given that a unitary matrix R requires that the product with its Hermitian conjugate is proportional to the unit matrix, namely, $RR^\dagger \propto \sigma_0$. In this regard, we find that the singlet pair potential is unitary since $\hat{\Delta}^s(\mathbf{k})[\hat{\Delta}^s(\mathbf{k})]^\dagger = |d_0(\mathbf{k})|^2 \sigma_0$, while the triplet pair potential can develop both unitary and nonunitary components as,

$$\hat{\Delta}^t(\mathbf{k})[\hat{\Delta}^t(\mathbf{k})]^\dagger = |\mathbf{d}(\mathbf{k})|^2 \sigma_0 + \mathbf{P} \cdot \boldsymbol{\sigma}, \quad (16)$$

where $\mathbf{P} = i\mathbf{d} \times \mathbf{d}^*$ characterizes the spin polarization of Cooper pairs and its finite value reflects time-reversal symmetry breaking [62]. Following the discussion presented in this part, it is possible to explore superconductivity, which can emerge intrinsically due to e. g., electron interactions as in Eq. (11) and, depending on the type of pairing channel, spin-singlet and spin-triplet pair potential can be studied. It is worth noting that superconducting states can be also induced by means of the so-called proximity effect when placing superconductors in contact with normal state materials, thereby enabling the possibility for superconducting states with properties coming from the normal materials. In what follows we will discuss intrinsic superconductivity in UMs and later will focus on hybrid systems formed by superconductors and UMs.

A. Intrinsic superconductivity in unconventional magnets

Most of the studies that addressed intrinsic superconductivity in UMs focused on the coexistence of superconductivity and altermagnetism in a single material as well as the possible generation of superconductivity by spin fluctuations in AMs. One of the initial works investigated the formation of superconductivity in a $d_{x^2-y^2}$ -wave AM under the presence of Rashba spin-orbit coupling (SOC) [142] since it naturally appears during the growing process of AMs on substrates [303]. In particular, the authors consider an extended attractive Hubbard interaction allowing for both spin-singlet s - and equal spin-triplet p -wave pairing channels, where their respective pair potentials are found within a self-consistent approach by an expression similar to Eq. (11) in the $d_{x^2-y^2}$ -wave AM modelled by the third expression of Eqs. (8) under Rashba SOC. The system was then shown to host a mixture of spin-singlet s -wave and spin-triplet p -wave superconductivity due to the simultaneous effect of breaking time-reversal symmetry by altermagnetism and inversion symmetry by SOC [142]. Another key aspect of this study is that it reports dominant p -wave superconductivity when the combined action of time-reversal and four-fold rotational around the z axis symmetries is preserved [142]; this symmetry combination is also preserved in AMs and raises an intriguing role of $d_{x^2-y^2}$ -wave altermagnetism on the type of emergent superconductivity. In an almost parallel study, superconductivity and

altermagnetism was addressed in a system with itinerant electrons and magnetic sites but without SOC [143], where the onsite exchange interaction between itinerant and localized spins induces a spin splitting, expected in AMs, and is also responsible for an electron-magnon coupling due to fluctuations in the localized spins. Interestingly, Ref. [143] found that, while nonmagnetic sites are essential for d -wave altermagnetism, a symmetry also exhibited by the splitting of magnon bands, the electron-magnon coupling gives rise to electron-electron interactions (as the one leading to Eq. (11)) but mediated by two magnons, which then produce a dominant equal spin-triplet p -wave superconductivity with sizeable spin polarization determined by \mathbf{P} in Eq. (16), perhaps already anticipated in Ref. [128]. This electron-magnon induced superconductivity was then also confirmed under many-body effects [291], carried out within the strong-coupling approach of the Eliashberg theory [304, 305]. Within the weak coupling limit, the spin-triplet odd-momentum superconducting state can be dominant by the electron-phonon coupling [306].

In a subsequent study, the role of magnetic exchange interactions in AMs was further explored as a mechanism to drive superconductivity [131], where the chosen system involved a multi-orbital t - J model on a square-octagon lattice. By allowing all (charge, spin, and pairing) mean-field channels [131], distinct phases appear, such as the coexistence of altermagnetism and superconductivity having a mixture of spin-singlet d -wave and mixed spin-triplet s -wave as well as a d -type pair-density wave due to the Fermi surface nesting, thus reflecting the intriguing role of altermagnetism for realizing nontrivial states. Moreover, in a study earlier than Refs. [131, 291], it was shown that finite momentum superconductivity can naturally appear in $d_{x^2-y^2}$ -wave AMs with spin-singlet $d_{x^2-y^2}$ -wave superconductivity even in the absence of net magnetization, as long as their nodes coincide; here, intrinsic superconductivity is due to an effective nearest-neighbor attraction for spin-singlet pairing, where the pair potential is found from an equation similar to Eq. (11) but with the momentum decomposition allowing for a finite center-of-mass momentum of Cooper pairs; see also Refs. [132–134, 147, 222] for other theoretical studies supporting the appearance of finite momentum superconductivity in AMs. Another studied aspect of altermagnetism is its potential for modifying the parity symmetry, which was shown in Ref. [292] with the appearance of spin-triplet f -wave superconductivity in d -wave AMs with spin-singlet and spin-triplet pair potentials. Besides AMs, superconductivity was very recently studied in PUMs taking into account a pair potential from the simplest electron-phonon mediated interaction similar to Eq. (11), which then was shown to produce spin-singlet s -wave and equal spin-triplet p -wave superconductivity [148]. Taking altogether, the theoretical advances on intrinsic superconductivity in unconventional magnetism uncovered the potential of UMs for hosting novel superconducting phases.

B. Possible superconducting pair correlations due to unconventional magnetism

In order to further uncover the role of unconventional magnetism for allowing novel superconducting states, and given that the pair potential is intimately related to the pair amplitude $F_{\sigma\sigma'}(\mathbf{k}, \mathbf{k}', \omega_n)$ via Eq. (11), we now analyze the symmetries of $F_{\sigma\sigma'}(\mathbf{k}, \mathbf{k}', \omega_n)$. With this, we can identify the emergent superconducting correlations in UMs with superconductivity. To carry out this task, it is necessary to remind that the pair amplitude represents a two-electron wavefunction and, therefore, fulfills the antisymmetry condition imposed by the fermionic nature of paired electrons under the total exchange of involved quantum numbers as

$$F_{\sigma\sigma'}(\mathbf{k}, \mathbf{k}', \omega_n) = -F_{\sigma'\sigma}(\mathbf{k}', \mathbf{k}, \omega_n). \quad (17)$$

This condition here involves momenta, spins, and Matsubara frequencies but, in general, the pair amplitude can depend on other quantum numbers such as bands, valley, layer, etc., see Refs. [1, 9, 15, 307, 308]. Interestingly, the antisymmetry condition given by Eq. (17) implies that the parity of the momentum part, the spin configuration, and the frequency dependence are linked. As such, under the individual exchange of such quantum numbers, the pair amplitude can be either *even* (E) or *odd* (O), provided the total exchange of quantum numbers makes the pair amplitude antisymmetric. At this point, it is also useful to decompose the spin symmetry and write the pair amplitudes as a 2×2 matrix in spin space as for the pair potential in Eq. (14) and Eq. (15),

$$\hat{F}(\mathbf{k}, \omega_n) = [F_s(\mathbf{k}, \omega_n) + \mathbf{F}_t(\mathbf{k}, \omega_n) \cdot \boldsymbol{\sigma}](i\sigma_y), \quad (18)$$

where $F_s(\mathbf{k}, \omega_n)$ is the spin-singlet pair amplitude, while $\mathbf{F}_t(\mathbf{k}, \omega_n)$ is the vector of spin-triplet pair components $\mathbf{F}_t(\mathbf{k}, \omega_n) = (F_x(\mathbf{k}, \omega_n), F_y(\mathbf{k}, \omega_n), F_z(\mathbf{k}, \omega_n))$. The singlet and triplet parts are given by: $F_s(\mathbf{k}, \omega_n) = [F_{\uparrow\downarrow}(\mathbf{k}, \omega_n) - F_{\downarrow\uparrow}(\mathbf{k}, \omega_n)]/2$, $F_x(\mathbf{k}, \omega_n) = [-F_{\uparrow\uparrow}(\mathbf{k}, \omega_n) + F_{\downarrow\downarrow}(\mathbf{k}, \omega_n)]/2$, $F_y(\mathbf{k}, \omega_n) = [F_{\uparrow\uparrow}(\mathbf{k}, \omega_n) + F_{\downarrow\downarrow}(\mathbf{k}, \omega_n)]/(2i)$, $F_z(\mathbf{k}, \omega_n) = [F_{\uparrow\downarrow}(\mathbf{k}, \omega_n) + F_{\downarrow\uparrow}(\mathbf{k}, \omega_n)]/2$; details on the decomposition of pair symmetries noted here can be found in Refs. [1, 9, 15, 309]. Moreover, it can be also defined a spin polarization of Cooper pairs associated to the pair amplitudes as $\hat{\mathbf{P}} = i\mathbf{F}_t \times \mathbf{F}_t^*$, which is akin to \mathbf{P} in Eq. (16). The expressions for the pair amplitudes given here are similar to those for the singlet and triplet parts of the pair potential given in the paragraph below Eq. (15).

Now, going back to identifying the symmetry of the pair amplitudes, we realize that, due to the antisymmetry condition, the spin-singlet pair amplitude can have either even-frequency even-parity symmetry or odd-frequency odd-parity symmetry. By a similar analysis, we find that the spin-triplet pair amplitudes can exhibit either even-frequency odd-parity or odd-frequency even-parity. As a result, taking into account frequencies, spins, and parity, there exist four pair symmetry classes that respect

Magnet / SC	singlet <i>s</i> -wave	singlet <i>d</i> -wave	triplet chiral <i>p</i> -wave	triplet helical <i>p</i> -wave
<i>d</i> -wave altermagnet	<i>s</i> -wave ESE	<i>d</i> -wave ESE	<i>p</i> -wave ETO($\parallel \mathbf{d}$)	<i>p</i> -wave ETO($\parallel \mathbf{d}$)
	<i>d</i> -wave OTE($\parallel \hat{z}$)	<i>g</i> -wave OTE($\parallel \hat{z}$)	<i>f</i> -wave OSO	<i>f</i> -wave ETO($\parallel \hat{z} \times \mathbf{d}$)
<i>p</i> -wave magnet	<i>s</i> -wave ESE	<i>d</i> -wave ESE	<i>p</i> -wave ETO($\parallel \mathbf{d}$)	<i>p</i> -wave ETO($\parallel \mathbf{d}$)
	<i>p</i> -wave ETO($\parallel \hat{z}$)	<i>f</i> -wave ETO($\parallel \hat{z}$)	<i>d</i> -wave ESE	<i>d</i> -wave OTE($\parallel \hat{z} \times \mathbf{d}$)

Table II. List of pair symmetries due to the combination of superconductivity and unconventional magnetism, characterized by AMs and PUMs as two representative examples of even- and odd-parity UMs. The top row and leftmost column show the type of superconductor and UM, respectively. The symmetries of the induced pair amplitudes are shown from the second column and second row. As an example, the cell in the position of the second column and second row shows that combining spin-singlet *s*-wave superconductivity with *d*-wave altermagnetism gives rise to two pair symmetry classes: *s*-wave ESE and *d*-wave OTE, with a *d*-vector parallel to the *z*-axis. We note that the symbols “*s, p, d, f, g, . . .*-wave” represent, respectively, the degree 0, 1, 2, 3, 4, . . . of the homogeneous polynomials of momenta given by the pair amplitudes. Taken from Ref. [145].

the antisymmetry condition: i) even-frequency spin-singlet even-parity (ESE), ii) even-frequency spin-triplet odd-parity (ETO), iii) odd-frequency spin-singlet odd-parity (OSO), and iv) odd-frequency spin-triplet even-parity (OTE); see more details about the OTE class in Refs. [9, 15, 219, 309–332]. It is worth noting that, while there exists a direct relation between pair amplitudes and pair potential via Eq. (5), the pair potential in Eq. (5) is not frequency dependent, and thus symmetric, but the pair amplitude given by Eq. (12) depends on frequency. A generalization of the pair potentials discussed here, such that they become frequency dependent, can be done within Eliashberg theory [304, 305, 333–338], see also Refs. [339, 340]. We will however concentrate on the four allowed pair symmetries, whose emergence, in spite of being allowed, depends on the unconventional magnetic system under investigation [145], with a particular relation to the breaking of the underlying symmetries of the system [62] (time translation, spatial translation, spin-rotation, inversion, etc.). Even though the resulting four pair symmetry classes have already been studied before in systems with relativistic SOC [9, 15, 219, 315, 320, 324, 325, 341], the full classification in even- and odd-parity UMs with superconductivity was only recently reported [145], see also Refs. [146–148, 155].

In order to unveil the role of unconventional magnetism for inducing novel superconducting correlations, let us first consider a *d*-wave AM with spin-singlet superconductivity. This is modelled by a BdG Hamiltonian given by Eq. (13) but with $\hat{H}(\mathbf{k}) = \xi_{\mathbf{k}}\sigma_0 + M_{\mathbf{k}}^d\sigma_z$ characterizing the *d*-wave AM, with the exchange field $M_{\mathbf{k}}^d$ given by Eq. (4) and $\xi_{\mathbf{k}}$ the kinetic term, while $\hat{\Delta}(\mathbf{k}) = i\sigma_y d_0(\mathbf{k})$ describes the spin-singlet pair potential discussed in the previous subsection. Then, by using Eq. (12) for the anomalous Green’s function, which is the same as obtaining the off-diagonal component of the Nambu Green’s function in Matsubara representation $\hat{G}(\mathbf{k}, i\omega_n) = (i\omega_n - H_{\text{BdG}}(\mathbf{k}))^{-1}$, the spin-singlet

and spin-triplet pair amplitudes can be obtained as [145]

$$F_s(\mathbf{k}, i\omega_n) = -\frac{d_0(\mathbf{k})Q_{\mathbf{k}}(\omega_n)}{[Q_{\mathbf{k}}(\omega_n)]^2 + 4[M_{\mathbf{k}}^d]^2\omega_n^2}, \quad (19)$$

$$F_t(\mathbf{k}, i\omega_n) = \frac{2i\omega_n d_0(\mathbf{k})M_{\mathbf{k}}^d \hat{z}}{[Q_{\mathbf{k}}(\omega_n)]^2 + 4[M_{\mathbf{k}}^d]^2\omega_n^2},$$

where $Q_{\mathbf{k}}(\omega_n) = \omega_n^2 + \xi_{\mathbf{k}}^2 - [M_{\mathbf{k}}^d]^2 + |d_0(\mathbf{k})|^2$. From Eqs. (19), we can identify the symmetries of superconducting correlations that emerge when combining *d*-wave altermagnetism with spin-singlet superconductors. The first property to note is that spin-singlet and spin-triplet pair amplitudes emerge, with the triplet parallel to \hat{z} , which reflects the role of *d*-wave altermagnetism as a mechanism to convert spin-singlet into spin-triplet. The spin-singlet pair amplitude, first expression in Eqs. (19), is even in both frequency and momentum given that $Q_{\mathbf{k}}(\omega_n) = Q_{-\mathbf{k}}(\omega_n)$, $Q_{\mathbf{k}}(\omega_n) = Q_{\mathbf{k}}(-\omega_n)$, and $d_0(\mathbf{k}) = d_0(-\mathbf{k})$. As a result, $F_s(\mathbf{k}, i\omega_n)$ has a pair symmetry that corresponds to the ESE class discussed at the beginning of this subsection. Depending on whether $d_0(\mathbf{k})$ describes a spin-singlet *s*-wave or spin-singlet *d*-wave pair potential, the spin-singlet pair amplitude $F_s(\mathbf{k}, i\omega_n)$ would acquire the *s*- or *d*-wave parity of the parent superconductor.

The situation becomes more interesting for the spin-triplet pair amplitude $F_t(\mathbf{k}, i\omega_n)$ given by the second expression in Eqs. (19). In fact, while such a pair component has a mixed spin-triplet symmetry, it develops an odd frequency dependence ($\sim \omega_n$ in the numerator) and a parity symmetry that results from the interplay between superconductivity (via $d_0(\mathbf{k})$) and *d*-wave altermagnetism (via $M_{\mathbf{k}}^d$). This implies that $F_t(\mathbf{k}, i\omega_n)$ has an odd-frequency spin-triplet even-parity and belongs to the OTE class. For a spin-singlet *s*-wave superconductor ($d_0(\mathbf{k}) = \Delta$), the even-parity of $F_t(\mathbf{k}, i\omega_n)$ corresponds to *d*-wave symmetry entirely determined by *d*-wave altermagnetism via $M_{\mathbf{k}}^d$; hence the parity of the AM is transferred to the emergent pair amplitude. For a spin-singlet *d*-wave superconductor, with a *d* vector as in Tab. III, the even-parity of $F_t(\mathbf{k}, i\omega_n)$ has a *g*-wave symmetry due to the combined action of the *d*-wave AM and *d*-wave superconductor; the amplitude and argument of the OTE pair

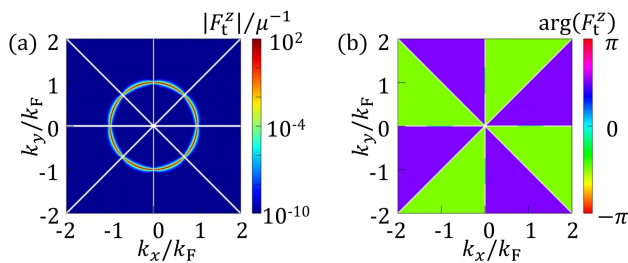


Figure 6. Emergent pair amplitudes in a $d_{x^2-y^2}$ -wave AM with spin-singlet d_{xy} -wave superconductivity. (a) Absolute value of the OTE pair amplitude given by Eq. (19) as a function of momenta. The diagonal lines indicate the nodes of the pair amplitude. (b) Argument of the OTE pair amplitude as a function of momenta, where the purple and green colors indicate $\pi/2$ and $-\pi/2$, respectively. Parameters: $\Delta = 0.01\mu$, $\omega_n = 0.5\Delta$ and $J = 0.3\Delta$. Adapted from Ref. [145].

amplitude are shown in Fig. 6, with a clear node structure that reflects its parity. The ESE and OTE pair symmetry classes due to d -wave altermagnetism and spin-singlet superconductivity are indicated in Tab. II. Ref. [145] also addressed the role of AMs with spin-triplet superconductivity as well as other PUMs with distinct types of superconductivity, which allowed to establish unconventional magnetism as a mechanism that not only mixes spins, thereby leading to a spin-singlet to spin-triplet conversion, but also transfers the parity symmetry to the emergent superconducting state, see Tab. II. Thus, it is possible to induce superconducting states with a higher parity [145], such as the f -wave pairing state in AMs with spin-triplet p -wave superconductivity as shown in Tab. II, already predicted before in Ref. [292] in the context of intrinsic superconductivity. Due to the direct relation between pair amplitude and pair potential, the classification carried out in Ref. [145] is expected to also hold for the pair potential under appropriate interactions, being thus useful to understand for appearance of intrinsic superconductivity in UMs. We can therefore conclude that unconventional magnetism is a promising ground for novel superconducting states.

C. Superconducting junctions formed by unconventional magnets and superconductors

Having discussed the effect of unconventional magnetism on the superconducting pair symmetries, in this part we address the emergent phenomena when UMs are placed in contact with a superconductor. In particular, we focus on NS hybrid junctions where N represents a normal state material, which can be any normal metal or UM, while S denotes a superconductor, as schematically shown in Fig. 7(a). NS junctions are the simplest superconducting junctions that permit us to analyze fundamental superconducting phenomena due to the combination of unconventional magnetism, superconductivity,

and the breaking of spatial translation at the junction's interface.

1. Modelling NS junctions

Before going further, it is important to remark that, when dealing with systems that are inhomogeneous in space, the pair potential is written in terms of two spatial coordinates; thus, the expression of the pair potential in spin space corresponding to Eq. (14) is given by,

$$\hat{\Delta}(\mathbf{r}, \mathbf{r}') = [d_0(\mathbf{r}, \mathbf{r}') + \mathbf{d}(\mathbf{r}, \mathbf{r}') \cdot \boldsymbol{\sigma}](i\sigma_y), \quad (20)$$

where $d_0(\mathbf{r}, \mathbf{r}')$ describes the spin-singlet pair potential and $\mathbf{d}(\mathbf{r}, \mathbf{r}')$ the vector of spin-triplet components. The individual components hold properties according to their symmetries, see more on Refs. [17, 298]. Since the analysis of NS junctions often involves finding the spectrum E and wavefunction Ψ , it is necessary to solve the eigenvalue problem associated to the BdG Hamiltonian, which is similar to the one given by Eq. (13) but for inhomogeneous systems. The eigenvalue problem in Nambu space is given by

$$\int dr' \mathcal{H}_{\text{BdG}}(\mathbf{r}, \mathbf{r}') \Psi(\mathbf{r}') = E \Psi(\mathbf{r}), \quad (21)$$

where $\Psi(\mathbf{r}) = (u_\uparrow(\mathbf{r}), u_\downarrow(\mathbf{r}), v_\uparrow(\mathbf{r}), v_\downarrow(\mathbf{r}))^T$ is the Nambu vector with electron- (u_σ) and hole-like (v_σ) parts, while $\mathcal{H}_{\text{BdG}}(\mathbf{r}, \mathbf{r}')$ is the BdG Hamiltonian written as

$$\mathcal{H}_{\text{BdG}}(\mathbf{r}, \mathbf{r}') = \begin{pmatrix} \delta(\mathbf{r} - \mathbf{r}') \hat{h}(\mathbf{r}') & \hat{\Delta}(\mathbf{r}, \mathbf{r}') \\ \hat{\Delta}^\dagger(\mathbf{r}, \mathbf{r}') & -\delta(\mathbf{r} - \mathbf{r}') \hat{h}(\mathbf{r}') \end{pmatrix}. \quad (22)$$

Here, $\hat{h}(\mathbf{r})$ is the Hamiltonian describing electrons and $\hat{\Delta}(\mathbf{r}, \mathbf{r}')$ the pair potential, both matrices in spin space. The eigenvalue problem given by Eq. (21) is also known as BdG equations. While $\hat{h}(\mathbf{r})$ is in general a 2×2 matrix in spin space with all its elements finite, in the absence of fields that couple spins $\hat{h}(\mathbf{r})$ is a diagonal matrix in spin space given by $\hat{h}(\mathbf{r}) = h(\mathbf{r}) + M(\mathbf{r})\sigma_z$, with $h(\mathbf{r}) = -(\hbar^2/2m)\nabla^2 - \mu(\mathbf{r}) + U(\mathbf{r})$, where $\mu(\mathbf{r})$ is the chemical potential that measures the filling of the band from the band bottom, $U(\mathbf{r})$ is a one-body potential characterizing the interface, and $M(\mathbf{r})$ describes the exchange field of an UM appropriately written from Eqs. (3) and (4). Thus, when spins are not coupled, the BdG equations can be decoupled, leading to simpler expressions to solve, as discussed e. g., in Refs. [17, 298]. This is the case, for instance, of a spin-singlet s -wave pair potential and in the absence of spin mixing fields and $M(\mathbf{r}) = 0$, where the BdG equations simply become

$$\begin{pmatrix} h(\mathbf{r}) & \Delta(\mathbf{r}) \\ \Delta^*(\mathbf{r}) & -h(\mathbf{r}) \end{pmatrix} \begin{pmatrix} u_\uparrow(\mathbf{r}) \\ v_\downarrow(\mathbf{r}) \end{pmatrix} = E \begin{pmatrix} u_\uparrow(\mathbf{r}) \\ v_\downarrow(\mathbf{r}) \end{pmatrix}, \quad (23)$$

$$\begin{pmatrix} h(\mathbf{r}) & -\Delta(\mathbf{r}) \\ -\Delta^*(\mathbf{r}) & -h(\mathbf{r}) \end{pmatrix} \begin{pmatrix} u_\downarrow(\mathbf{r}) \\ v_\uparrow(\mathbf{r}) \end{pmatrix} = E \begin{pmatrix} u_\downarrow(\mathbf{r}) \\ v_\uparrow(\mathbf{r}) \end{pmatrix}.$$

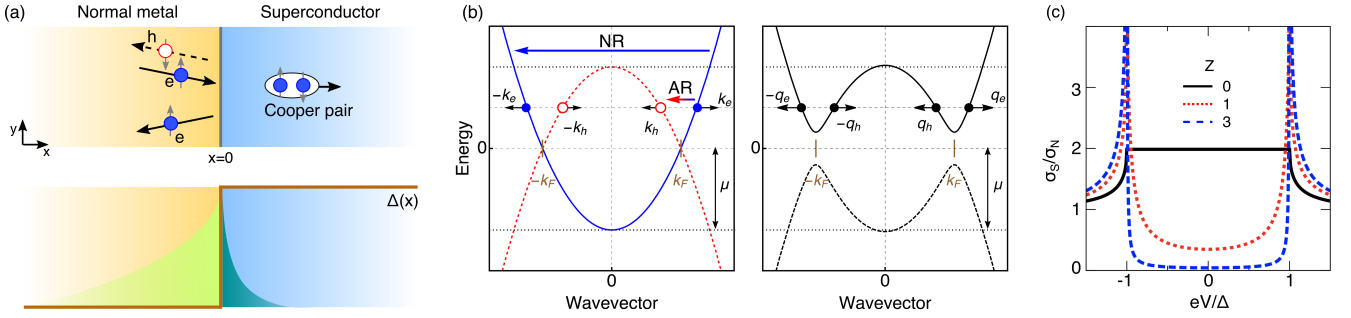


Figure 7. (a) Top: Andreev reflection in a NS junction formed by a semi-infinite normal metal (N, yellow) and a semi-infinite conventional superconductor (S, blue). An incident electron (filled blue circle) at the NS interface located at $x = 0$ (gray vertical line) can be reflected back either as an electron or as a hole (empty red circle). The reflection of an electron into a hole is known as Andreev reflection, a process that also allows the transfer of a Cooper pair (white ellipse with two filled circles) into the superconductor. The Andreev reflection discussed here implies that the reflection angle is the same as the angle of incidence (retroreflection). Bottom: The Andreev reflection carries superconducting correlations from the superconductor with pair potential $\Delta(x)$ (brown curve) into the normal metal, known as the proximity effect (light green region), and also modifies the superconducting correlations in the superconductor, known as the inverse proximity effect (blue-green region). (b) Energy versus momentum in the normal metal (left) and superconductor (right), indicating the right moving electrons and holes in the former as well as quasielectrons and quasiholes in the latter. (c) Tunneling conductance in the NS junction of (a) as a function of energy for distinct values of the interface barrier strength Z .

While for conventional superconductors, the BdG equations are simpler, under general circumstances, one always has to solve the Eq. (21), which is of course a challenging task. We also note that there are clever approximations that can reduce the complexity of the BdG equations, such as the so-called Andreev or semiclassical approximation where the chemical potential is the largest energy scale. The Andreev equations are simpler to solve than the BdG equations because they involve first derivatives in the single particle Hamiltonian in contrast to the second derivatives in $\hat{h}(\mathbf{r})$ of the BdG equations, see more in Refs. [17, 298].

To find the energies and wavefunctions of a NS junction along x with a spin-singlet s -wave pair potential $\Delta(\mathbf{r}) = \theta(x)\Delta$, we can just solve the BdG equations Eqs. (23) in terms of plane waves for a given single particle Hamiltonian $\hat{h}(\mathbf{r})$. This approach assumes that N and S are semi-infinite systems along x and that there is a pair potential only in the superconducting region S but no pair potential in the normal region N exists. While this is a simplification of what happens at interfaces between superconductors and normal state materials, it turns out that such an assumption already provides interesting insights on the emergent superconducting phenomena at such NS interfaces [342]. Upon appropriate modifications of the profile of the pair potential, it is also possible to model finite N and S regions in superconducting junctions, see e. g., Refs. [184, 212, 224, 225, 320, 326, 330, 341, 343]. The total solutions would then need to comply with the continuity of wavefunctions at the respective interfaces, such as at $x = 0$ in Fig. 7(a). Another possibility to model NS junctions with finite N and S regions is to carry out a tight-binding discretization of the BdG Hamiltonian within a tunneling Hamiltonian approach [17, 167, 180, 205, 215, 217, 219], thus allowing to ex-

plore finite size effects. Whenever necessary, we will refer to the type of approach used to model superconducting junctions, see also Refs. [297, 344–346].

2. Andreev reflections and Andreev bound states

To understand the most fundamental effect in superconducting junctions between superconductors and UMs, we here address charge transport in a NS junction modelled as discussed in the previous subsection. To start with, we first focus on a one-dimensional (1D) NS junction located at $x = 0$ when N is a normal metal and S a conventional spin-singlet s -wave superconductor; this will help us unveil the role of unconventional magnetism later. Then, to uncover the transport processes at the interface of NS junctions, we employ scattering states which are built by using the wavefunctions of the N and S regions [298, 342]. Thus, by taking the BdG equations given by Eq. (23) and using plane waves $\Psi(x) = Ae^{ikx}$, the BdG Hamiltonian gives the energies in the superconductor $E_k = \pm\sqrt{\xi_k^2 + \Delta^2}$, where $\xi_k = \hbar^2 k^2/2m - \mu$, while $E_k = \pm\xi_k$ are the normal energy bands in N. The associate wavevectors in N are $\pm k_{e(h)}$ with

$$k_{e(h)} = k_F \sqrt{1 \pm \frac{E}{\mu}}, \quad (24)$$

while in S are $\pm q_{e(h)}$ with

$$q_{e(h)} = k_F \sqrt{1 \pm \frac{\Omega}{\mu}}, \quad (25)$$

where $k_F = \sqrt{2m\mu/\hbar^2}$ is the Fermi wavevector, and

$$\Omega = \begin{cases} \sqrt{E^2 - |\Delta|^2}, & E \geq |\Delta| \\ i\sqrt{|\Delta|^2 - E^2}, & -|\Delta| \leq E \leq |\Delta| \\ -\sqrt{E^2 - |\Delta|^2}, & E \leq -|\Delta|. \end{cases} \quad (26)$$

Thus, the wavefunctions in N are given by

$$\begin{aligned} \Psi_{\pm k_e}(x) &= e^{\pm i k_e x} \begin{pmatrix} 1 \\ 0 \end{pmatrix}, \\ \Psi_{\pm k_h}(x) &= e^{\pm i k_h x} \begin{pmatrix} 0 \\ 1 \end{pmatrix}, \end{aligned} \quad (27)$$

while in S by

$$\begin{aligned} \Psi_{\pm q_e}(x) &= e^{\pm i q_e x} \begin{pmatrix} u \\ v \end{pmatrix}, \\ \Psi_{\pm q_h}(x) &= e^{\pm i q_h x} \begin{pmatrix} v \\ u \end{pmatrix}, \end{aligned} \quad (28)$$

where $u = \sqrt{1 + \Omega/E}/\sqrt{2}$ and $v = \sqrt{1 - \Omega/E}/\sqrt{2}$. The energy versus momentum in N and S as well as their associated wavevectors are shown in Fig. 7(b). To identify the scattering processes, we look at the direction of motion of the respective states at fixed wavevectors. The direction of motion of a state at the given wavevector can be obtained by looking at the group velocity

$$v_g(k) = \frac{1}{\hbar} \frac{dE(k)}{dk}, \quad (29)$$

where $E(k)$ is the energy dispersion discussed in the paragraph before Eq. (24), see also Fig. 7(b). This allows us to identify that electrons in N with k_e and $-k_e$ move to the right and left directions, respectively. Moreover, holes in N with k_h and $-k_h$ move to the left and right, respectively. In a very similar way, we can identify the direction of motion for the quasiparticles in S. The direction of motion in N and S is depicted by horizontal black arrows in Fig. 7(b). Having this allowed states in mind, we therefore find that a right moving electron $\Psi_{k_e}(x)$ from N can be reflected back at the NS interface into N either as a left-moving electron with $\Psi_{-k_e}(x)$ or as a left-moving hole with $\Psi_{k_h}(x)$. The reflection into a particle of the same kind is known as normal reflection (NR), while the reflection of an electron into a hole or vice-versa is known as Andreev reflection (AR) [347, 348], see Fig. 7(b); for more details on the AR, see Refs. [342]. The right moving electron from N can be also transmitted into S as a quasidelectron or quasihole, processes known as normal transmissions and Andreev transmissions, respectively. When scattering occurs at energies within the superconducting gap, the AR involves the transfer of a Cooper pair into S [342], sketched in Fig. 7(a). We can thus see that Andreev processes are unique to superconducting interfaces, which is why they represent perhaps one of

the most fundamental superconducting scattering effects, carrying information about the superconductor and the NS interface as well see next. The Andreev reflection is perhaps the most fundamental effect in superconducting junctions and does not have any analog in normal state heterostructures [342, 347, 348]. We can then quantify ARs and their effects in transport by constructing scattering states, which involve the discussed processes for a given particle moving towards the NS interface. For instance, for a right-moving electron towards the interface, we obtain in N and S,

$$\begin{aligned} \Psi_N(x) &= e^{i k_e x} \begin{pmatrix} 1 \\ 0 \end{pmatrix} + a e^{i k_h x} \begin{pmatrix} 0 \\ 1 \end{pmatrix} + b e^{-i k_e x} \begin{pmatrix} 1 \\ 0 \end{pmatrix}, \\ \Psi_S(x) &= c e^{i q_e x} \begin{pmatrix} u \\ v \end{pmatrix} + d e^{-i q_h x} \begin{pmatrix} v \\ u \end{pmatrix}. \end{aligned} \quad (30)$$

The coefficients in $\Psi_{N,S}(x)$ are then determined by the boundary conditions at the interface, which, including a delta potential barrier $U(x) = \lambda\delta(x)$ of barrier strength λ , we find

$$[\Psi_N(x)]_{x=0} = [\Psi_S(x)]_{x=0}, \quad (31)$$

$$[\partial_x \Psi_S(x)]_{x=0} - [\partial_x \Psi_N(x)]_{x=0} = \frac{2m\lambda}{\hbar^2} [\Psi_N(x)]_{x=0}.$$

Then, within the Andreev approximation where the chemical potential is the largest energy scale, we assume $k_{e(h)} \sim q_{e(h)} \sim k_F$. In this regime, the coefficients of $\Psi_{N,S}(x)$ take simple forms, and for the normal and Andreev reflections, one finds $a = \Gamma/[(1 + Z^2) - Z^2\Gamma^2]$ and $b = [iZ(1 - iZ)(\Gamma^2 - 1)]/[(1 + Z^2) - Z^2\Gamma^2]$, with $Z = m\lambda/(\hbar^2 k_F)$, $\Gamma = v/u$. We can then obtain the differential conductance at zero temperature $dI/dV = (2e^2/h)\sigma_S(E = eV)$, where [349]

$$\sigma_S = \begin{cases} \frac{2\sigma_N^2 \Delta^2}{(\sigma_N - 2)^2 \Delta^2 - 4(1 - \sigma_N)E^2}, & |E| < \Delta, \\ \frac{2\sigma_N E}{(2 - \sigma_N)\Omega + \sigma_N E}, & |E| > \Delta, \end{cases} \quad (32)$$

where $\sigma_N = 1/(1 + Z^2)$ is the transmissivity in the normal state and we have used that $\sigma_S = (1 - |b|^2 + |a|^2)$. The role of ARs is thus to increase σ_S , while NRs tend to reduce it [342, 349]. The conductance σ_S as a function of energy is presented in Fig. 7(c) for distinct values of Z which captures the barrier strength. Without any barrier $Z = 0$, the junction is transparent and $\sigma_N = 1$, which then leads to a constant conductance $\sigma_S = 2$ within the superconducting gap due to perfect AR $|a| = 1$ and $|b| = 0$, see black curve in Fig. 7(c). The finite constant subgap conductance at $Z = 0$ is therefore a signature of Cooper pair transport, which is remarkable given that the AR coefficient is obtained in N; the AR hence carries superconducting information deep into N. At finite Z , normal reflections appear and reduce the subgap conductance, see dotted red curve in Fig. 7(c). At very large Z , the normal transmissivity is very small and leads to

very small values of the subgap conductance, as indeed seen in the dashed blue curve in Fig. 7(c). Conductance can thus provide information about the superconducting interface, via ARs, and also about the superconductor. While the physics discussed so far in this part is well-known, it will help us understand how unconventional magnetism affects the Andreev transport in superconducting junctions.

We are now ready to analyse the scattering processes at the NS interface located at $x = 0$ with N being an UM and S a conventional superconductor. For UMs, we consider d -wave AMs and p -wave UMs discussed in Section II, and then follow the same steps as the ones we carried out before for finding the conductance [Eq. (32)] when N is just a normal metal. We also assume that our system is infinite along y so that k_y is still a good quantum number. Moreover, we have to distinguish between up and down spins, even though spins are not necessarily coupled since the exchange field in UMs we consider to be along z , see Section II. Hence, the 4×4 BdG matrix can be written in terms of two independent 2×2 blocks. Without carrying out any calculation, it is important to have an intuition about the role of unconventional magnetism. For this reason, in Fig. 8 we show the Fermi surfaces and energy dispersions at positive energies of each UM, including d_{xy} - and $d_{x^2-y^2}$ -wave AMs as well as p_x - and p_y -wave UMs. By inspecting the Fermi surface of d_{xy} -wave AMs and p_y -wave UMs [Fig. 8(a,f)], we notice that opposite spin states have k_y and $-k_y$, reflecting that ARs as traveling waves are always allowed but depend on

the spin splitting of the energy dispersion. In the case of a $d_{x^2-y^2}$ -wave AM and p_x -wave UM [Fig. 8(b,e)], the states with k_y and $-k_y$ have the same spins; here, NR is possible as a traveling wave but the AR becomes an evanescent wave. Further insights can be also obtained from Fig. 8, where we show the energy dispersions and also indicate the possible scattering states when incident electrons with spin up and down towards the interface. Keeping all the discussions in mind, and in order to quantify the contributions from NR and ARs to charge conductance, we now write down the scattering state in N ($x < 0$) for an incident electron from N with spin up towards the NS interface,

$$\begin{aligned}\Psi_{\text{N}}^{\uparrow}(x, k_y) &= e^{ik_y y} \left[\Psi_{p_{e\uparrow}^+}(x) + a_{\uparrow} \Psi_{p_{h\downarrow}^-}(x) + b_{\uparrow} \Psi_{p_{e\uparrow}^-}(x) \right], \\ \Psi_{\text{N}}^{\downarrow}(x, k_y) &= e^{ik_y y} \left[\Psi_{p_{e\downarrow}^+}(x) + a_{\downarrow} \Psi_{p_{h\uparrow}^-}(x) + b_{\downarrow} \Psi_{p_{e\downarrow}^-}(x) \right],\end{aligned}\quad (33)$$

where $\Psi_{p_{e\uparrow}^+}(x) = e^{ip_{e\uparrow}^+ x} (1, 0, 0, 0)^T$, $\Psi_{p_{h\downarrow}^-}(x) = e^{ip_{h\downarrow}^- x} (0, 0, 0, 1)^T$, $\Psi_{p_{e\uparrow}^-}(x) = e^{ip_{e\uparrow}^- x} (1, 0, 0, 0)^T$, $\Psi_{p_{e\downarrow}^+}(x) = e^{ip_{e\downarrow}^+ x} (0, 1, 0, 0)^T$, $\Psi_{p_{h\uparrow}^-}(x) = e^{ip_{h\uparrow}^- x} (0, 0, 1, 0)^T$, $\Psi_{p_{e\downarrow}^-}(x) = e^{ip_{e\downarrow}^- x} (0, 1, 0, 0)^T$. Moreover, the coefficients a_{σ} and b_{σ} represent the amplitudes of Andreev and normal reflections for an incident electron with spin $\sigma = \uparrow, \downarrow$. Moreover, $p_{e\sigma}^{\pm}$ and $p_{h\sigma}^{\pm}$ are wavevectors in N and obtained from the energy dispersion for UMs. In the case of AMs, they are given by

$$\begin{aligned}p_{e\sigma}^{\pm} &= -\frac{2\sigma m J \sin 2\beta}{\hbar^2 k_{\text{F}}^2 + 2\sigma m J \cos 2\beta} k_y \pm \frac{\hbar k_{\text{F}}^2}{\hbar^2 k_{\text{F}}^2 + 2\sigma m J \cos 2\beta} \sqrt{2m \left(1 + \frac{2\sigma m J \cos 2\beta}{\hbar^2 k_{\text{F}}^2} \right) (\mu + E) - \hbar^2 k_y^2 + \frac{4m^2 J^2}{\hbar^2 k_{\text{F}}^4} k_y^2}, \\ p_{h\sigma}^{\pm} &= \frac{2\sigma m J \sin 2\beta}{\hbar^2 k_{\text{F}}^2 + 2\sigma m J \cos 2\beta} k_y \mp \frac{\hbar k_{\text{F}}^2}{\hbar^2 k_{\text{F}}^2 + 2\sigma m J \cos 2\beta} \sqrt{2m \left(1 + \frac{2\sigma m J \cos 2\beta}{\hbar^2 k_{\text{F}}^2} \right) (\mu - E) - \hbar^2 k_y^2 + \frac{4m^2 J^2}{\hbar^2 k_{\text{F}}^4} k_y^2},\end{aligned}\quad (34)$$

while for p -wave UMs we have

$$\begin{aligned}p_{e\sigma}^{\pm} &= -\frac{\sigma m J \cos \beta}{\hbar^2 k_{\text{F}}} \pm \sqrt{\frac{2m}{\hbar^2} (\mu + E) - \left(k_y + \frac{\sigma m J \sin \beta}{\hbar^2 k_{\text{F}}} \right)^2 + \frac{m^2 J^2}{\hbar^4 k_{\text{F}}^2}}, \\ p_{h\sigma}^{\pm} &= \frac{\sigma m J \cos \beta}{\hbar^2 k_{\text{F}}} \mp \sqrt{\frac{2m}{\hbar^2} (\mu - E) - \left(k_y - \frac{\sigma m J \sin \beta}{\hbar^2 k_{\text{F}}} \right)^2 + \frac{m^2 J^2}{\hbar^4 k_{\text{F}}^2}}.\end{aligned}\quad (35)$$

We also note that the scattering states given by Eqs. (33) also hold when replacing N by a ferromagnet with magnetization along z , but the wavevectors are then

given by [350]

$$\begin{aligned}p_{e\sigma}^{\pm} &= \pm \sqrt{\frac{2m}{\hbar^2} (\mu - \sigma J + E) - k_y^2}, \\ p_{h\sigma}^{\pm} &= \mp \sqrt{\frac{2m}{\hbar^2} (\mu + \sigma J - E) - k_y^2}.\end{aligned}\quad (36)$$

The expressions for the wavevectors in AMs written above coincide with those used in [150, 184] to study

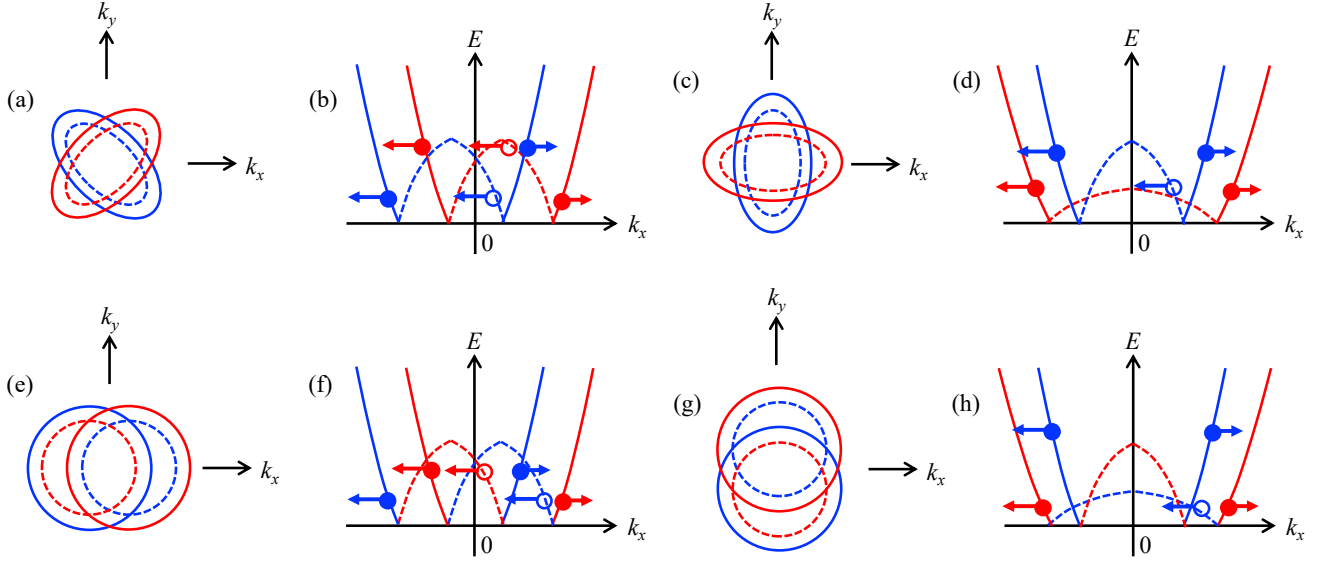


Figure 8. Fermi surfaces and energy dispersions in UMIs, including d -wave AMs (a-d) and p -wave UMIs (e-h). More precisely, (a,c,e,g) shows the quasiparticle energy contour at $E > 0$ for (a) d_{xy} and (c) $d_{x^2-y^2}$ -wave AMs, while (e,g) for p_x - and p_y -wave UMIs. The solid red and blue lines represent the electron energy bands for up and down spins, respectively. Dotted red and blue lines stand for the hole energy bands with up and down spins, respectively. (b,d,f,h) Sketch of scattering states due to right moving electrons with spin up and down at distinct energies, which involve ARs and NRs for (e) $d_{x^2-y^2}$ and (d) d_{xy} -wave AMs, and (f) p_x and (h) p_y -wave UMIs. Filled (empty) red and blue circles denote the electron (hole) with up and down spin at an energy E , and arrows represent the direction of the traveling wave of electrons and holes, respectively.

ARs in d -wave AMs, while our expressions slightly differ from the expressions employed in [152] to study ARs in p -wave UMIs due to the definition of the p -wave magnetic order. In the S region, the wavevectors are still the same as those given by Eqs. (25) but the wavefunctions need to be written taking into account up and down spins, see e. g., Refs. [341, 351]. Having the scattering states in N [Eq. (33)], which now represents an UMI, and S, we can use Eqs. (31) upon appropriate modifications, to find the coefficients a_σ and b_σ representing ARs and NRs. It is worth noting here that since the exchange fields of UMIs are momentum dependent, one needs to be careful when deriving the boundary conditions [150]: antisymmetrization of the unconventional magnet field is needed in order to maintain Hermiticity of the Hamiltonian. In our case, this can be done by replacing the momentum operator as $k_x \rightarrow \{k_x, \theta(-x)\}/2$, where $\{\cdot\}$ is the anticommutator; see Refs. [150] and [148] for AMs and PUMs, respectively. In doing so, it is possible to find analytical solutions for the scattering processes, although the expressions are lengthy and, instead of writing them, we next discuss their behavior under the impact of unconventional magnetism.

In Fig. 9, we present the tunneling conductance as a function of energy in NS junctions without a potential barrier $Z = 0$ modelled as discussed in the previous paragraph: N and S represent semi-infinite of a magnetic material with exchange field J and a conventional spin-singlet s -wave superconductor. For completeness, in Fig. 9(a) we consider N to be a ferromagnet, while

in Fig. 9(b,c) we take it to be a d_{xy} -wave and $d_{x^2-y^2}$ -wave AMs, respectively. In Fig. 9(d,e) we consider N to describe $p_x(y)$ -wave UMIs. Addressing multiple types of magnetic order is useful in order to identify the role of unconventional magnetism on conductance. In NS junctions with N being a ferromagnet, the finite values of the exchange field J reduce the constant subgap conductance while leaving a larger value at zero energy. The reduction of the subgap conductance can be understood to originate from the split Fermi surfaces due to J (see inset), a situation that then suppress Andreev reflection processes [350, 352]. In the case of N being a d -wave AM, the situation has some similarities but also differences with respect to the ferromagnet case which depends on the orientation of the alternating magnetic field, compare Fig. 9(b,c) and Fig. 9(a). In fact, for NS junctions with d_{xy} -wave AMs [Fig. 9(b)], the conductance within the superconducting gap only slightly feels the variations of the exchange field J , remaining roughly constant at values equal to $\sigma_S \approx 2\sigma_N$ [150, 151]. The insensitivity of the conductance in d_{xy} -wave AMs to variations of the exchange field originates because, when integrating over all incident angles towards the interface, the majority and minority spin bands contribute equally, which then gives rise to a vanishing total spin polarization of incident states (see also inset); that is why the conductance for a d_{xy} -wave AM behaves as for a normal metal without spin polarization. This conductance behavior is thus different from what occurs when N is a ferromagnet but it is similar when N is a normal metal [Fig. 7(c)], point-

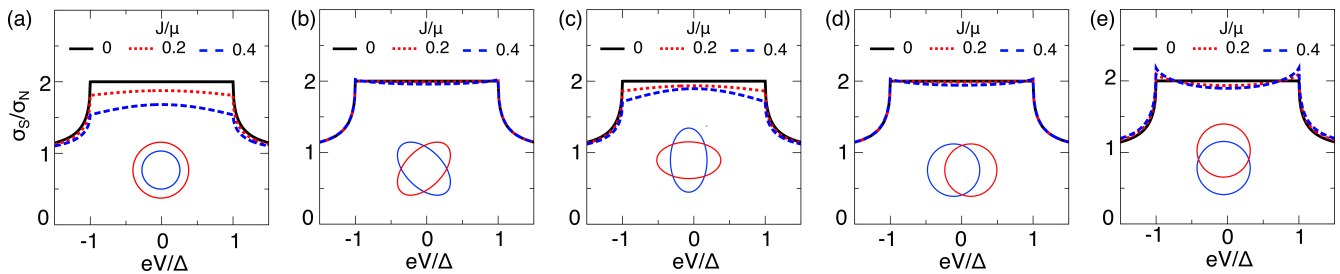


Figure 9. Tunneling conductance integrated in k_y as a function of energy eV in NS junctions formed by semi-infinite UMs and a semi-infinite conventional superconductor, where N is a ferromagnet (a), d_{xy} -wave AM (b), a $d_{x^2-y^2}$ -wave AM (c), a p_x -wave UM (d), and a p_y -wave UM (e). The conductance is normalized with the normal transmissivity $\sigma_N = 1/(1 + Z^2)$, with Z characterizing the strength of the barrier here taken $Z = 0$. Distinct curves represent distinct values of the strength of the exchange field in the respective magnet, while the insets depict the Fermi surfaces in each case. Parameters: $\mu = 1$, $\Delta = 0.001\mu$, $J = 0.2\mu$.

ing out an intriguing difference of AMs with respect to ferromagnets despite both breaking time-reversal symmetry. For NS junctions where N region is a $d_{x^2-y^2}$ in Fig. 9(c), the subgap conductance exhibits an overall reduction as the exchange field increases [150], a behavior similar to the one when N is a ferromagnet, see Fig. 9(a). This happens because the trajectories with a dominant contribution to the charge transport are those exhibiting a normal incidence to the interface, a regime where the Fermi surface of the AM is similar to a ferromagnet because one spin species is larger than the other, compare insets in Fig. 9(a,c). We have verified that when the barrier strength takes finite values, characterized by $Z \neq 0$, the subgap conductance reduces.

In relation to NS junctions where N is a semi-infinite p -wave magnet, we find slightly different behavior from the one discussed for d -wave AMs and ferromagnets, depending on the orientation of the exchange field of the UM. When N is a p_x -wave UM, the conductance is largely insensitive to variations of the exchange field J [Fig. 9(d)], akin to what occurs in d_{xy} -wave AMs and indicating that Andreev reflections are dominant. The almost constant value of the subgap conductance when N is a p_x -wave UM originates from the shift of the Fermi surfaces of the p_x -wave UM along the k_x -direction. The slight variation of the subgap conductance indicates that the mismatch of the Fermi surface exists in the used model given by Eq.(1). In Ref. [152], however, the shape of spin-resolved Fermi surface does not change with J and the subgap conductance is constant within the superconducting gap. Interestingly, when N is a p_y -wave UM, the increase of J modifying the conductance in such a way that reduces it within the superconducting gap but enhances it at the gap edges $\pm\Delta$ and also outside the gap, as shown in Fig. 9(e). This implies that Andreev scattering tends to be suppressed in NS junctions with N being a p_y -wave UM. The reason for this behavior is that there are no available Fermi surfaces corresponding to ARs for quasiparticles with large transverse momentum. The discussed effect was first predicted in Ref. [152] and recently also confirmed in Ref. [148]. Ref. [152] also addressed con-

ductance in NS junctions with N being a p -wave magnet and S being a p -wave superconductor, a system shown to produce zero-bias conductance peaks which acquires a nontrivial dependence on the magnetic order. Thus, UMs affect the charge conductance in NS junctions.

So far we have assumed that the UM is semi-infinite and it is thus natural to wonder what happens to the conductance when the UM has a finite length. These ideas were explored in Refs. [151, 153, 154, 156] which involved AMs but not PUMs. To understand the conductance features in superconducting junctions with AMs of finite length, it is important to understand the underlying properties of N_1N_2S junctions, where N_1 and S are semi-infinite normal and superconducting regions, while N_2 is a finite normal region. In this case, an incident electron from N_1 gets transmitted to N_2 , which then experiences confinement effects due to the finite length of N_2 and also Andreev reflections at the N_2S interface [212]. The interplay of confinement and ARs give rise to the formation of discrete states within the superconducting gap having electron and hole characters, also known as Andreev bound states (ABSs). This phenomenon already appears when N_2 is just a normal metal, where ABSs have been revealed to produce conductance features that help identify the type of superconductor [212]. In the case of N_1N_2S junctions where N_1 and S are a semi-infinite normal metal and a spin-singlet s -wave superconductor, Ref. [151] predicted that ABSs appear and can even produce zero-bias peaks for $d_{x^2-y^2}$ -wave AMs [Fig. 10]; this suggests a strong dependence of conductance on the alternating orientation. Moreover, in a similar type of N_1N_2S junction, Ref. [153] found that a special type of AR occurs, known as specular AR when the reflection angle is inverted with respect to the angle of incidence [353], which induces a positive nonlocal conductance and can be useful for realizing Cooper pair splitters. Later, Ref. [156] explored conductance and ABSs in N_1N_2S junctions with N_2 being a d -wave AM and S being a d -wave superconductor, a system motivated by the need to understand the impact of the d -wave nature in both materials; the ABSs in Ref. [156] are referred to as

de Gennes and Saint-James states. Interestingly, while the d -wave nature of AMs induces ABSs already when S is a conventional spin-singlet s -wave superconductor [151], having a d -wave superconductor affects the levels around zero energy which then produce distinct features in the tunneling conductance, see Fig. 10(a-d). For a N_2 finite region being a $d_{x^2-y^2}$ -wave AM, the tunneling conductance develops a zero-bias peak due to the formation of zero-energy ABSs; this effect occurs because the spin-split bands in $d_{x^2-y^2}$ -wave AMs enhance the mismatch between electron and hole wave vectors, resulting in a sizable phase accumulation in the process of sequential NRs and ARs inside the altermagnetic region N_2 ; these zero-bias peaks originate due to confinement effects in the finite region N_2 [212]. In contrast, for a N_2 finite region being a d_{xy} -wave AM, ABSs with a different profile appear and lead to a V-shape profile of the tunneling conductance around zero energy, but with a finite value at zero energy, see Fig. 10(c,d). While these studies indeed reveal the intriguing impact of unconventional magnetism in superconducting systems, there are still phenomena that need to be explored such as crossed ARs [157] and also Andreev physics in PUMs [354] as well as in superconducting junctions with higher momentum UMs. The so far reported strong dependence of the ABSs and their conductance signatures in junctions with d -wave altermagnetism and superconductivity unveils novel superconducting phenomena that can be further exploited for the design of e.g., Andreev qubits [355–357], see also Refs. [21, 23].

3. Proximity effect and inverse proximity effect

In the previous part, we have seen that Andreev processes in superconducting junctions are able to carry information about the superconductor deep into a non-superconducting UM material when placed in very close proximity. We have shown that the carried information strongly depends on the properties of both the UM and superconductor, raising a natural question about the nature of superconductivity when combining UMs and superconductors in the form of hybrid junctions. This question was partially addressed in Subsection III B, where we showed that distinct types of superconducting correlations emerge when an entire 2D UM has homogeneous superconductivity, provided spatial invariance is preserved. However, in junctions, such as those where ARs have been studied and where spatial invariance is broken, the nature of superconductivity still remains unknown and we plan to study it in this part.

For simplicity, let us first point out some basic features about superconducting correlations in NS junctions located at $x = 0$ and with a pair potential $\Delta(x) = \theta(x)\Delta$; here N and S are semi-infinite regions of a normal metal and a conventional superconductor, respectively. The superconducting correlations can then be obtained from the anomalous part of the Nambu Green's

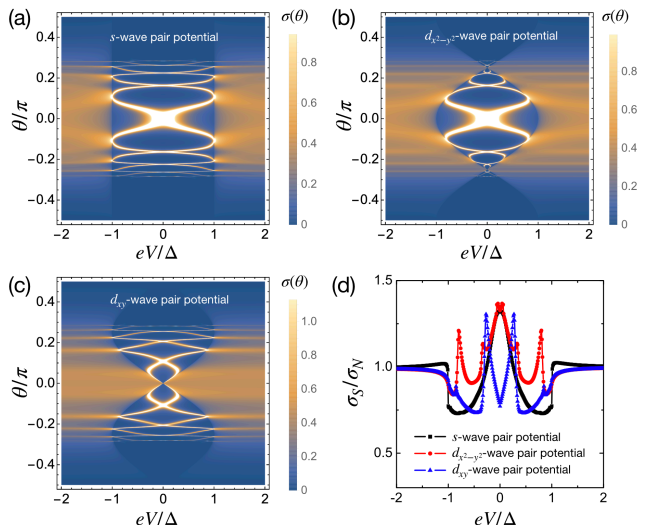


Figure 10. Tunneling conductance as a function of energy eV and the injection angle to the interface θ in N_1N_2S junctions, where N_1 is a semi-infinite normal metal, N_2 is a d -wave AM of length L , and S a semi-infinite superconductor that can have spin-singlet s -wave (a) or d -wave pair potentials (b,c). A barrier potential characterized by Z is assumed at the interface between N_1 and N_2 ; also, θ denotes the injection angle defined as $k_y = k_F \sin \theta$, with k_F being the Fermi wavevector. (d) The total tunneling conductance integrated in θ as a function of eV corresponding to (a-c). Parameters: $k_FL = 10$ and $Z = 2$, $J = 0.3\mu$, $\Delta = 0.001\mu$. Adapted from Ref. [156].

function $\hat{G}(x, x', k_y, \omega_n)$ associated with the BdG Hamiltonian of the system, as discussed in Subsection III B; since momentum along x is not a good quantum number, $\hat{G}(x, x', k_y, \omega_n)$ depends on two spatial coordinates [9, 15, 17, 308]. For NS junctions, it is useful to calculate the Nambu Green's function by using scattering states [15, 164, 326, 359, 360], so that the semi-infinite nature of N and S are taken into account. Alternatively, one can use a recursive Green's function approach within a tight-binding description, also proven useful for calculating the Green's function of semi-infinite superconducting systems [146, 358]. Under general conditions, even though the pair potential in N is zero, it is possible to induce a nonzero pair amplitude in N , with a characteristic length $\xi_N = \hbar v_F/E$ [361, 362], which at zero energy is kept all the way to infinity and signals the superconducting coherence; at finite temperatures, one recovers $\xi_N \approx 1/T$, after doing an appropriate analytic continuation $E \rightarrow i\omega_n$. Analogously, an Andreev reflected hole has the opposite velocity at zero energy and traces the same phase in a phase coherence fashion. Both the induced pair amplitude in N and the Andreev reflections have been shown to be directly related to each other and to be at the core of what is known as the superconducting *proximity effect* [15, 160, 320, 341, 363], where the part of N closest to S acquires superconducting correlations, see light green region in N of the bottom panel of Fig. 7(a). Furthermore, in the same way as the N region

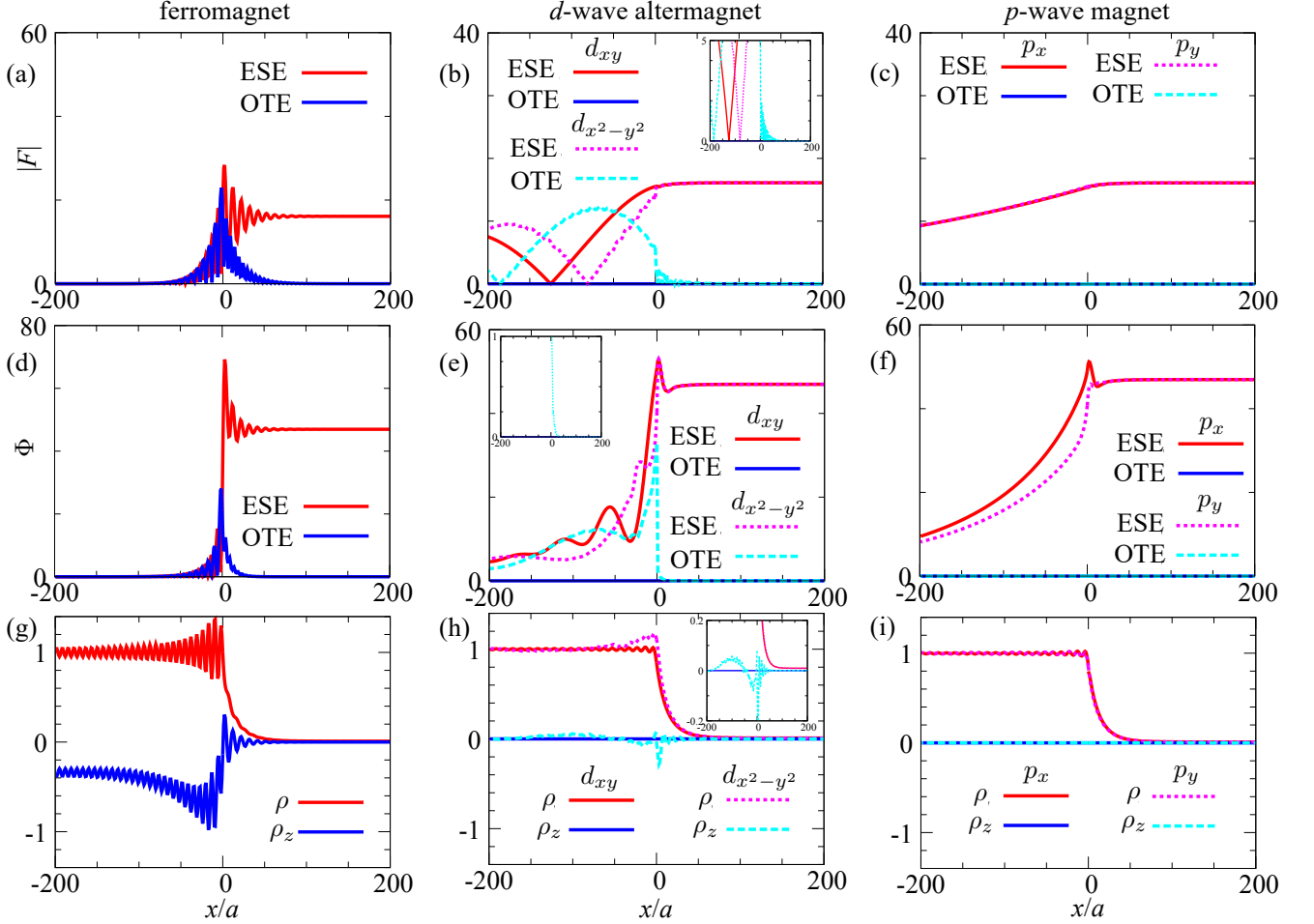


Figure 11. (a-c) Absolute value of the zero-frequency local pair amplitudes as a function of space at $k_y = 0.02\pi$ in NS junctions without potential barrier, where the interface is located at $x = 0$ and the S (N) regions correspond to a conventional spin-singlet s -wave superconductor (magnetic system) situated at $x > 0$ ($x < 0$). Distinct panels correspond to distinct N regions, including a ferromagnet (a), d -wave AM (b), p -wave UM (c). The pair amplitudes are obtained within a recursive Green's function approach. (d-f) Square absolute value of the pair amplitudes of (a-c) integrated in k_y . (g-i) Space dependence of the electronic LDOS and local spin-density along z , both integrated in k_y and normalized with respect to the LDOS at $E = 0$ and $\Delta = 0$ for the systems corresponding to (a-c). Tight-binding parameters: $a = 1$, $\mu = 0.1t$, $\Delta = 0.02t$, $m_z = t_x = t_y = t_{xy} = t_{x^2-y^2} = 0.1t$. Adapted from Ref. [358].

gets affected by the superconductor, the region of S closest to N over a range $\xi_S = \hbar v_F / \Delta$ also suffers changes intimately connected to the nature of N. For instance, given that S can be a conventional spin-singlet s -wave superconductor, it is possible to induce superconducting correlations with a distinct symmetry, which gives rise to an effect known as the *inverse proximity effect*; this effect has been mostly studied when N is a magnetic material which then induces a magnetic moment in the superconductor [361, 364–366] but recently also addressed under the presence of ABSs [367]. The inverse proximity effect is depicted by a blue-green region in S of the bottom panel of Fig. 7(a).

To understand the proximity effect and the inverse proximity effect in NS junctions formed by UMs, in

what follows we discuss the emergent pair amplitudes from Ref. [358] obtained for semi-infinite UMs and semi-infinite spin-singlet s -wave superconductors. We consider a NS junction along x located at $x = 0$, such that the pair potential is finite only in S, $\Delta(x) = \theta(x)\Delta$; to model N and S, a tight-binding (TB) description of the UMs and superconductors is taken with an appropriate discretization along x but keeping k_y a good quantum number, as discussed in Ref. [358], see also Section III. Here, within a TB representation, we remind that the strength of the exchange fields for a ferromagnet, d_{xy} -wave AM, $d_{x^2-y^2}$ -wave AM, p_x -wave UM, and p_y -wave UM are denoted by m_z , t_{xy} , $t_{x^2-y^2}$, t_x and t_y , respectively; see Subsection II A. Then, the pair amplitudes are found within a recursive Green's function approach as discussed in

Ref. [358]. Under general circumstances, NS junctions formed by UMs host four pair symmetries, which include the ESE, OSO, ETO, and OTE classes discussed in Subsection III B, where the first, second, and third capital letters represent the even (odd) symmetry of frequency, spin, and momentum parity, respectively. Moreover, the main role of the interface in NS junctions is that it breaks the spatial invariance, a mechanism that leads to the co-existence of even- and odd-parity states even when the bulk of S is a conventional spin-singlet s -wave parity [15]. Thus, here we also expect four pair symmetry classes due to the interplay of unconventional magnetism and breaking of spatial invariance at the NS interface. In Fig. 11, we show the absolute value of the local pair amplitudes as a function of space $x = x'$ at lowest frequency and fixed k_y for NS junctions with N being either a ferromagnet, a d -wave AM, or a p -wave UM; here $x < 0$ and $x > 0$ correspond to N and S, respectively. In Fig. 11(d-f), we also plot the square absolute value of the pair amplitudes of panels Fig. 11(a-c) integrated in the transverse momentum k_y . For completeness, in Fig. 11(g-i) we also present the zero-energy electronic LDOS and local spin density along z integrated in k_y . The first feature to notice here is that, by symmetry, the odd-parity pair amplitudes OSO and ETO vanish locally at $x = x'$, leaving only ESE and OTE pair classes as allowed superconducting correlations. Depending on the nature of magnetism in N, the ESE and OTE pair amplitudes, however, exhibit intriguing properties that reflect the nature of both the proximity effect and the inverse proximity effect. For NS junctions with N being a ferromagnet in Fig. 11(a,d), ESE and OTE pair amplitudes are induced locally in space with a leakage into N over distances determined by $\xi_F \approx 1/\sqrt{J}$, which determines the proximity effect into the ferromagnet; note that penetration length ξ_F is much shorter than ξ_N in normal metals [361, 362]. There is also a finite value of OTE pairing in S, which decays in an oscillatory fashion from the interface over $\xi_S = 100a$ for this case and is accompanied by a decaying LDOS as well as a finite local spin density along z [Fig. 11(g)]; this altogether signals the inverse proximity effect. The finite value of the ESE pair amplitude in the S region of Fig. 11(a,d) simply reflects the spin-singlet s -wave nature of the considered parent superconductor.

In the case of d -wave AMs in Fig. 11(b,e), the ESE pair amplitude induced in N develops an oscillatory profile with distinct periodicities that depend on the interplay between the chemical potential, the transverse momentum k_y , and the type of d -wave magnetic order; an apparent decay into N is also seen, which is, however, slower than in ferromagnets [Fig. 11(a,d)]. A similar oscillatory profile was reported before in NS junctions with Rashba SOC [341]. Moreover, an OTE pairing can be also induced in the $d_{x^2-y^2}$ -wave AM, which exhibits an oscillatory decaying profile from the interface towards the bulk of S for distances within ξ_S , see Fig. 11(b,e). No OTE is induced in NS junctions with d_{xy} -wave AMs because its even parity is formed by an odd dependence in space

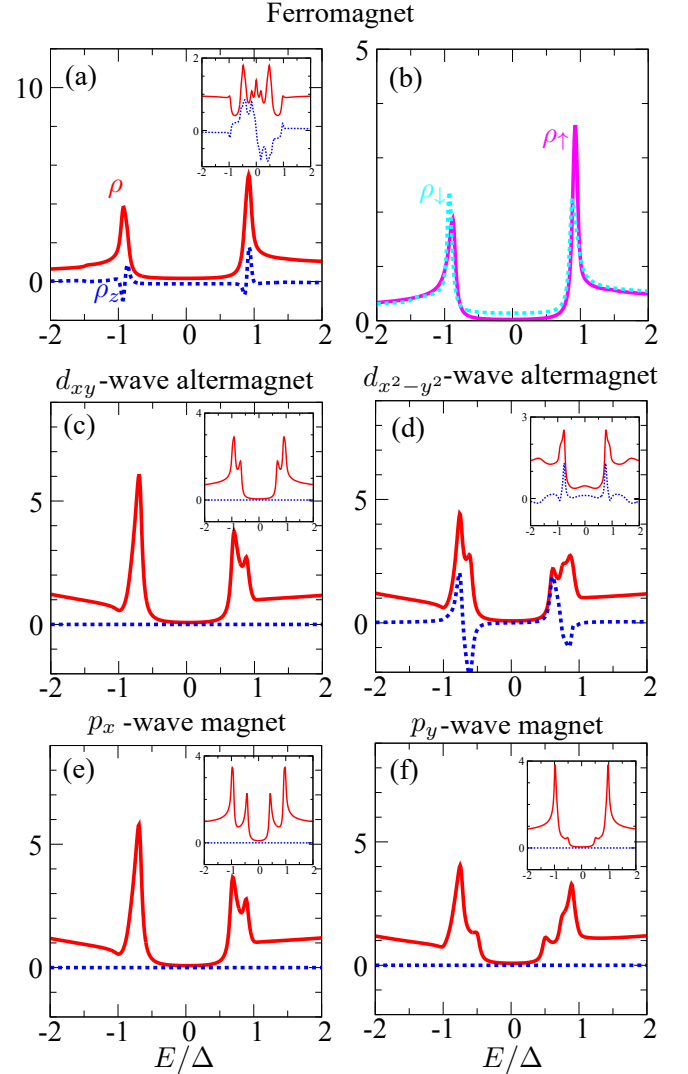


Figure 12. Energy dependence of the LDOS and spin density along z in the S region close to the interface of a NS junction, where N is a magnetic material of finite length L_N and S is a semi-infinite spin-singlet s -wave superconductor. The DOS and spin density are integrated in k_y , and normalized with respect to its value at $E = 0$ and $\Delta = 0$. (a) DOS and spin density for a ferromagnet; (b) LDOS for up and down spins in a ferromagnet. (c-f) The same as in (a) but for d -wave AMs and p -wave UMs. Insets show the LDOS and spin density at $\mu = 4t$, $m_z = t_x = t_y = t_{xy} = t_{x^2-y^2} = 0.4t$. Tight-binding parameters: $L_N = 10a$, $\mu = 0.1t$, $\Delta = 0.02t$, $m_z = t_x = t_y = t_{xy} = t_{x^2-y^2} = 0.1t$, $x = 1a$. Adapted from Ref. [358].

along x and an odd dependence in k_y , which leads to a vanishing amplitude locally in x . We note that, while a finite LDOS in both d -wave AMs is found, a finite local spin density is only present close to the interface of NS junctions with $d_{x^2-y^2}$ -wave AMs when OTE pairing is present, see Fig. 11(h). Thus, the absence of OTE in NS junctions with d_{xy} -wave AMs is accompanied by the

absence of spin density along z , see Fig. 11(h). For NS junctions with p -wave magnets, an odd-parity symmetry in k_y restricts the formation of OTE as for d_{xy} -wave AMs, while ESE is induced into N in an oscillatory decaying fashion that is distinct to what happens in d -wave magnets, see Fig. 11(c,f). In this case, the LDOS in N develops weak oscillations with the same periodicity as the ESE pair amplitude and decays from the interface into S, while vanishing local spin density is obtained in NS junctions with both types of p -wave UMs, see Fig. 11(i). In all cases discussed here, the vanishing LDOS deep in S already indicates the conventional nature of the parent superconductor, which exhibits a U-shaped LDOS and is independent of the magnetic nature of N. We can therefore see that the proximity effect in NS junctions based on UMs is governed by penetration lengths in the UMs that are entirely associated to their type of magnetic nature. Moreover, while a clear inverse proximity effect is predicted in $d_{x^2-y^2}$ -wave AMs, the preliminary findings of Ref. [358] suggests vanishing values for the local amplitudes in d_{xy} -wave AMs and PUMs.

Further insights on the inverse proximity effect can be obtained from Fig. 12, where we show the LDOS and local spin density integrated over k_y inside S but very close to the interface of a NS junction. Since it is known that the inverse proximity effect is sensitive to the appearance of ABSs [367], we consider a finite length N region made of a magnetic material, which is expected to host ABSs due to confinement in N [198, 199, 205, 212]. One of the main features is that LDOS exhibits subgap peaks representing the emergence of ABSs, whose position however depends on the magnetic order and chemical potential, see Fig. 12 and also insets. Another interesting feature is that, while the LDOS is always finite and develops a U-shape profile, the local spin density develops finite values only for the $d_{x^2-y^2}$ -wave AM and ferromagnet but vanishes otherwise. This behavior holds even for a stronger chemical potential and exchange field, supporting the absence of induced local pair amplitudes that contribute to the inverse proximity effect in NS junctions formed by d_{xy} -wave AMs and p -wave UMs, see insets. These results, however, do not rule out the formation of nonlocal superconducting correlations as contributing sources to the inverse proximity effect in such systems [368], but their relevance still remains unexplored. Having discussed the proximity effect and the inverse proximity effect in terms of emergent superconducting correlations, it is important to remark some points needed for adding more fundamental understanding of superconductivity in UMs. Thus, while a direct relationship is known to exist between the discussed proximity effects and Andreev processes, the method used to obtain Fig. 11 does not allow to identify it; to discover such a relationship, the superconducting correlations need to be calculated by using a scattering Green's function approach, which involves scattering states defined in terms of Andreev and normal processes [15, 164, 326, 359, 360]. Furthermore, the understanding of the proximity effect as well as the inverse proximity

effect would enormously benefit from the investigation of superconducting correlations in hybrid systems with UMs under realistic conditions, such as the unavoidable finite size [219, 369] as well as the intrinsic multiple degrees of freedom [308, 316, 327, 370–372].

D. Emergent superconducting phenomena in unconventional magnets

One particular aspect of combining unconventional magnetism with superconductivity is that it leads to novel phenomena even when considering conventional superconductors. One of the most fundamental consequences of such a combination was discussed in Subsection III B and involves the realization of novel superconducting pair symmetries, where unconventional magnetism not only affects the spin symmetry but also the parity in momentum, see Table II. In this regard, spin-triplet Cooper pairs can be realized in AMs and also in PUMs [145], which, under appropriate material design, can pave the way for superconducting spintronics [3–8] without net magnetization [60, 373]. Besides spin-triplet Cooper pairs, the interest in UMs has already led to interesting studies that demonstrate the utility of AMs for even more intriguing superconducting phenomena. Among the most salient examples, of fundamental and applied relevance, we highlight the utilization of d -wave altermagnetism for realizing topological superconductivity [142, 149, 191–193], superconducting diodes [132, 222], magnetoelectric effects [239, 240], and thermoelectric effects [293, 294], see also Fig. 13. These studies demonstrate the impact of unconventional magnetism for advancing the search of novel superconducting phenomena in distinct areas, an aspect that will very likely lead to useful quantum applications in the near future. In this part, we briefly review the four examples of novel superconducting effects highlighted above.

1. Topological superconductivity

Topological superconductivity is a topological phase of matter that is characterized by the formation of boundary states known as Majorana zero modes or simply as Majorana modes [10, 11, 17]. The intrinsic spatial non-locality and topological nature of Majorana states are useful for designing qubits that are robust against local sources of decoherence [18, 21, 22, 24], which highlights the enormous potential of topological superconductivity. In terms of ingredients for topological superconductivity, initial proposals showed that such a topological phase needs unconventional spin-triplet p -wave superconductivity [10, 11], which is however scarce in nature [62]. By now, it is well-understood that topological superconductivity can be engineered by using common ingredients, such as spin-orbit coupling, conventional spin-singlet s -wave superconductivity, and magnetism [12, 17]. Follow-

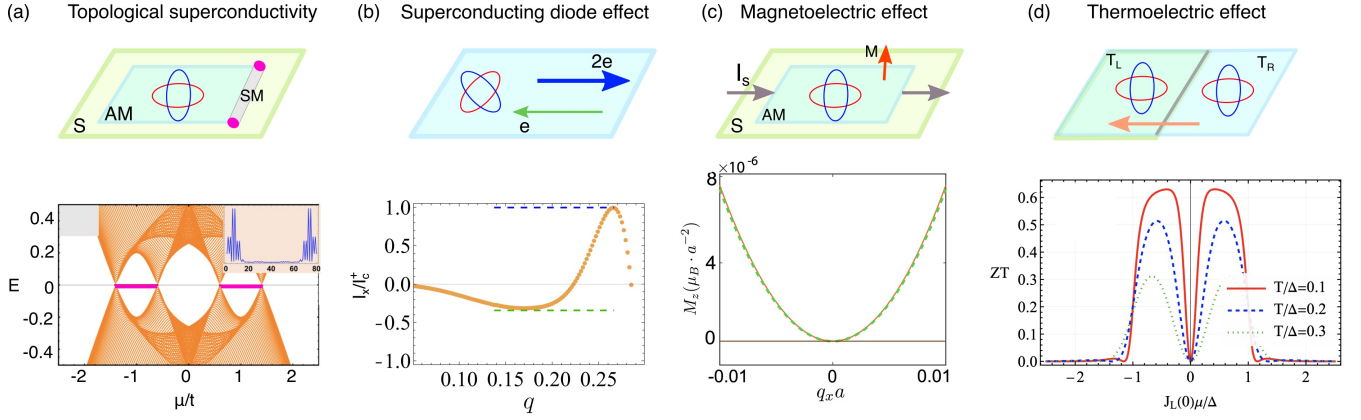


Figure 13. Emergent phenomena in superconducting systems with altermagnetism. (a) Top: 1D topological superconductivity in a hybrid system formed by a conventional superconductor S (light green), a $d_{x^2-y^2}$ -wave AM (cyan), and a semiconductor nanowire (gray); the semiconductor becomes a 1D topological superconductor with Majorana modes at its ends (magenta filled circles). Bottom: Low-energy spectrum as a function of the chemical potential, with Majorana modes depicted in magenta; inset: wavefunctions of the Majorana modes. Reprinted figure with permission from Sayed Ali Akbar Ghorashi, Taylor L. Hughes, and Jennifer Cano, Phys. Rev. Lett. 133, 106601 (2024) [192]; Copyright (2025) by the American Physical Society. (b) Top: Superconducting diode effect in a d_{xy} -wave AM with intrinsic conventional superconductivity, which originates due to a nonreciprocity in the supercurrents (blue and green arrows). Bottom: Supercurrent along x normalized by the positive maximum supercurrent I_c^+ as a function of the momentum q for the Fulde–Ferrell state. The blue and green dashed lines mark I_c^+ and I_c^- , respectively. Reproduced under the terms of the CC-BY 4.0 license and adapted with permission from the authors of Ref. [132]. (c) Top: Magnetoelectric effect in a hybrid system formed by a $d_{x^2-y^2}$ -wave AM and a conventional superconductor. By applying a supercurrent I_s induces an out of plane magnetization M (red arrow) that characterizes the magnetoelectric effect. Bottom: Magnetization along z as a function of the momentum q_x at a finite exchange field; the magnetization is represented by the red curve, while the green dashed curve shows the second-order spin susceptibility multiplied by q_x^2 . Reprinted figures with permission from Jin-Xin Hu, Oles Matsyshyn, Justin C. W. Song, Phys. Rev. Lett. 134, 026001 (2025) [240]; Copyright (2025) by the American Physical Society. (d) Top: The thermoelectric effect in a hybrid system formed by two $d_{x^2-y^2}$ -wave AMs (cyan) at different temperatures $T_{L,R}$ with the left AM coupled to a conventional superconductor (green). A finite temperature difference induces an electric voltage which then allows the flow of an electric current (orange), signalling the thermoelectric effect. Bottom: Figure of merit, which characterizes the power conversion efficiency, as a function of the exchange field in the left AM for distinct temperature differences T . Reprinted figures with permission from Pavlo O. Sukhachov, Erik Wegner Hodt, and Jacob Linder, Phys. Rev. B 110, 094508 (2024) [294]; Copyright (2025) by the American Physical Society.

ing these ideas, several experiments have reported measurements with signatures that seem consistent with Majorana physics [13, 14, 248], although several studies have also challenged the interpretation of such results as they might come from trivial states and hence not related to Majorana modes [201, 204, 205]. Another concern in all these works is that the magnetism needed to reach the topological superconducting phase, coming from either a ferromagnet or external magnetic fields, is detrimental for conventional superconductivity e. g., due to Zeeman depairing effects. All these challenges suggest the need to explore other detection protocols and, most importantly, alternative materials with less detrimental effects for superconductivity.

With the advent of AMs, a new door opened in the field of topological superconductivity because such unconventional magnets exhibit a spin-splitting of energy bands like ferromagnets while maintaining zero net magnetization, thus being more friendly towards superconductivity. In this regard, topological superconductivity was initially addressed as an intrinsic phenomenon [142] by taking into account $d_{x^2-y^2}$ -wave altermagnetism and

Rashba SOC with an extended attractive Hubbard interaction for spin-singlet and spin-triplet pairing channels. Ref. [142] found that altermagnetism is favorable for spin-triplet p -wave superconductivity, which then can realize topological superconductivity with distinct types of Majorana modes, including chiral and helical propagating Majorana modes as well as localized Majorana corner modes. Interestingly, the combination of time-reversal symmetry and the four-fold rotation along the z -axis, inherent to AMs, enforces the emergence of Majorana corner modes, thus unveiling the potential of altermagnetism for topological superconductivity and Majorana physics. Beyond intrinsic topological superconductivity, unconventional magnetism has shown to be promising for realizing Majorana physics in hybrid systems formed by UMs and superconductors. For instance, Majorana corner modes were predicted in Ref. [193] by simply coupling a conventional superconductor, a 2D topological insulator and a AMs, where the Majorana states can be controlled by the direction of the Néel vector; see also Ref. [191] for a similar study by combining DIII topological superconductors and d -wave AMs. The combi-

nation of AMs with conventional superconductors was more detailed addressed in Ref. [192], which predicted the realization of topological superconductivity without net magnetization in 1D and 2D with Majorana edge modes and Majorana chiral (and corner) modes, respectively. Of particular relevance is the realization of 1D topological superconductivity by coupling a 1D semiconductor to a $d_{x^2-y^2}$ -wave AM with conventional spin-singlet s -wave superconductivity Ref. [192], see the top panel of Fig. 13(a). The 1D hybrid model belongs to the BDI symmetry class, which has an integer topological invariant \mathbb{Z} and realizes a topological phase when the exchange field when $\sqrt{\Delta^2 + (t - \mu)^2} < J < \sqrt{\Delta^2 + (t + \mu)^2}$, where J is the exchange field, μ the chemical potential in a tight-binding model, and t the hopping strength, see Ref. [192]. The emergence of Majorana modes is shown in the bottom panel of Fig. 13(a), where the energy spectrum of a finite size 1D hybrid system is presented and the Majorana modes appear at zero energy and localized at the system ends. Ref. [194] also showed that p -wave magnetism can be utilized for realizing topological superconductivity, which, together with Ref. [192], clearly demonstrate the tremendous potential of UMs for realizing Majorana modes. More recently, p -wave UMs have been shown to be a crucial ingredient for the emergence of Majorana flat bands when combining them in a hybrid system together with a conventional superconductor [195]. The authors showed that a zero-bias conductance peak signals the anomalous proximity effect [313, 315, 374–377] and can be an indicator of Majorana flat band physics [195], paving the route for another front to explore topological superconductivity. It is worth noting that the field requires further investigations to uncover the overall potential of unconventional magnetism for designing Majorana modes without net magnetization, which could involve addressing higher angular momentum UMs.

2. Superconducting diode effect

The superconducting diode effect (SDE) has recently attracted great fundamental and application-oriented interests, largely due to its experimental demonstration in several materials [227, 378–381]; see also Ref. [237]. Broadly speaking, the diode effect is based on the conduction of current primarily along one direction and shown to be key building blocks for several electronic components [382–387]. The SDE, on the other hand, is based on the supercurrents of superconductors which become different in opposite directions, see top panel of Fig. 13(b). Thus, superconducting diodes exhibit functionalities that are superior than those of diodes in the normal state which suffer from energy losses due to unavoidable finite resistance [388, 389]. The SDE can therefore enable energy-saving applications using superconducting circuits in the future [237]. It is by now known that both the time-reversal and the inversion symmetry breaking are necessary conditions for the realization of the SDE

although not sufficient [230, 231, 237, 385, 390, 391], an idea that has already led to the prediction of the SDE in bulk superconductors [227, 230, 231, 378, 392–395]. Together with breaking time-reversal and inversion symmetries, Ref. [396] showed that breaking x -inverting symmetries are also needed to realize the superconducting diode effect. The symmetry constraints for the SDE have shown to also result in the emergence of finite momentum Cooper pairs, like those in Fulde-Ferrell-Larkin-Ovchinnikov states, as well as different depairing effects between supercurrents with opposite directions [229, 230]. To quantify the efficiency of the SDE, and hence measure the nonreciprocity of the system, it is often used the quality factor defined as,

$$\eta = \frac{I_c^+ - |I_c^-|}{I_c^+ + |I_c^-|}, \quad (37)$$

where I_c^+ and I_c^- are the maximum and minimum supercurrents (or critical currents) in opposite directions. A nonzero value of the quality factor, $\eta \neq 0$, indicates the emergence of the SDE; a perfect diode efficiency is reached when $\eta = 1$, which would imply having a supercurrent only along one direction.

Most of the recent activity on the SDE with relatively high quality factors has involved systems with Rashba SOC, conventional superconductivity, and applied magnetic fields [230, 231, 237, 392]. While these are indeed relevant, the applied magnetic fields are often detrimental to superconductivity. Motivated by this fact, the SDE has very recently been explored in AMs [132, 220, 222], which, as discussed in Section III, break time-reversal symmetry without an external magnetic field and exhibit zero net magnetization [60], conditions that are friendly with superconductivity. AMs can thus be useful for realizing field-free superconducting diodes. The first study addressing the intrinsic SDE in AMs is Ref. [132], where the authors consider a d_{xy} -wave AM and superconductivity due to attractive interactions as in the BCS theory. Within the framework of Ginzburg-Landau theory, Ref. [132] finds the stabilization of pair density wave states, such as the Fulde-Ferrell and Fulde-Ferrell* states, which intrinsically break inversion symmetry and carry a finite momentum. In Ref. [132], a Fulde-Ferrell state is characterized by a single phase, while the Fulde-Ferrell* state by two phases. Notably, when exploring the supercurrents, the authors of Ref. [132] found a nonreciprocal behavior that not only distinguishes between Fulde-Ferrell and Fulde-Ferrell* states but also signals the emergence of the SDE in the absence of any external magnetic field. The bottom panel of Fig. 13(b) shows the supercurrent for the Fulde-Ferrell states as a function of momentum, revealing that I_c^+ and I_c^- are distinct and enable a field-free SDE with efficiency of $\eta = 0.5$ [132]. A similar idea was a bit later addressed in Ref. [222] but with a $d_{x^2-y^2}$ -wave AM and spin-singlet pairing on nearest-neighbor bonds, which, treated within a self-consistent approach, allowed the authors to find a SDE having perfect efficiencies of $\eta = 1$ under an external magnetic field.

The results of the perfect SDE are ascribed to the native finite-momentum superconductivity in AMs [222], which the authors also show to be connected to a topological phase transition in AM under external magnetism [283]. We also note that hybrid systems formed by AMs and superconductors have also been explored [220], where an electric field seems to be needed for the SDE, which is predicted to also control the diode's efficiency. We can therefore conclude that the unique spin properties of AMs are promising for realizing superconducting diodes with a broad range of efficiencies and zero and finite magnetic fields. Even though the search for superconducting diodes in UMs is still in its infancy, it is very likely that other types of UMs will enrich the device functionality without relying on complicated mechanisms.

3. Magnetoelectric effect

The intrinsic altermagnetic properties have also been shown to be the key for inducing a magnetoelectric effect [239, 240], a key mechanism for superconducting spintronics [3–8]. In fact, the magnetoelectric effect in superconductors occurs when an applied supercurrent generates a finite spin polarization [397–399], thus offering a powerful way to induce a net magnetization and a good control of spins without dissipation; see also [400–405] for recent works on the magnetoelectric effect in superconductors. One of the key ingredients for the magnetoelectric effect is the breaking of inversion symmetry, e.g., due to SOC [397–399], where spins couple to the motion of Cooper pairs and lead to a net spin polarization tied to the applied supercurrent. These conditions are often satisfied in time-reversal invariant noncentrosymmetric superconductors [406], where an applied supercurrent \mathbf{I}_s generates a magnetization \mathbf{M} with a linear relationship between them, $\mathbf{M} \propto \mathbf{c} \times \mathbf{I}_s$, where \mathbf{c} indicates the polar axis of the superconductor with Rashba SOC.

With the discovery of AMs, the exploration of the superconducting magnetoelectric effect has experienced another impetus since the altermagnetism offers unique spin-dependent properties without relying on SOC and at zero net magnetization. This allowed the study of the superconducting magnetoelectric effect in systems formed by centrosymmetric superconductors and AMs [239, 240]; these studies predict a nonlinear superconducting magnetoelectric effect where an out of plane magnetization induced due to an applied supercurrent in an AM-superconductor hybrid system, see top panel of Fig. 13(c). To be more precise, Ref. [240] found that the emergent net magnetization is a second-order nonlinear effect given by $\delta M_c^{(2)} = \chi_{ab}^c q_a q_b$, where $a, b = x, y$ is the supercurrent direction, $c = x, y, z$ the magnetization direction, and $q_{a,b}$ the Cooper pair momentum due to the applied supercurrent $\mathbf{I}_s \propto \mathbf{q}$. Moreover, the coefficient χ_{ab}^c is the second-order spin susceptibility and is nonzero only when time-reversal symmetry is broken due to altermagnetism [240]. To visualize the nonlinear behav-

ior of the magnetization, the bottom panel of Fig. 13(c) shows the results of Ref. [240] for an applied supercurrent along x as a function of momentum. The authors of Ref. [240] also argue that such a second-order nonlinear superconducting magnetoelectric effect can be the dominant contribution in the out-of-plane magnetization due to the large spin splitting of AMs. Thus, unlike non-centrosymmetric superconductors with SOC, AMs allow for a nonlinear magnetoelectric effect in centrosymmetric superconductors that can be useful for a nondissipative control of magnetization. We expect that the predictions of Refs. [239, 240] will motivate further studies to fully exploit the distinct parities of UMs towards an efficient approach for superconducting spintronics.

4. Thermoelectric effect

Another line of research that has recently benefited from the interplay between altermagnetism and superconductivity is thermoelectricity, explored by combining a hybrid system formed by d -wave AMs and a conventional superconductor in Ref. [294], see top panel of Fig. 13(d). Under generic circumstances, thermoelectricity is based on the direct conversion of temperature gradients into electrical quantities, a phenomenon known as the thermoelectric effect [407–410]; see also Refs. [323, 331, 411–420]. One of the key requirements for inducing a thermoelectric effect is the breakdown of particle-hole symmetry, which, although intrinsic in superconductors, can be broken by magnetic fields. A large body of works considered hybrids systems between superconductors and ferromagnets, which managed to produce high efficiencies with figures of merit reaching even $ZT \approx 40$ in hybrid systems based on two spin-split superconductors [421], see also Ref. [422]. These findings put ferromagnet-superconductor hybrid systems as promising for energy harvesting and cooling of electronics at cryogenic temperatures. Despite the notable properties, ferromagnets introduce undesirable stray magnetic fields that are detrimental when combining multiple structures [423–429], thus limiting the scalability of thermoelectric devices based on superconductors. The drawbacks of ferromagnets clearly point towards the need of finding other materials without stray fields for the thermoelectric effect in superconductors.

Ref. [294] showed that the above issue can be resolved in superconducting junctions with $d_{x^2-y^2}$ -wave AMs, as schematically shown in Fig. 13(d). Unlike ferromagnets, AMs exhibit a momentum dependent spin splitting of energy bands without any net magnetization, which was shown to be useful for stray-field-free devices with high storage densities. The momentum dependent spin splitting of AMs enables the breaking of particle-hole symmetry for each spin, while coupling to another AM renders the interface spin active, mechanisms that permit to realize a thermoelectric response without any magnetic field. One of the main findings of Ref. [294] is that the

AM-superconductor hybrid junction can reach a figure of merit with reasonable efficiencies, as seen in the bottom panel of Fig. 13(d). The authors further showed that the behavior of the figure of merit, as well as the Seebeck coefficient, is similar to that a ferromagnet-superconductor system when temperature is varied [294]. This study thus opens new possibilities for exploring thermoelectricity in superconductors with unconventional magnetism, which could even further offer new ways for caloritronics in superconductors [421, 430–432].

IV. JOSEPHSON JUNCTIONS WITH UNCONVENTIONAL MAGNETS

In the previous section, we have delved into the understanding of the interplay between superconductivity with unconventional magnetism and also discussed the emergent phenomena when UMs are placed in contact with a superconductor. In this part, we focus on superconducting junctions formed by two superconductors linked by an UM, also known as Josephson junctions (JJs). In these junctions, Andreev reflections at both superconducting interfaces lead to the formation of Andreev bound states (ABSs) when there is a finite phase difference between the pair potentials of the superconductors [168, 342]. The phase-dependent ABSs due to Andreev processes are responsible for the transfer of Cooper pairs between superconductors without any applied voltage [163, 166, 172, 174–177, 433–439], which signals the flow of a dissipationless supercurrent also known as the Josephson effect [440]. Due to the superconducting nature, the ABSs and Josephson effect have been shown to be extremely useful for identifying the type of emergent superconductivity [164, 165, 168, 170, 178, 179, 441] and also relevant for designing superconducting devices [19–21, 442–447]. In this section, we address the emergence of ABSs in JJs formed by superconductors and UMs and how the distinct types of magnetic order produce measurable signatures in the phase-biased Josephson effect.

A. Modelling Josephson junctions

To capture the fundamental aspects of phase-biased JJs, such as ABSs and the Josephson effect, there are two complementary approaches that are useful for pedagogical purposes. For this, it is important to specify that the JJs we consider here are formed along x by two conventional spin-singlet s -wave superconductors coupled via an UM, with a pair potential profile given by

$$\hat{\Delta}(x) = \begin{cases} \Delta e^{i\varphi_L}, & x \in S_L \\ 0, & x \in \text{UM}, \\ \Delta e^{i\varphi_R}, & x \in S_R, \end{cases} \quad (38)$$

where Δ is the pair potential amplitude assumed to be the finite and the same in both left (L) and right (R)

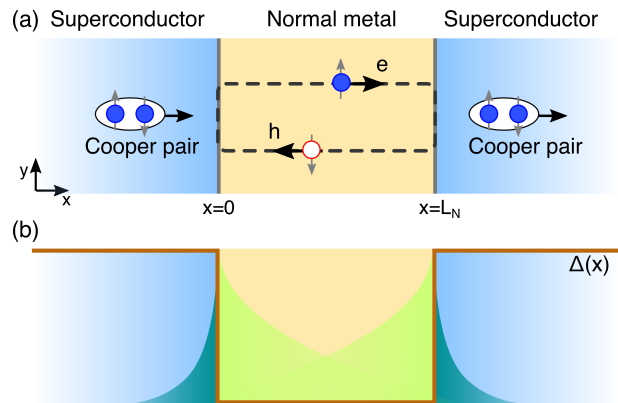


Figure 14. Sketch of a Josephson junction along x formed by two superconductors connected by a normal metal, with interfaces located at $x = 0$ and $x = L_N$. (a) Due to Andreev reflections at both interfaces picking up the superconducting phases, Andreev bound states emerge within the superconducting gap in the normal region, a process that also involves the transfer of Cooper pairs between superconductors. (b) Due to the proximity effect, the normal region acquires superconducting correlations (light green), while the superconducting correlations in the superconductors acquire properties of the normal region (blue-green). Here, the amplitude of the pair potential $\Delta(x)$ in the junction is indicated in brown color.

superconductors, while no superconductivity is taken in the UM. Moreover, $\varphi_{L,R}$ is the phase in the pair potentials of the left/right superconductor, whose phase difference $\varphi = \varphi_R - \varphi_L$ plays an important role in JJs as we will see and consider in the following subsections of this part. For now, we can specify the length of the UM to be L_N , a quantity that is often used to distinguish between short ($L_N \ll \xi_S$) and long ($L_N \gg \xi_S$) JJs, with ξ_S being the superconducting coherence length [166], see also Refs. [448, 449]. We can also model the interfaces by delta-like potentials $U(x) = V_L\delta(x) + V_R\delta(x - L_N)$. Note that, while the pair potential needs to be in principle obtained self-consistently [297, 450, 451], assuming the profile given by Eq. (38) is reasonable and proven to help understand the formation of ABSs and the Josephson effect [165, 168, 298]. In a very similar way one can model the pair potential of unconventional superconductors [17, 298]. In relation to the description of the superconductors and UMs, we can model them by using either continuum models or their tight-binding representations, as we explain next.

1. Continuum model

In this situation, the superconductors and the UMs are described by the continuum models given by Eqs. (3) and (4). Then, the properties of JJs can be explored via the scattering approach in the same way as we discussed in Subsection III D. For simplicity, we assume that the interfaces of the JJ along x are located at $x = 0$ and

$x = L_N$, with L_N being the length of the UM, while momentum k_y is still a good quantum number along the transverse direction. Taking a BdG Hamiltonian for each section of the JJ, with the pair potential given by Eq. (38), one constructs scattering states incident on the interfaces, which are then appropriately matched at such interfaces and scattering coefficients are found. These scattering coefficients can then be used to calculate the ABSs, Green's functions, and supercurrents; for more details see e. g., Refs. [15, 17, 164, 166, 174–177, 326, 360]. See also Refs. [452]. Within the scattering formalism, the supercurrent can be obtained as [175, 177]

$$I(\varphi) = \int_{-k_F}^{k_F} \bar{I}(\varphi, k_y) dk_y, \quad (39)$$

$$\bar{I}(\varphi, k_y) = \frac{e\Delta}{2\hbar\beta} \sum_{\omega_n, \sigma} \left[\frac{q_e^n + q_h^n}{\Omega_n} \right] \left[\frac{a_{e\sigma}(\varphi)}{q_e^n} - \frac{a_{h\sigma}(\varphi)}{q_h^n} \right]$$

where $\beta = 1/(\kappa_B T)$, with κ_B being the Boltzmann constant and T the temperature, $\Omega_n = \sqrt{\omega_n^2 + \Delta^2}$, $\omega_n = \pi\kappa_B T$, $q_{e(h)}^n = k_F \sqrt{1 \pm i(\Omega_n/\mu) - (k_y/k_F)^2}$, while $a_{e\sigma}$ and $a_{h\sigma}$ represent four types of Andreev reflection coefficients from by injections of electron-like and hole-like quasiparticles with $\sigma = \uparrow, \downarrow$ from the left superconductor. As explained above and in Subsection III D, the Andreev reflection coefficients are obtained by matching the scattering states at the interfaces, see Ref. [184] for the Andreev coefficients in JJs based on AMs. Eq. (39) is known as the Furusaki-Tsukada formula [175, 177] and nicely reflects the direct relationship between the amplitude of Andreev processes with the Josephson current $I(\varphi)$. To evaluate $I(\varphi)$ in Eq. (39), we can then parametrize the transverse component of the wave vector $k_y = k_F \sin(\theta)$ by the angle of incidence $\theta \in [-\pi/2, \pi/2]$ on the left-most region, such that the integration is carried out over the angle θ . We would also like to point out that the scattering coefficients form the so-called S-matrix, and that is why their poles define the formation of ABSs [166, 177, 453]. Thus, by finding the Andreev coefficient $a_{e\sigma}$, we can also calculate the ABSs within this scattering approach. We lastly note that it is even possible to take into account the finite size of the superconductors under appropriate construction of the required scattering states accompanied by their boundary conditions, see Refs. [17, 320, 330, 343].

2. Tight-binding model

When multiple degrees of freedom are present, the continuum approach to treat JJs becomes challenging. An alternative way is to treat the system in real space within a tight-binding approach, where the JJ Hamiltonian is discretized along x and written as

$$H_{JJ}(k_y) = H_{UM} + H_{S_L} + H_{S_R} + H_T, \quad (40)$$

where each element on the right-hand side is a matrix in real space and their dependence on the transverse momentum k_y is omitted for simplicity. In Eq. (40), H_{UM} describes the UM, while $H_{L(R)}$ describes the left (right) superconductor and H_T the coupling between UM and superconductors. We consider that the superconductors are of length $L_S = Ma$, with M the number of sites in each superconductor, while $L_N = Na$ the length of the UM with N being the number of lattice sites; a is the lattice spacing, taken to be the same in each region. The elements of $H_{JJ}(k_y)$ are given by

$$H_{UM}(k_y) = \sum_j c_j^\dagger \hat{u}_N(k_y) c_j + c_{j+1}^\dagger \hat{t}_N(k_y) c_j + \text{h.c.},$$

$$H_{S_\alpha}(k_y) = \sum_j c_{\alpha j}^\dagger \hat{u}_S(k_y) c_{\alpha j} + c_{\alpha j+1}^\dagger \hat{t}_S(k_y) c_{\alpha j} + \text{h.c.},$$

$$+ \sum_j \Delta e^{i\varphi_\alpha} [c_{\alpha j\uparrow} c_{\alpha j\downarrow} - c_{\alpha j\downarrow} c_{\alpha j\uparrow}] + \text{h.c.},$$

$$H_T(k_y) = \hat{V}_L c_L^\dagger c_{L_M} + \hat{V}_R c_R^\dagger c_{R_1} + \text{h.c.} \quad (41)$$

where $c_j = (c_{j\uparrow}, c_{j\downarrow})^T$, $c_{\alpha j} = (c_{\alpha j\uparrow}, c_{\alpha j\downarrow})^T$, while $c_{j\uparrow}$ annihilates an electronic states at site j and spin σ in the UM; similarly, $c_{\alpha j\uparrow}$ annihilates an electronic states at site j and spin σ in the superconductor $\alpha = L/R$, and Δ is the amplitude of the spin-singlet s -wave pair potential.

$$\hat{u}_N = [-\mu + 4t_1 - 2t_1 \cos k_y] \sigma_0$$

$$+ [-t_{x^2-y^2} \cos k_y + t_y \sin k_y] \sigma_z,$$

$$\hat{t}_N = -t_1 \sigma_0 + \left[-it_{xy} \sin k_y + \frac{t_{x^2-y^2}}{2} - i\frac{t_x}{2} \right] \sigma_z, \quad (42)$$

$$\hat{u}_S = [-\mu + 4t_1 - 2t_1 \cos k_y] \sigma_0,$$

$$\hat{t}_S = -t_1 \sigma_0,$$

$$\hat{V}_{L,R} = -t_{\text{int}} t_1 \sigma_0,$$

where μ and t_1 are the chemical potential and the hopping integral, $\sigma_{0,x,y,z}$ is the Pauli matrices in spin space and $t_{\text{int}} \in [0, 1]$ is the parameter that controls the tunneling amplitude at the interface. Having the tight-binding Hamiltonian given by Eq. (40), we can calculate the spectrum E_n by diagonalizing $H_{JJ}(k_y)$. Moreover, this information can be used to find the free energy F , which then allows us to calculate the zero temperature Josephson current as

$$I(\varphi) = \frac{e}{\hbar} \int dk_y \frac{dF(\varphi, k_y)}{d\varphi} \quad (43)$$

where $F(\varphi, k_y) = \sum_{n < 0} E_n(\varphi, k_y)$.

While Eq. (43) is useful for finite length systems, it gets computationally expensive when the systems are large. In that case, we can opt e. g., for incorporating the superconductors via self-energies within a recursive Green's function approach, see Refs. [146, 454]. Within this approach, the Green's function in the middle two sites of the UM can be obtained, which then allows us to calculate

the LDOS and Josephson current as [455–457]

$$\begin{aligned}\rho(\varphi) &= -\frac{1}{\pi} \int \text{ImTr}' \hat{G}_{00}(\varphi, k_y, E) dk_y, \\ I(\varphi) &= \frac{iet_1}{\hbar\beta} \int \text{Tr}' \sum_{\omega_n} [\hat{G}_{01}(\varphi, k_y, i\omega_n) \\ &\quad - \hat{G}_{10}(\varphi, k_y, i\omega_n)] dk_y,\end{aligned}\quad (44)$$

where $\beta = 1/(\kappa_B T)$, \hat{G}_{ij} are the Green's function in Nambu space in the two middle sites ($i, j = 0, 1$) of the UM, Tr' means that the trace is taken only over the electron subspace, and the integration is carried out within $[-\pi, \pi]$. Moreover, in the first equation we have carried out the analytic continuation to real energies $i\omega_n \rightarrow E + i\delta$, t_1 is hopping in the UM. We also point out that having the Green's function in the middle sites of the UM is also useful for exploring the ABSs, which are obtained from the poles of the Green's function by solving $\det[\hat{G}_{00}^{-1}(k_y, \omega)] = 0$ for ω , see also [297]. In what follows, we discuss the formation of ABSs, the phase-dependent supercurrents, and the emergent phenomena due to the interplay between unconventional magnetism and the Josephson effect that was reported so far.

B. Formation of Andreev bound states and their spectral signatures

To understand the impact of unconventional magnetism on the ABSs, we first remind their formation in JJs formed by semi-infinite conventional spin-singlet s -wave superconductors and a normal metal [433], see Fig. 14(a). For a short normal metal, there is a pair of spin-degenerate ABSs that emerge within the pair potential Δ and given by $E_{\pm}(\varphi) = \pm\Delta\sqrt{1 - \sigma_N \sin^2(\varphi/2)}$, see Ref. [433]; here, φ is the superconducting phase difference and σ_N the normal transparency. The first feature to stress that the ABSs are 2π -periodic, with $E_{\pm}(\varphi = 0) = \pm\Delta$ and $E_{\pm}(\varphi = \pi) = \pm\Delta\sqrt{1 - \sigma_N}$. Moreover, in the full transparent regime $\sigma_N = 1$, the ABSs are $E_{\pm} = \pm\Delta\cos(\varphi)$, implying that the subgap spectrum is gapless at $\varphi = \pi$ since the ABSs reach zero energy. In the tunneling regime $\sigma_N = 0$, the ABSs are independent of the phase and are located near the gap edges $E_{\pm} = \pm\Delta$. For a nonzero normal transmission below full transparencies, the subgap spectrum is always gapped; for instance, at $\varphi = \pi$, the ABSs are given by $E_{\pm}(\varphi = \pi) = \pm\Delta\sqrt{1 - \sigma_N}$, hence the subgap spectrum exhibits an energy gap. When the normal metal becomes longer, more energy levels appear at subgap energies and the cosine-like dispersion with the phase changes to a linear dispersion in the long junction regime [180, 297, 433].

The features discussed in the previous paragraph are well-known and will help understand how the behaviour of the ABSs is affected when considering UMs instead of a normal metal connecting semi-infinite spin-singlet s -wave superconductors in a JJ, a question addressed in

Ref. [146]. The ABSs of a short JJ as a function of the superconducting phase difference are shown in Fig. 15(a-d) at fixed transverse momentum k_y , obtained from the poles of \hat{G}_{00} in Eq. (44). The first property to highlight is that, under general conditions, the JJ hosts four ABSs that are spin split and strongly dependent on the transverse momentum k_y but with a distinct phase dependence depending on the type of UM. For a JJ with a d_{xy} -wave AM, the ABSs are spin split only when $k_y \neq 0$, with avoided crossings (gap) around zero energy between positive and negative ABSs of the same spin, very likely due to a normal transmission effect across the UM, see Fig. 15(a). The authors of Ref. [146] also showed that the ABSs profile changes when k_y takes other values, where the energy gaps due to the avoided crossings reduce and even reach zero energy at distinct φ , including $\varphi = 0$; this signals a phase shift of the ABSs due to d_{xy} -wave altermagnetism. For JJs with a $d_{x^2-y^2}$ -wave AM, the ABSs also exhibit a spin splitting as in the d_{xy} -wave AM but their phase-dependence is slightly different, see Fig. 15(b). For instance, even $k_y = 0$, the ABSs are split in spin since there already is a finite strength of the $d_{x^2-y^2}$ -wave field at this transverse momentum, see Eqs. (8) and Ref. [146]. In this case, ABSs with distinct spins develop zero-energy crossings at distinct values of φ , an effect that depends on k_y and also occurs at $\varphi = 0$, unveiling also a phase shift due to $d_{x^2-y^2}$ -wave altermagnetism in JJs. These features of the ABSs were also reported in Ref. [182]. Thus, ABSs in JJs with d -wave AMs exhibit a distinct phase dependence with respect to JJs with superconductors linked by a normal metal.

When it comes to JJs with PUM, the ABSs behave slightly similar to the ABSs in JJs with a normal metal but also exhibit some differences, see Fig. 15(c,d). In both types of PUMs the ABSs develop a cosine-like profile with a finite energy gap at $n\pi$, with $n \in \mathbb{Z}$, but the spin splitting is distinct; only the ABSs in JJs with a p_y -wave UM seem to form a visible spin splitting since k_y here enters as a magnetic field, see Fig. 15(c,d). Ref. [146] shows that other values than the chosen in Fig. 15(d) give a larger spin splitting. With this, we can say that the ABSs in JJs formed by conventional superconductors and PUMs are different from what we discussed for JJs with AMs. At the same time, the ABSs in JJs with AMs and PUMs exhibit features that are distinct from JJs with normal metals, hence uncovering the impact of unconventional magnetism on the formation of ABSs.

In terms of detection schemes of ABSs, one way is to explore their spectral signatures e. g., in the LDOS of the UM, which can be accessed via conductance by tunnel coupling a normal probe to the neighbourhood of the junction [345]. Following this idea, Ref. [146] obtained the LDOS by using the first expression of Eqs. (44), which we present in Fig. 15(e-h) for the LDOS at fixed k_y and in Fig. 15(i-l) for the LDOS integrated in k_y . In general, the high intensity regions at fixed transverse momentum in the LDOS of Fig. 15(e-h) clearly correspond to the formation of ABSs in Fig. 15(a-d) for d - and p -

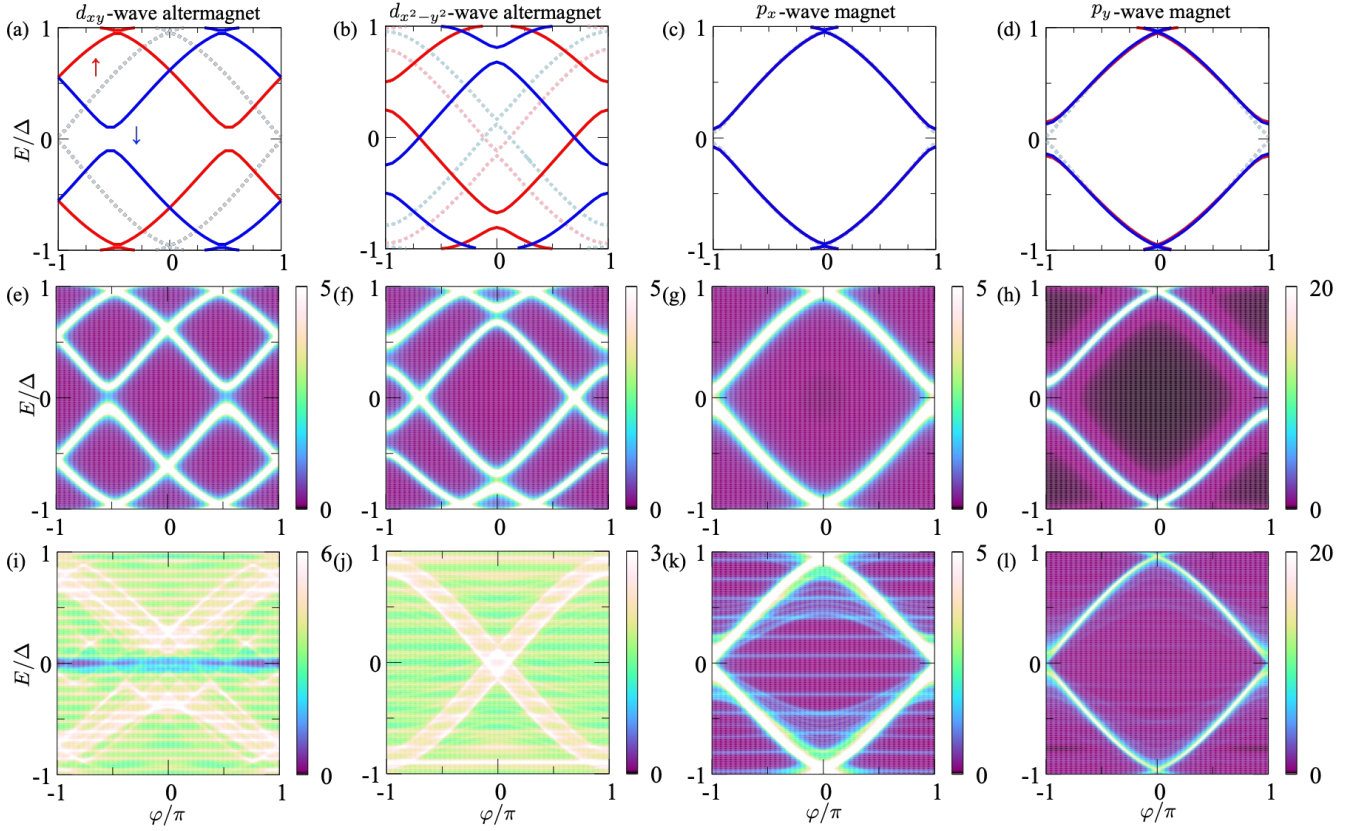


Figure 15. ABSs and their spectral signatures via LDOS in Josephson junctions based on UMs obtained from a tight-binding model. (a-d) ABSs as a function of the superconducting phase difference φ , obtained from the poles of the Green's function in the middle of the UM at $k_y = 0.2\pi$. Light red and light blue curves represent the ABSs at $k_y = 0$. (e-h) Electronic LDOS obtained from the Green's function used in (a-d) as a function of energy and phase difference at $k_y = 0.2\pi$ in the middle of the UM ($x = 14a$). (i-l) Electronic LDOS for (e-h) integrated over the transverse momentum k_y in the middle of the UM at $x = 14a$ as a function of energy and phase difference. Tight-binding parameters: $a = 1$, $L_N = 30a$, $t_{x(y)} = 0.4t$, $t_{xy} = 0.42t$, $t_{x^2-y^2} = 0.4t$, $\Delta = 0.02t$, $t_{\text{int}} = 0.95$, $\mu = 1.5t$, $\delta = 0.01\Delta$. Here, τ controls the transparency across the UM. Adapted from Ref. [146].

wave UMs, where the visibility of the gaps around zero energy depends on the broadening which is inevitable under realistic conditions. At fixed k_y , the ABSs reaching zero energy are very likely to produce zero-energy LDOS peaks, see e. .g., Fig. 15(f,g). The signatures of the ABSs become more intriguing when looking at the integrated LDOS over k_y , where, due to the strong dependence of the ABSs on k_y , the LDOS features are not simple to analyze, see Fig. 15(i-l). Nevertheless, it is still possible to identify a rather soft gap around zero energy in JJs with a d_{xy} -wave AM [Fig. 15(i)], which Ref. [146] showed it to have a V-shape. In contrast, JJs with $d_{x^2-y^2}$ -wave AMs exhibit subgap structure that develops large values near to $\varphi = 0$, see Fig. 15(j). In the case of JJs with p -wave UMs in Fig. 15(k,l), the ABSs are less challenging to identify, albeit the gap around zero energy does not survive the transverse momentum integration. It is also worth noting that the horizontal branches in Fig. 15(k) correspond to dispersionless traces of ABSs appearing at distinct k_y but do not affect the overall visibility of

the phase-dependent branches. The discussed spectral features in AMs and PUMs correspond to a fixed exchange field; when such a field increases, Ref. [146] found that the subgap spectrum oscillates for JJs with AMs, with the periodicity determined by the exchange field of the respective AM. In JJs with p -wave UMs, increasing the exchange field remains roughly constant the LDOS, with rather small variations in the case of p_y -wave UM at large exchange fields. We thus close this part by stressing that the formation of ABSs in JJs with UMs strongly depends on the type of unconventional magnetism and on the transverse direction, signatures that can be with caution identified via LDOS. It remains an open problem the behavior of ABSs in JJs with UMs having higher angular momentum dependence which will definitely shed more light on the importance of the interplay between superconductivity and unconventional magnetism.

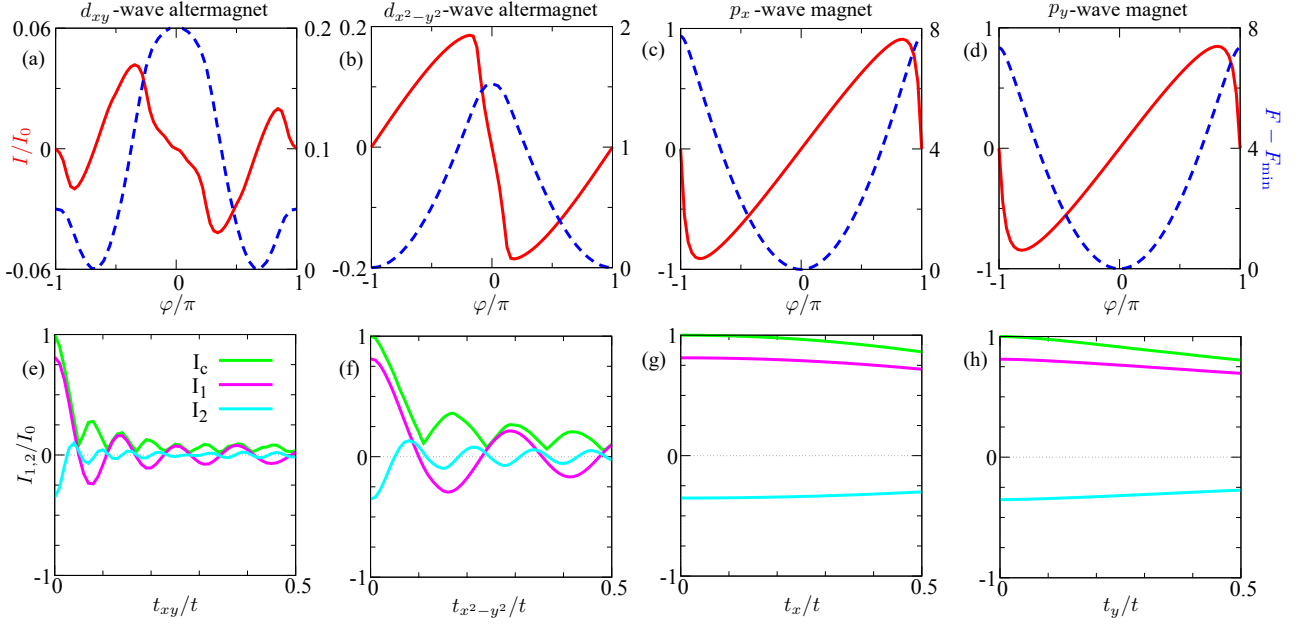


Figure 16. Josephson effect in JJs formed by conventional spin-singlet s -wave superconductors and UMs. (a-d) Current-phase curves indicated by red curves for JJs with d_{xy} - and $d_{x^2-y^2}$ -wave AMs as well as for JJs with a p_x -wave UM, with a p_y -wave UM. The blue curves depict the respective free energy. The strength of the exchange field in (a-d) is the same as in Fig. 15(a-d), and I_0 is the critical current without magnetic order. (e-f) Critical current I_c and first and second harmonics $I_{1,2}$ of the Josephson current $I(\varphi)$ as a function of the exchange field in the respective UM. Here, I_c , I_1 , and I_2 are shown by green, magenta, and cyan curves, respectively. Parameters: $T = 0.025T_c$, $T_c = 0.01t$; rest of parameters are same as in Fig. 15. Adapted from [146].

C. The Josephson effect and current-phase characteristics

Having identified the effect of unconventional magnetism on the formation of ABSs, we now discuss the phase-dependent supercurrents $I(\phi)$ characterizing Cooper pair transport across JJs with UMs, studied in Ref. [146] for AMs and PUMs. The Josephson effect in JJs with AMs was also studied in Refs. [181–186, 458]. Before addressing the Josephson effect in UMs, it is worth reminding the Josephson effect when conventional superconductors are linked by a short normal metal or simply when two conventional superconductors are directly coupled. In this case, the supercurrent is given by [439]

$$I(\varphi) = \frac{I_c \sigma_N \sin(\varphi)}{\sqrt{1 - \sigma_N \sin^2(\varphi/2)}} \tanh \left[\frac{E(\varphi)}{2\kappa_B T} \right], \quad (45)$$

where $E(\varphi) = \Delta \sqrt{1 - \sigma_N \sin^2(\varphi/2)}$, $I_c = e\Delta/2\hbar$, σ_N the normal transparency introduced in Eq. (IVB) and T the temperature. Thus, in the tunneling regime ($\sigma_N \ll 1$), the supercurrent in conventional JJs is given by $I(\varphi) = I_c \sin(\varphi)$, first derived by [459], which has a maximum at $\varphi = \pi/2$; in the full transparent regime ($\sigma_N = 1$), the supercurrent is given by $I(\varphi) = I_c \text{sgn}(\cos(\varphi/2)) \sin(\varphi/2)$, first derived Kulik and Omelyanchuk [460], with a maximum at $\varphi = \pi$. In both cases, the supercurrent is an odd function of the phase, $I(\varphi) = -I(\varphi)$, it is 2π -

periodic with the phase, it vanishes at integer values of the phase $I(\varphi) = 0$ for $\varphi = n\pi$, with $n \in \mathbb{Z}$, and the positive and negative maxima are equal $I_c = I_c^\pm$, with $I_c^\pm = \max_\varphi [\pm I(\varphi)]$. Below we will see that these seemingly standard properties of conventional JJs are strongly affected by unconventional magnetism.

For JJs with UMs, the supercurrent in Ref. [146] is obtained using the second expression of Eqs. (44) for the system associated to Fig. 15, where two semi-infinite spin-singlet s -wave superconductors are linked via an UM. The respective supercurrents as a function of the superconducting phase difference φ are presented in Fig. 16(a-d) for JJs with d -wave AMs and p -wave UMs. Therein, we also show the corresponding free energy $F(\varphi)$ as a function of φ , whose minimum value $F_{\min} = \min_\varphi [F(\varphi)]$ is subtracted for visualization purposes, see blue curves in Fig. 16(a-d). The first observation in Fig. 16(a-d) is that the current-phase curves and the free energies share some similarities and also strong differences depending on the type of UM. Among the similarities is that the supercurrent $I(\varphi)$ and the free energy $F(\varphi)$ exhibit a 2π -periodicity with φ , while $I(\varphi)$ in all cases exhibits zero value at $n\pi$ with $n \in \mathbb{Z}$, and the positive/negative maxima are equal. However, $I(\varphi)$ and $F(\varphi)$ acquire a distinct dependence with respect to the superconducting phase difference that unveils the type of JJ. In the case of JJs with a d_{xy} -wave AM, the current-phase curve develops minima and maxima around $\varphi = \pm\pi$ and $\varphi = 0$, respectively, see Fig. 16(a); this supercurrent behaviour is

accompanied by a free energy with minima at $\varphi \neq 0, \pi$, and hence signals the emergence of a φ -JJ as a result of d -wave altermagnetism, see also Ref. [184]. We note that φ -JJs were initially predicted in Ref. [189]. In JJs with $d_{x^2-y^2}$ -wave AMs, the current-phase curve has a sine-like behaviour but is shifted by π , which is also accompanied by minima of the free energy at $\varphi = \pm\pi$, see Fig. 16(b) and Ref. [146]; this behaviour corresponds to a π -JJ, also reported in Refs. [181–184, 186, 458]. In the case of JJs with p -wave UMs, the phase-dependent supercurrents $I(\varphi)$ have a regular sine-like behavior with a sharp transition across $\varphi = \pm\pi$ due to a presumably high transmission as seen in the Andreev spectrum of Fig. 15(k,l). The corresponding free energy for JJs with p -wave UMs has a single minimum at $\varphi = 0$ and hence represents a regular 0-JJ.

We can gain further understanding of the supercurrent by inspecting the maximum current $I_c = \max_{\varphi}[I(\varphi)]$, known as critical current, presented in Fig. 16(e-h) as a function of the exchange field for each UM [146]. Moreover, since the Josephson current can be decomposed in terms of even and odd harmonics of φ as $I(\varphi) = \sum_m [I_m \sin n\varphi + J_m \cos n\varphi]$, in Fig. 16(e-h) we also show the nonzero first and second harmonics $I_{1,2}$. We note that Refs. [146, 184] showed that $J_n = 0$ in JJs with AMs and PUMs due to their intrinsic symmetries, see also Ref. [188]. The first observation is that the critical currents for d -wave AMs exhibit an oscillatory decay as the exchange fields increase, with a distinct periodicity tied to the type of altermagnetism, see Fig. 16(e,f) and Ref. [146]. The oscillatory profile can be understood in terms of the oscillatory profile of their first and second harmonics as depicted by cyan and magenta curves in Fig. 16(e,f). In the case of p -wave magnets, the critical currents do not oscillate but develop a slow decay as the exchange fields increase, a phenomenon explained in Ref. [146] to be the result of the non-detrimental effect of preserving time-reversal symmetry in PUMs and the spin-singlet Cooper pairs in the parent conventional superconductors. The oscillations in critical currents are common in magnetic systems with a net magnetization [2] and also in topological junctions with Majorana states [180, 197–200, 223, 461, 462], which both phenomena are absent here in the discussed JJs based on UMs and conventional superconductors. Taking the critical current properties and the discussion made in the previous paragraph, we can say that UMs represent a rich playground for anomalous current-phase characteristics and also for designing distinct types of JJs by simply using conventional superconductors.

Besides JJs formed by conventional superconductors and UMs, Ref. [156] very recently studied in JJs formed by d -wave superconductors and a d -wave AM [Fig. 17 (a)] and the main findings we show in Fig. 17 (c-d). In this case, the sign of the d -wave pair potential changes on the Fermi surface, in contrast to what occurs in conventional spin-singlet s -superconductors. This property can enhance the $\sin(2\varphi)$ component of the Josephson current

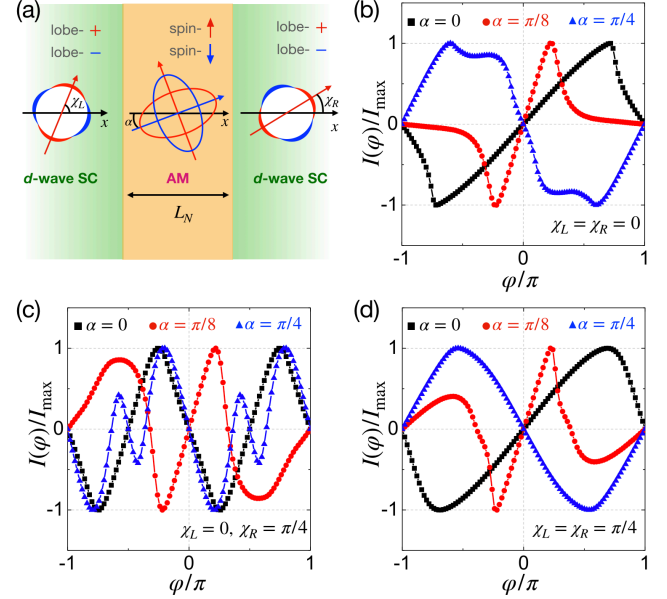


Figure 17. Current-phase characteristics $I(\varphi)$ in JJs formed by semi-infinite d -wave superconductors and a d -wave AM of finite length L_N . (a) Sketch of the JJ without interface barriers, where the angles $\chi_{L/R}$ indicate the orientation of the pair potential lobe with respect to the x -axis in the left/right superconductor. Also, α denotes the orientation of the exchange field lobe with respect to the x -axis. (b-d) $I(\varphi)$ for $\chi_{L/R} = 0$ (b), $\chi_L = 0$ and $\chi_R = \pi/4$ (c), and $\chi_{L/R} = \pi/4$ (d). Parameters: $k_F L_N = 30$, $J = 0.2\mu$, $\kappa_B T = 0.0108\Delta$. Adapted from Ref. [156].

$I(\varphi)$ and realize the φ -junction [187, 188] in asymmetric junctions [189, 463]. In the JJs based on d -wave superconductors and a d -wave AM, the current-phase curves are generally expressed as $\sum_n I_n \sin(n\varphi)$. Since the lobe angles with respect to the interface change, the current-phase curves exhibit $0-\pi$ transitions in the symmetric junctions [Fig. 17 (b)(d)]. Particularly, for asymmetric $0^\circ-\pi/4$ junction, the first-order harmonic of Josephson current I_1 reappears when the AM has neither $d_{x^2-y^2}$ nor d_{xy} symmetry, as shown in Fig. 17 (c) where the Josephson current is finite at $\varphi = \pm\pi/2$ for $\alpha = \pi/8$. Such behavior is in sharp contrast to that in a $0^\circ-\pi/4$ junction with a ferromagnet [464], where the first-order sinusoidal component never appears in the current-phase curve. It is shown in Ref. [156] that the intriguing behavior of the Josephson current in JJs formed by d -wave superconductors and a d -wave AM is strongly tied to the underlying symmetries in AMs, which involve the combination of time-reversal symmetry \mathcal{T} as the time-reversal operator, \mathcal{M}_{xz} as the mirror reflection operator with respect to xz -plane, and \mathcal{C}_4 the fourfold rotation symmetry with respect to z axis. More precisely, Ref. [156] showed that the symmetries $\mathcal{M}_1 = \mathcal{T}\mathcal{M}_{xz}$ and $\mathcal{M}_2 = \mathcal{T}\mathcal{M}_{xz}\mathcal{C}_4$ give rise to the protected nodal points at $\varphi = \pm\pi/2$ for $d_{x^2-y^2}$ - and d_{xy} -AM, respectively. As a result, the interplay between d -wave superconductivity and d -wave alter-

magnetism offers a good controllability of distinct types of JJs, which might be of utility for designing Josephson devices [19, 23, 445, 447].

D. Emergent phenomena due the interplay between unconventional magnetism and the Josephson effect

Apart from the already discussed unusual current-phase characteristics, the combination of unconventional magnetism and the Josephson effect also leads to novel superconducting correlations and can be used to engineer nonreciprocal Josephson transport. In particular, we stress the prediction of odd-frequency spin-triplet pairing [146] and the realization of the Josephson diode effect [221], emergent phenomena that hold fundamental relevance for understanding superconductivity in JJs with UMs and also applied importance for superconducting electronics. In the following, we discuss these two discoveries.

1. Odd-frequency spin-triplet pairing

As discussed in Subsection III B, the interplay between superconductivity and unconventional magnetism leads to novel superconducting correlations. Motivated by these results, Ref. [146] predicted the formation of several superconducting pair symmetries by exploiting the Josephson effect and unconventional magnetism. The superconducting correlations were obtained from the anomalous electron-hole component of the Nambu Matsubara Green's functions as discussed in Section III B for a JJ formed along x by semi-infinite spin-singlet s -wave superconductors linked by UMs; periodic boundary conditions along the transverse direction is taken, such that k_y is a good quantum number. Among UMs, Ref. [146] considered d -wave AMs and p -wave UMs, which, when coupled to the superconductors, were shown to host superconducting correlations having symmetries similar but also distinct to that of the parent superconductor. Notably, for p -wave UMs and d -wave AMs, Ref. [146] finds spin-triplet superconducting correlations belong to the ETO and OTE symmetry classes discussed in Subsection III B, respectively, whose parity symmetry is determined by the symmetry of unconventional magnetism. For instance, for JJs with d_{xy} -wave AMs, the OTE pair amplitude has an even parity that is determined by the combination of the odd dependence under the exchange of spatial coordinates and odd in k_y ; the oddness in k_y entirely arises due to the magnetic order, given that the altermagnetic field of a d_{xy} -wave AM is odd under k_y . Similarly, the parity symmetry of the OTE pairing in JJs with $d_{x^2-y^2}$ -wave AMs is determined by the evenness in space and in momentum along the transverse direction. The role of AMs for affecting the parity of emergent superconducting correlations was already discussed

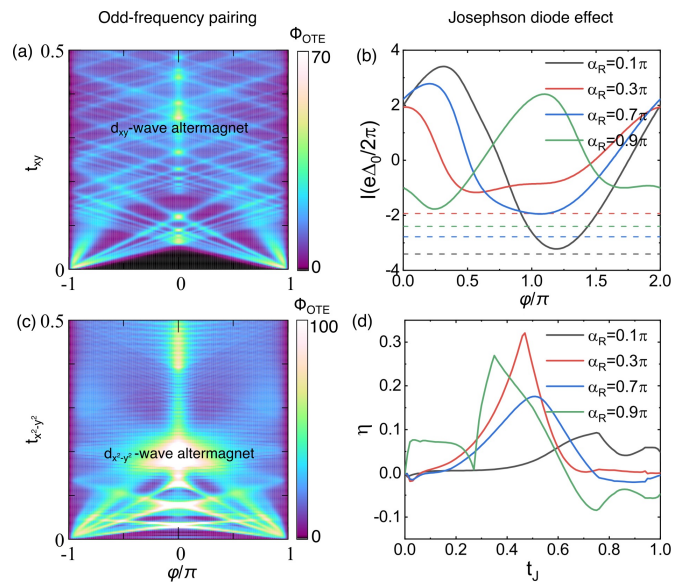


Figure 18. Emergent phenomena in JJs based on AMs. (a,c) Odd-frequency spin-triplet even-parity pairing: Square absolute value of the OTE pair amplitude integrated over k_y as a function of the strength of the altermagnetic field and the superconducting phase difference. The OTE pair amplitude is obtained in the middle of a d -wave AM connecting two semi-infinite conventional superconductors at lowest Matsubara frequency within a recursive Green's function approach. Tight-binding parameters: $a = 1$, $L_N = 30a$, $\Delta = 0.02t$, $t_{\text{int}} = 0.95$, $\mu = 1.5t$, $T_c = 0.01t$, and $T = 0.025T_c$. Adapted from Ref. [146]. (b,d) Josephson diode effect: (a): Current-phase curves for distinct values of the orientation angle α_R of the AM lobes with respect to the x -axis. (d): Josephson diode efficiency η as a function of the strength of the altermagnetic field for distinct values of α_R . Reprinted figures with permission from Qiang Cheng, Yue Mao, and Qing-Feng Sun, Phys. Rev. B. 110, 014518 (2024) [221]; Copyright (2025) by the American Physical Society.

in Subsection III B. However, the most relevant finding of Ref. [146] is that the formation of OTE pairing can be controlled by the interplay between altermagnetism and the Josephson effect. To visualize this fact, we show in Fig. 18(a,b) the square absolute value of the OTE pairing in the middle of a d -wave AM integrated over k_y as a function of the altermagnetic field and the superconducting phase difference φ , see also Ref. [146]. As observed, a finite OTE pairing is induced only when both the altermagnetic field and φ , which not only unveils the formation of novel superconducting correlations but also suggest that they are important in the proximity effect of JJs formed by AMs. An interesting open problem is perhaps to explore how long in space survive these pair correlations, which could take us further to understand and realize a long-range proximity effect in JJs with AMs and their extension to PUMs as well. Studies of this kind are necessary for envisaging Josephson devices hosting spin-polarized supercurrents [3] useful for superconducting spintronics [3–8], which can be achieved using UMs

at zero net magnetization.

2. The Josephson diode effect

In the Josephson diode effect, nonreciprocity occurs in the supercurrents $I(\varphi)$ driven by the Josephson effect [223–225, 229, 235, 236, 465–469], which by now has already motivated an intense experimental activity [232, 233, 237, 378, 470–474]. More specifically, in a similar way as for the superconducting diode effect in bulk superconductors, the Josephson diode effect involves the nonreciprocity of maximum and minimum critical currents $I_c^+ \neq I_c^-$, where $I_c^\pm = \max_\varphi[\pm I(\varphi)]$. Thus, the Josephson diode efficiency is quantified by quality factor $\eta = (I_c^+ - |I_c^-|)/(I_c^+ + |I_c^-|)$ given by Eq. (37) but involving the maximum and minimum Josephson currents. We can also see that the antisymmetric dependence of the supercurrent with the phase φ is broken, namely, $I(\varphi) \neq -I(-\varphi)$; hence, the Josephson diode effect requires current-phase curves that are distinct to what is obtained in conventional JJs. As for the superconducting diode discussed in Subsection IIID 2, the Josephson diode effect also requires breaking time-reversal and inversion symmetries as necessary but not sufficient conditions. Ref. [396] showed that, breaking time-reversal and inversion symmetries, needs to be combined with breaking x -inverting symmetries in order to induce nonreciprocal Josephson transport. These conditions can be easily achieved in JJs formed by semiconductors which exhibit intrinsic SOC under the presence of external magnetic fields breaking time-reversal and x -inverting symmetries. In terms of supercurrent harmonics, when the Josephson current is decomposed as $I(\varphi) = \sum_m [I_m \sin(m\varphi) + J_m \cos(m\varphi)]$, the discussed symmetry Josephson diode requirements were shown in Ref. [224] to be directly connected to the Josephson current exhibiting the simultaneous coexistence of the harmonics $\sin(\varphi)$, $\sin(2\varphi)$, and $\cos(\varphi)$ [224]. Thus, a Josephson diode effect is possible when I_1 , I_2 and J_1 coexist, maximizing the efficiency η when such harmonics are comparable in magnitude [396].

Given the requirements for Josephson diodes, JJs formed by AMs represent an interesting and promising ground. This is because AMs exhibit broken time-reversal symmetry and have a momentum dependent magnetic field akin to SOC but of not relativistic origin, already shown to be important for superconducting diodes in bulk superconductors and whose extension to JJs is hence natural, see Subsection IIID 2. Exploring AMs for Josephson diodes is further supported by the findings of Refs. [146, 156] discussed in Subsection IV C, where the current-phase characteristics of JJs with AMs were shown to exhibit multiple harmonics ($I_{1,2}$), thus being promising for the Josephson diode effect according to Ref. [224] if an additional mechanism is able to allow for J_1 . In this regard, J_1 can be induced e. g., by an external magnetic field or perhaps other spin-dependent

fields, which then implies that $I(\varphi) \neq -I(-\varphi)$ and the Josephson diode effect can be realized. So far, only one study reported the Josephson diode effect in a JJ formed by conventional spin-singlet s -wave superconductors with d -wave altermagnetism and also Rashba SOC [221]. In the top panel of Fig. 18(b), the current-phase curves of Ref. [221] are shown for distinct values of the orientation angle that controls the d -wave altermagnetism and the Rashba SOC. The distinct values of maximum and minimum values of $I(\varphi)$ and the finite quality factors in the bottom panel of Fig. 18(b) clearly show the emergence of the Josephson diode effect using d -wave AMs. While these findings are indeed encouraging, Ref. [221] showed that the Josephson diode needs the simultaneous presence of altermagnetism and Rashba SOC, vanishing if SOC is zero. This then makes us wonder if it is possible at all to realize Josephson diodes by simply using AMs, or they need to be combined with PUMs or other higher angular momentum UMs since, under certain circumstances, they also offer a spin splitting of energy bands. Pursuing these ideas have an immediate impact in superconducting electronics where Josephson diodes can be utilized.

V. EXPERIMENTAL ADVANCES

Having discussed the theoretical efforts due to unconventional magnetism in superconductors, this part addresses the experimental advances. Since the field is still at its infancy, almost all the reported experiments involve normal state AMs [48, 49, 66–73, 75–82, 84–104, 110, 475–477]; see also Refs. [60, 61] for recent reviews on AMs. These experiments measured the band splitting in AMs [70, 71, 75–77, 79, 81, 82] as well as anomalous and spin transport effects [48, 72, 75, 84–89], spin currents [90–98, 110], magnetooptical effects [99–104]. So far, UMs with an odd-parity magnetic order have not been experimentally studied, although there exist interesting predictions regarding Mn_3GaN and CeNiAsO for p -wave UMs [55]. In the case of superconductivity and unconventional magnetism, as we have already mentioned in the introduction, superconductivity has been observed in thin films of strained RuO_2 [135–137] and indications of superconductivity also exists in monolayer FeSe [138]. Since these materials are also promising for altermagnetism [60, 61], it seems that intrinsic superconductivity in altermagnets, or the coexistence of superconductivity and altermagnetism, might be indeed possible. In superconducting junctions, only a single study has very recently been reported [159], which addresses superconducting transport via Andreev reflections in junctions formed by MnTe , expected to be altermagnetic, and In superconductor.

In what follows, we briefly discuss the normal state experiments on AMs reporting their spin splitting and d -wave nature as well as the generation of spin currents, of particular importance for novel superconducting phe-

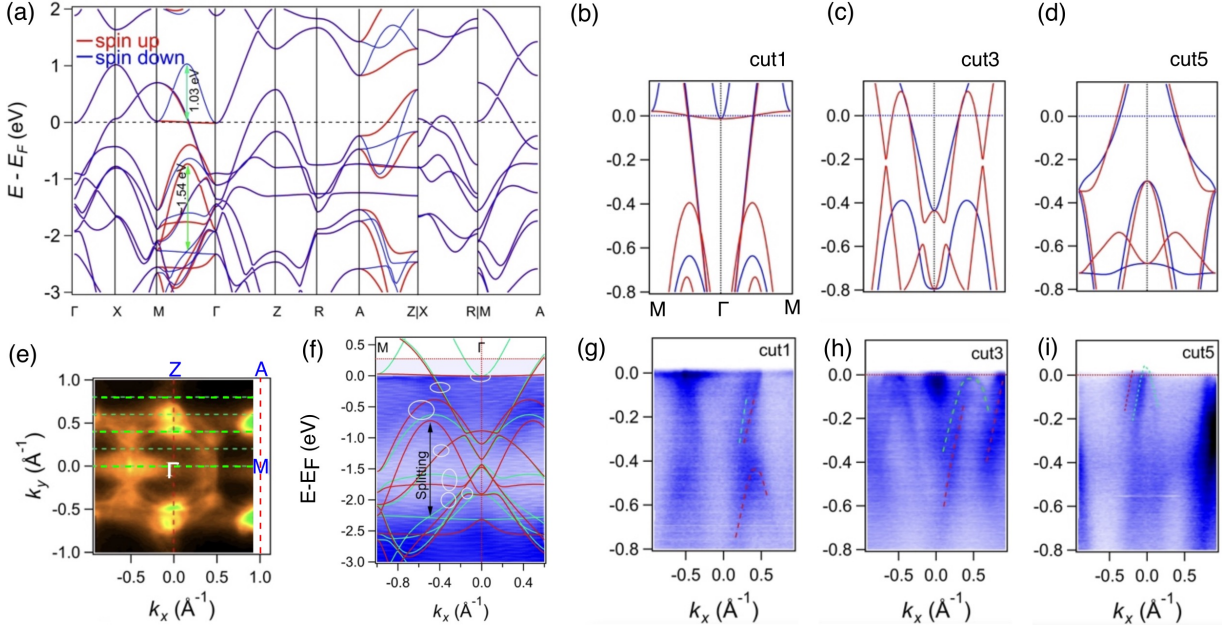


Figure 19. Measurement of the band splitting in the Γ MAZ plane of RuO_2 . (a) Electronic band structure along high symmetry lines for the altermagnetic phase of RuO_2 , shifted upward by 0.36 eV; spin up and down bands are indicated by red and blue, respectively. (b-d) Calculated band structure along cuts 1, 3, 5, indicated by the brightest green dashed lines in the Fermi surface in the Γ MAZ plane (e). (f) ARPES spectra with a wide energy range along Γ M direction, with the calculated band structure overlaid; the blue color is changed to green to avoid confusion with the blue background. The band splitting is indicated by the double black arrow. (g-i) ARPES spectra of cuts parallel to the Γ M direction with an equal k_z offset of $0.2(\Gamma Z)$ between each other. Reproduced under the terms of the CC-BY 4.0 license and adapted with permission from the authors of Ref. [71].

nomena as we argue below. Moreover, we also delve into the experiments in the superconducting state, on strained superconductivity in RuO_2 and the Andreev reflection in MnTe/In junctions.

A. Spin splitting and d -wave altermagnetic nature in the normal state

One of the first properties that attracted experimental interest in AMs has been the spin splitting of energy bands [70, 71, 75–77, 79, 81, 82]. As we have discussed in the introduction and also in Section II, the band splitting has a nonrelativistic origin and is, therefore, distinct to what happens in spin-orbit coupled materials. This band splitting is a result of opposite-spin sublattices linked by the crystal-rotation symmetries [52]. Moreover, since there is zero net magnetization in AMs, the band splitting is also different from what occurs in ferromagnets. As a result, the band splitting in AMs is a unique altermagnetic property. While several experiments have reported consistent evidence of band splitting in AMs, there have also been studies that challenge the altermagnetic nature of RuO_2 . In this regard, a recent study [478] reported the absence of altermagnetic spin splitting in RuO_2 , while Refs. [479, 480] indicate that the ground state of RuO_2 is nonmagnetic. Ref. [480] also suggested multiple scattering as the source of the magnetic signals

reported earlier in RuO_2 [475] and argued that the altermagnetic signals seen in such a material likely have extrinsic origin. It is worth noting that a recent theoretical study suggested that the adequate characterization of the amount of Ru vacancies can actually promote the formation of a magnetic state in RuO_2 [481] at a lower and more realistic Hubbard U than that used in Refs. [45, 48]; see also Refs. [70, 83, 482–484] for recent supporting evidence of altermagnetism in RuO_2 . These studies thus reflect the intense activities in the field of altermagnetism, highlighting that more experiments are needed to expand the understanding of RuO_2 and perhaps extend this motivation to measure the spin splitting in other altermagnetic materials as already reported for MnTe [77].

In spite of the controversy exposed in the previous paragraph, the confirmation of altermagnet-induced band splitting would be a great breakthrough in the field. In light of this, now we would like to describe the band splitting and identification of the d -wave parity in the altermagnet RuO_2 reported in Ref. [71]; the great interest in this material justifies its consideration. Single crystals of RuO_2 were grown by chemical vapor transport method and conventional synchrotron-based angle photoemission spectroscopy (ARPES) was used to measure the spin band splitting [71], see Fig. 19. In Fig. 19(a), the bandstructure along high symmetry lines in the altermagnetic phase shows a distinct spin splitting along

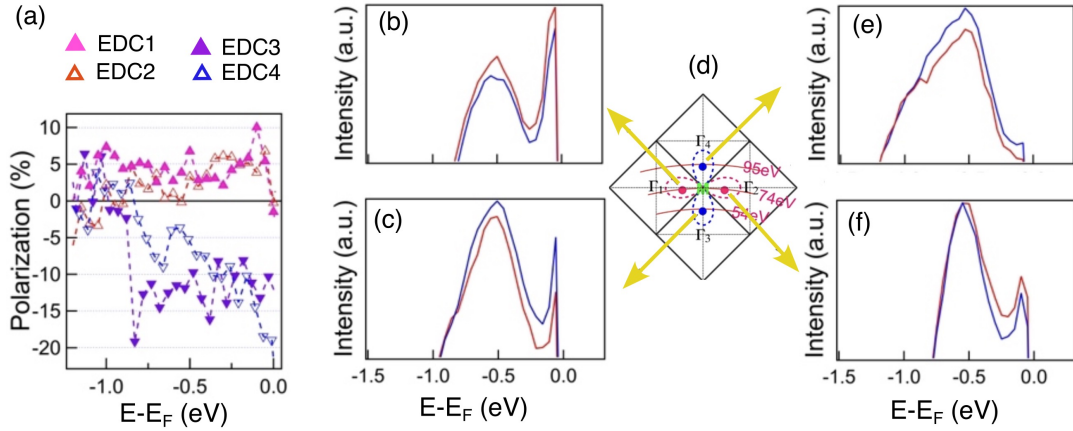


Figure 20. Experimental identification of the d -wave antiferromagnetic order in RuO_2 . (a) Spin polarization along EDC 1-4 symmetrically around the M point, at momenta on the left/right and above/below M, after removing the linear background. EDC stands for energy distribution curve. (b) Zoomed-in view of the intensity of spin-polarized EDCs along EDC1 at the left point of M. The red and blue curves indicate up and down spins, respectively. (c,e,f) The same as in (b) but for momenta at the right, above, and below the M point. (d) shows the cross-section of the Brillouin Zone and the high symmetry points, where the four points where the spin EDCs are obtained. The left/right and above/below momenta points are depicted by red and blue filled circles in (d), respectively, and are located along $\Gamma_1\text{M}\Gamma_2$ and $\Gamma_3\text{M}\Gamma_4$. (d) also indicates the photon energies at which spin-ARPES spectra was acquired. Reproduced under the terms of the CC-BY 4.0 license and adapted with permission from the authors of Ref. [71].

ΓM and AZ directions; along ΓM direction, an energy splitting of 1.54eV is predicted, see also Ref. [52]. The spin splitting is perhaps more clearly seen in Fig. 19(b-d), which shows the bandstructure along three cuts parallel to ΓM and along ΓZ in the Fermi surface shown in Fig. 19(e). The band splitting seen in Fig. 19(a-d) is confirmed in Fig. 19(f-i), where the ARPES spectra are presented and measured with energy and angular resolutions set to $\sim 20\text{meV}$ and 0.1° , respectively at 22°K . By overlaying the theoretical bandstructure, the authors of Ref. [71] estimate the largest band splitting of 1.54eV to be within the energy range of -0.7eV and -2.5eV , see Fig. 19(f). The band dispersion from ARPES measurements can be seen to adjust well to the bandstructure calculations, albeit experimental data seem to have large broadening effects and low energy resolution, compare Fig. 19(b-d) and Fig. 19(g-i). These findings thus support the induced band splitting in antiferromagnetic RuO_2 , even though more studies are necessary to settle the controversy about the antiferromagnetic nature of this effect.

A key property of AMs, which distinguishes them from conventional magnets, is that their magnetic order has an even-parity symmetry. One of the simplest AMs have d -wave symmetry, which was predicted for RuO_2 [52]. This property was also addressed in the experimental study of Ref. [71] by means of spin-ARPES with an energy resolution set to $\sim 100\text{meV}$ at 11°K . The key findings of Ref. [71] that reveal the d -wave nature of the antiferromagnet RuO_2 are shown in Fig. 20. As we discussed in Section II, the d -wave parity of AMs is reflected in the four lobe structure with an alternating spin whose direction flips after a $\pi/2$ rotation, see Fig. 20(d). To measure the d -

wave antiferromagnetic texture, the authors of Ref. [71] chose four points, one per lobe (filled blue/red circles), and measured the spin polarization by means of spin-ARPES at distinct photon energies. The measured polarization is largely positive and reaches a maximum of 10% for the points along $\Gamma_1\text{M}\Gamma_2$, while it is negative and with a maximum of up to 20% for the points along $\Gamma_3\text{M}\Gamma_4$. These features already reveal an opposite behavior for the spin polarization, which supports the d -wave nature of RuO_2 . More insights are obtained from Fig. 20(b,c) and Fig. 20(e,f), which show the intensity of the spin-polarized energy distribution curves for each spin. In this case, the contribution from spin up at the left point of M along $\Gamma_1\text{M}$ exhibits a larger value than its spin-down counterpart, which indicates a spin-up polarization, see Fig. 20(b). For the bottom point of M along $\Gamma_3\text{M}$, the spin-down part is larger than the spin-up contribution, thus favouring a spin-down polarization that is of opposite sign as the one obtained for the point along $\Gamma_1\text{M}$, see Fig. 20(c). Following a similar analysis, at the right and top points along the $\text{M}\Gamma_2$ and $\text{M}\Gamma_4$, respectively, the authors of Ref. [71] measure a spin-up and spin-down polarizations. Thus, the measurements discussed here support the antiferromagnet nature of RuO_2 . Despite the ongoing controversy, it is important to highlight these experiments as they can inspire other studies which can then help understand the symmetries of the unconventional magnetic order. Establishing the band splitting and detecting the parity symmetries of AMs would be very useful when combining them with superconductors, as these properties are crucial for engineering novel superconducting phenomena such as spin-triplet higher mo-

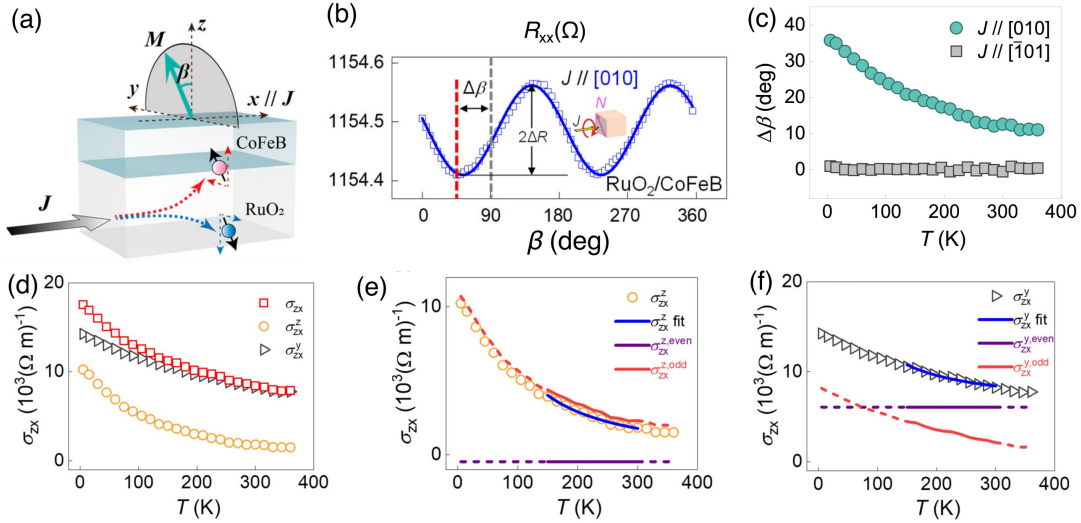


Figure 21. Detection of spin currents in altermagnetic RuO₂. (a) Scheme of the spin Hall magnetoresistance measurement in a RuO₂/CoFeB heterostructure, while scanning a 4T magnetic field M in a plane perpendicular to the electric field; here, β is the angle between the magnetic field and the normal direction z , $\Delta\beta$ is a phase shift, and x is the direction of the dc current J parallel to the [010] crystallographic direction. The current J favors the separation of spins, indicated by dotted red and cyan arrows. (b) Spin Hall magnetoresistance as a function of β at 5°K and with J parallel to [010]. The magenta arrow indicates the direction of the Néel vector. (c) Temperature dependence of the phase shift $\Delta\beta$ obtained from the spin Hall magnetoresistance measurements. (d-e) Spin Hall conductivities as a function of temperature, showing the total and the y - and z polarized components σ_{zx} , σ_{zx}^y , and σ_{zx}^z . Reproduced with permission from the authors of Ref. [98].

momentum Cooper pairs [145, 146] and controllable $0 - \pi$ transitions in Josephson junctions [146, 156, 184].

B. Spin currents in the normal state

A spin current is characterized by the flow of the spins of electrons in the absence of a charge current and represents a unique way to carry information [39, 40, 245]. The ability to generate spin currents with spin torques in magnets offers a robust way for controlling the magnetization, a crucial task towards efficient spintronics [40, 485]. In AMs, the spin splitting of energy bands, and their associated anisotropic spin distribution of Fermi surface, has been shown to be an interesting way for inducing transverse spin currents [83, 90–98, 110], thus reflecting the importance of altermagnetism; see also Refs. [113, 114]. This spin current has a nonrelativistic origin, is odd under time-reversal symmetry, can be reversed by switching the Néel vector, and exhibits an unusual spin polarization that makes AMs promising for spin-torque devices. We remind that spin currents induced by relativistic spin-orbit coupling, as in the spin Hall effect, are even under time-reversal symmetry [486]. As pointed out above, the nonrelativistic spin currents have attracted the interest of several groups and, very recently, their magnetic origin in altermagnetic RuO₂ as well as their direct connection to the Néel vector have been experimentally addressed in Ref. [98]. The key results of Ref. [98] are shown in Fig. 21, where spin Hall magnetoresistance measurements were carried out to identify the spin current polarization in

a RuO₂/CoFeB heterostructure [Fig. 21(a)]. The magnetoresistance R was measured using the four-point method under an applied dc current of $100\mu\text{A}$ along x , while an external magnetic field M was rotated in the $y - z$ plane having an angle β with z , see Fig. 21(a). The magnetoresistance at 5°K as a function of β is presented in Fig. 21(b), which develops a sinusoidal profile given by $\cos(\beta - \Delta\beta)$; here, $\Delta\beta$ is a phase shift of the angle β , which is absent in conventional magnetoresistance measurements [487]. For the applied dc current along x in RuO₂(101), the spin current develops terms along y and z directions, which leads to a magnetoresistance minimum when the magnetization is parallel to the spin current polarization and away from $\beta = 90^\circ$. When measuring the temperature dependence of the phase shift $\Delta\beta$ in Fig. 21(c), the authors find that it acquires a vanishing value when the applied current J is parallel to $[\bar{1}01]$, while $\Delta\beta$ develops large values when the current is along [010] and decrease as temperature increases. These findings suggest that the temperature dependence has an impact on the corresponding spin Hall conductivities, whose temperature dependence is presented in Fig. 21(d-f). For clarity, Fig. 21(d) shows the total, the z polarized, and the y polarized spin Hall conductivities as a function of temperature, while Fig. 21(e,f) shows the respective conductivity components along z and y as well as their time-reversal odd and even contributions. Since the even spin conductivity is independent of scattering due to its intrinsic bandstructure origin, its temperature dependence is expected to be weak [93]. Thus, the strong temperature dependence of the total spin conductivities can be

only attributed to the odd contribution, which, as we discussed before is tied to the altermagnetic band splitting in RuO₂. By taking the ratio between odd spin conductivity contributions along y and z , the authors of Ref. [98] have also estimated the angle between the direction of the time-reversal odd spin current polarization and z ; they found that time-reversal odd spin current polarization is roughly parallel to the Néel vector for a range of temperatures within 5°K and 360°K. The results of Ref. [98] support the magnetic origin of the nonrelativistic spin currents in RuO₂ and its polarization along the Néel vector of such a material. We stress that more studies are needed to further support the altermagnetic origin of spin currents in the predicted AMs. Experiments of this type will be extremely useful also when contacting AMs with superconductors towards a new era of superconducting spintronics where spin currents in the superconducting state are fundamental [4, 5].

C. Intrinsic superconductivity in strained RuO₂ films

The possibility of intrinsic superconductivity in UMs has not been directly addressed yet experimentally, but there exist theoretical proposals suggesting altermagnetic spin fluctuations as a mechanism to induce superconductivity [128] as well as the possibility of finite momentum superconductivity without any net magnetization due to the coexistence of superconductivity and altermagnetism [129–134]. Despite the lack of experimental evidence of intrinsic superconductivity, there exist measurements of superconductivity in materials which are believed to be altermagnets. This is the case of RuO₂, where strain-induced superconductivity was reported in Ref. [135–137]. Moreover, a recent theoretical work [138] has suggested that monolayer FeSe, known to host superconductivity [488–490], can manifest altermagnetism due to their intrinsic time-reversal symmetry breaking. Altermagnetism was also predicted to appear in the parent cuprate La₂CuO₄ of a high-temperature superconductor [53], while very recently also the ground state of the strongly correlated CuAg(SO₄)₂ [141] has been reported to be altermagnetic [140]. Given the interest in RuO₂, we now discuss the experiment performed in Ref. [135] reporting intrinsic strain-induced superconductivity. Thin films of RuO₂ were epitaxially grown on single-crystal TiO₂ along the [110] direction, see top panel of Fig. 22(a). The film thickness was adjusted in the range of 26 – 32nm in order to be able to apply large values of epitaxial strain. To identify the superconducting state, the authors measure the resistivity ρ as a function of temperature by a four-probe method in a cryostat having a 9T superconducting magnet and a ³He refrigerator. They found that ρ drops to zero at the critical temperature $T_{c,zero} = 1.6^\circ\text{K}$ and with a midpoint temperature of $T_{c,mid} = 1.7^\circ\text{K}$; by applying an external magnetic field, the transition temperature moves towards

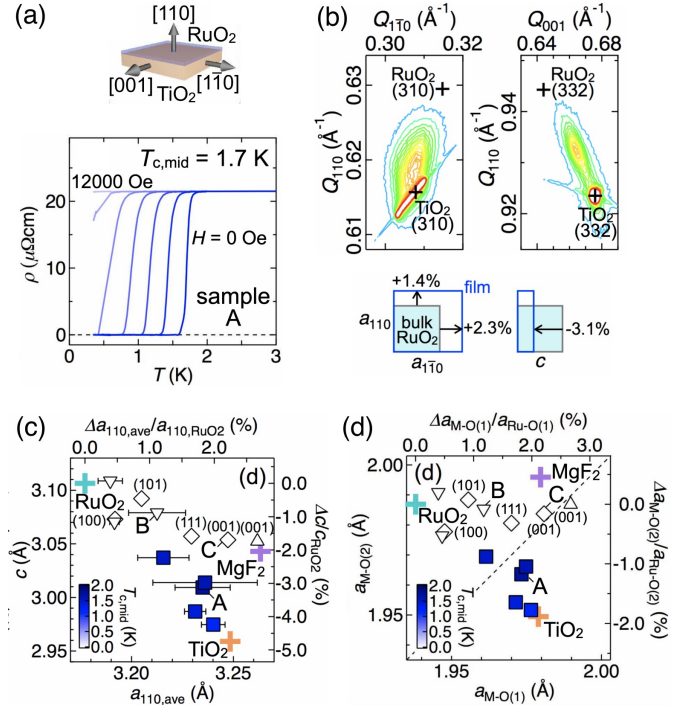


Figure 22. Measurement of superconductivity induced by strain in RuO₂ films. (a) The top panel shows a sketch of a RuO₂ film (light blue) grown on TiO₂ (light orange) along the [110] direction, referred to as sample A. The bottom panel depicts the in-plane resistivity ρ as a function of temperature for distinct values of an applied magnetic field parallel to the out-of-plane direction in steps of 2000Oe. A superconducting transition at $T_{c,zero} = 1.6^\circ\text{K}$, with a midpoint temperature of $T_{c,mid} = 1.7^\circ\text{K}$. (b) X-ray diffraction maps in reciprocal space taken for asymmetric reflections along [110] and [001] in-plane directions. The cross symbol “+” indicates the peak positions obtained from bulk lattice parameters for RuO₂ and TiO₂. Bottom panels depict the variations in the lattice parameters (a_{110} and $a_{1\bar{1}0}$) with respect to their bulk values in RuO₂. (c) Mapping of the average lattice parameter along [110] and [1 $\bar{1}$ 0] versus the lattice parameter c along [001], with the color indicating $T_{c,mid}$, while the ends of the horizontal bars mark a_{110} and $a_{1\bar{1}0}$. (d). Bond lengths between metal (M) atoms and oxygen (O) for RuO₂ films, including the bulk values of RuO₂, TiO₂, and MgF₂, while the symbols color coded by $T_{c,mid}$. Reprinted figures with permission from Masaki Uchida, Takuya Nomoto, Maki Musashi, Ryotaro Arita, and Masashi Kawasaki, Phys. Rev. Lett. 125, 147001 (2020) [135]; Copyright (2025) by the American Physical Society.

lower values. The authors also considered RuO₂ films on other substrates but did not obtain signs of superconductivity, which points towards the importance of strain for inducing superconductivity. From reciprocal space mappings, the authors show how epitaxial strain modifies the lattice parameters (a_{110} , $a_{1\bar{1}0}$, and c) of the RuO₂ films along three directions orthogonal to each other, achieving an anisotropic extension of a_{110} and $a_{1\bar{1}0}$ and a reduction of c , see Fig. 22(b). To identify the link between epitaxial strain and superconductivity, Fig. 22(c) presents the

mapping of the average lattice parameters a_{110} , $a_{1\bar{1}0}$ versus c , with the main signature being the appearance of superconductivity only in RuO_2 films grown along [110] on TiO_2 when c is reduced by +2% or more. This behavior was also identified by looking at the bond lengths between e. g., Ru and O atoms, denoted by $a_{\text{M-O}(1)}$ and $a_{\text{M-O}(2)}$, shown in Fig. 22(d); the most important feature in this case is the decrease of $a_{\text{M-O}(2)}$ as the bulk value of TiO_2 is reached, while $a_{\text{M-O}(1)}$ undergoes an increase. The authors further explore that soft phonon modes might be playing an important role for the emergence of superconductivity in strained RuO_2 films.

The interesting results of Ref. [135] motivate us to raise a natural question: is altermagnetism, predicted in RuO_2 [52] and with already experimental evidence [71], present in the strain-induced superconducting state reported in Ref. [135]? Moreover, it is worth noting that the critical temperature below which RuO_2 becomes superconducting is much lower than those predicted to realize altermagnetism [52], hence raising questions about the coexistence of altermagnetism and superconductivity in RuO_2 . If superconductivity and altermagnetism coexist, would it be possible to raise the superconducting critical temperature e. g., by strain engineering [136], such that the emergent effects are of utility for realistic quantum applications? We hope that these questions will motivate the community and the answer comes up soon. For now, we believe that realizing strain induced superconductivity in other altermagnetic candidates is a promising ground.

D. Signature of Andreev transport in altermagnet-superconductor junctions

The interplay between unconventional magnetism and superconductivity is a promising ground to explore emergent superconducting phenomena, as suggested by many theoretical works during the past two years, see e. g., Refs. [145, 146, 150–153, 156, 184]. Perhaps the simplest devices where this interplay can be addressed involves superconducting junctions formed by known superconductors and UMs. As discussed in Section III, when placing an UM in contact with a superconductor, superconducting correlations are induced in the UM by means of the proximity effect, which is directly linked to Andreev reflections [15, 160]. We remind that, in the Andreev reflection process, an incoming electron is reflected back as a hole at the normal-superconductor interface and thereby enhancing the differential conductance dI/dV [160, 349]. Thus, differential conductance is able to reveal the emergence of superconductivity and also the symmetry of its underlying order parameter [164]. In the case of AMs and PUMs, theoretical studies showed a strong dependence of Andreev transport on the orientation of the UMs [152, 156], which can be taken as a signature of emergent superconducting effects [145]. The simplicity of the recipe for exploring Andreev transport has already motivated an experimental study in altermagnet-

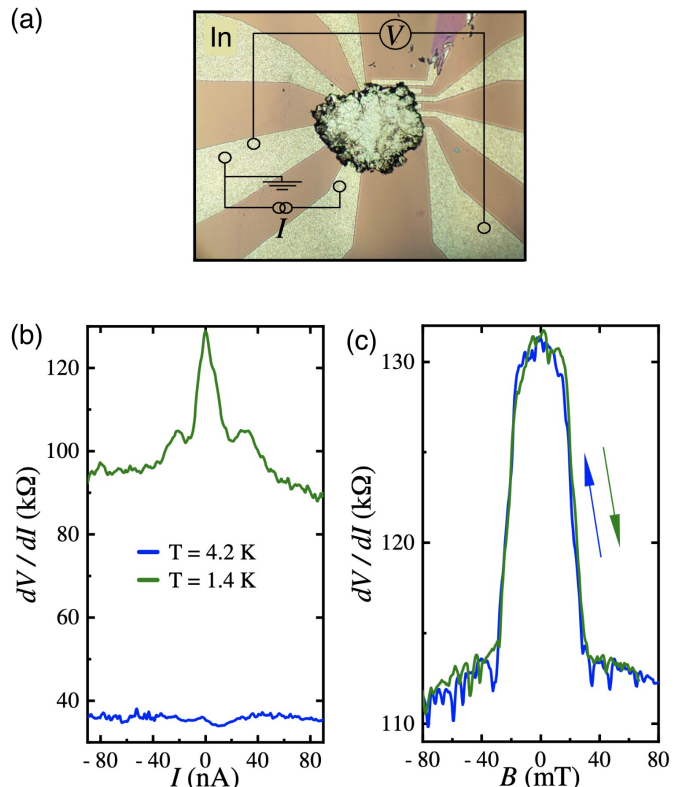


Figure 23. Andreev reflection in a NS junction formed by altermagnetic MnTe and superconducting In. (a) Image of the sample with electrical connections. A single crystal MnTe flake is transferred to the In leads pattern, so planar In-MnTe junctions are formed at the bottom surface of the flake. (b) Differential resistance of a single In-MnTe junction as a function of the dc current I for two distinct temperatures as. (c) Zero-bias resistance peak as a function of the magnetic field for two sweep directions. Reprinted figures from Physica B: Condensed Matter 696, 416602 (2025), Andreev reflection for MnTe altermagnet candidate, D. Yu. Kazmin, V.D. Esin, Yu. S. Barash, A. V. Timonina, N. N. Kolesnikov, E. V. Deviatov [159], Copyright (2025), with permission from Elsevier.

superconductor junctions, which was recently published in Ref. [159]. In particular, the authors of Ref. [159] considered a NS junction, where N is made of MnTe in the normal state and S is determined by Indium (In), see Fig. 23(a). To remind, MnTe is a g -wave altermagnet [52] and its nonrelativistic band splitting has already been experimentally reported [75, 77, 258] as well as its optical properties [101] and a spontaneous Hall effect [287]; the quality of MnTe was also studied in magnetization measurements [491]. Moreover, indium becomes superconducting below a critical temperature of $T_c \approx 3.4$ K and has a superconducting gap of $\Delta_{\text{In}} = 0.55$ meV [492]; indium is a type I spin-singlet s -wave BCS superconductor [493, 494]. The authors of Ref. [159] fabricated MnTe-In planar junctions with transparent NS interfaces and measure electron transport across the junction by a common three-point technique, obtained in a dilution refrigera-

tor equipped with a superconducting solenoid. Fig. 23(b) shows the measured differential resistance dV/dI as a function of the applied current I across a single MnTe-In junction at 4.2°K and 1.4°K: this reveals that the differential resistance (of the order of 40k Ω) has a extremely weak dependence on the applied current but its high value reflects the nature of the MnTe-In interface [159]. At low temperatures 1.4°K, where indium is a superconductor, the differential resistance is further increased following a nonlinear behaviour that reaches values even larger than 100k Ω [Fig. 23(b)]. Interestingly, for currents within ± 40 A, the differential resistance develops a symmetric increased profile centered at $I = 0$, with symmetric small peaks at ± 40 A that resembles the superconducting gap and a large zero-bias resistance peak resembling standard Andreev physics at disordered interfaces [349, 495, 496]. The authors also explain that the unusual dV/dI can be also seen to arise due to edge electrostatics which promote the depletion of carriers concentration at the NS interface, hence affecting the transport [497]. Moreover, when measuring the differential resistance as a function of an applied magnetic field, the zero-bias resistance appears for magnetic fields within ± 40 T, which is an relevant feature given that these values are close to the critical field of indium [492]. The authors of Ref. [159] also verified these findings in two distinct samples at 1.2°K.

Since the behavior of dV/dI reported in Ref. [159] only emerges when indium is superconducting, they are very likely reflecting Andreev transport but it is also fair to say that there exist some intriguing questions. The most pressing concern is perhaps the size of the induced superconducting gap, which seems to be much larger than the bulk value in indium (0.55meV), see Fig. 23(b,c). The specific profile of the differential resistance, and the respective conductance, still deserves to be further explored since, to date, no theoretical study has addressed transport in NS junctions with a g -wave AM such as MnTe; a recent study, however, already anticipates higher angular momentum spin triplet pairs when combining g -wave AMs with conventional superconductivity [145] but Andreev transport needs to be addressed in order to provide further understanding of the experiment carried out in Ref. [159]. Similarly, it would be important to clarify about the presence of altermagnetism at the conditions of the experiment of Ref. [159], specially whether altermagnetism still survives at the low temperatures. Another open question is about the possible effects due to the finite size of MnTe could be also playing a role in the subgap structure of differential resistance via e.g. confinement [205, 212]; it has recently been shown that confinement favors the presence of ABSs in AMs [156]. Novel superconducting phenomena might already be present at the interface of the MnTe-In junctions studied in Ref. [159] and its confirmation would require additional efforts on both the experimental and the theoretical fronts. Nevertheless, experiments like the one carried out in Ref. [159] is indeed encouraging to further exploit

the potential of unconventional magnetism for realizing novel superconducting effects. We hope that the physics discussed here will motivate to address the Josephson effect and perhaps the realization of superconducting devices by combining superconductors and unconventional magnets.

VI. CONCLUSIONS AND OUTLOOK

In this review article, we have summarized the recent advances on emergent superconducting phenomena emerging due to the interplay between unconventional magnetism and superconductivity. We have first provided an introduction to the field of unconventional magnetism in the normal state, making emphasis on their theoretical understanding and how to model magnetic orders with even- and odd-parities. We have pointed out the fact that d -wave altermagnets and p -wave unconventional magnets represent the magnetic counterparts of unconventional d - and p -wave superconductors. We have then discussed how the interplay of unconventional magnetism and superconductivity gives rise to the emergence of novel superconducting phenomena. In this part we have stressed that unconventional magnets not only convert spin-singlet into spin-triplet superconducting correlations but also transfer their parity, thus producing novel superconducting states with higher angular momentum that would not exist otherwise. Therein, we have also highlighted the importance of altermagnetism for realizing finite momentum superconductivity, topological superconductivity, superconducting diodes, non-trivial light-matter coupling, magnetoelectric and thermoelectric effects. Later, we have presented a thorough discussion of emergent physics in hybrid systems formed by unconventional magnets and superconductors, which we have accompanied by details on how to model such hybrid systems. In particular, we have clarified the signatures of unconventional magnetism in Andreev transport, proximity and inverse proximity effects, and also in the Josephson effect, where altermagnetism is e. g., the key to induce $0-\pi$ and φ -Josephson junctions. Here, we have also stressed that unconventional magnetism in Josephson junctions promotes the emergence of highly controllable odd-frequency pairing by means of the Josephson effect. Furthermore, we have summarized the recent experimental progress, highlighting the need of experimental signatures of the band splitting in altermagnets and the identification of their altermagnetic nature as well as the challenges to fabricate systems where altermagnetism coexists with superconductivity and its impact when contacting with superconductors.

Even though the field that combines unconventional magnetism and superconductivity is still in its infancy, the great efforts of the community bring us closer to understand its potential for truly novel superconducting phenomena that can be useful for quantum applications. Of particular relevance is that the special spin-

momentum locking in unconventional magnets already establishes new approaches for engineering spin-triplet Cooper pairs as well as their utilization for superconducting spintronics, topological superconductivity, thermoelectricity and multifunctional Josephson circuits, all at zero net magnetization and hence favorable for scalable superconducting devices. Despite the great interest, most of the research has addressed d -wave altermagnets and p -wave magnets in combination with superconductivity, thus leaving largely unexplored other types of unconventional magnets possessing magnetic order with higher angular momenta. The interplay between these unconventional magnets and superconductivity is very likely to offer far more exciting opportunities for novel phenomena. Furthermore, on the experimental front, several questions are still open, such as the identification of unconventional magnets by conductance measurements or their impact on the Josephson effect, to name just two examples. Nevertheless, we believe that the existent theoretical predictions of novel superconducting phenomena will motivate experiments hopefully in the very near future.

ACKNOWLEDGMENTS

We thank Y. Asano, P. Buset, D. Chakraborty, P.-H. Fu, J.-X. Hu, S. Ikegaya, M. Junzhang, S. Kashiwaya, J. Knolle, J. Linder, K. Maeda, T. Mizushima, N. Nagaosa, R. Seoane, P. Sukhachov, X. Qiu, M. Uchida, W. J. Zhao for useful discussions. Y. F. and K. Y. acknowledge financial support from the Sumitomo Foundation. B. L. acknowledges financial support from the National Natural Science Foundation of China (project 12474049). Y. T. acknowledges financial support from JSPS with Grants-in-Aid for Scientific Research (KAKENHI Grants Nos. 23K17668, 24K00583, 24K00556, and 24K00578). J. C. acknowledges financial support from the Carl Trygger's Foundation (Grant No. 22: 2093), the Sweden-Japan Foundation (Grant No. BA24-0003), and the Swedish Research Council (Vetenskapsrådet Grant No. 2021-04121),

-
- [1] F. S. Bergeret, A. F. Volkov, and K. B. Efetov, Odd triplet superconductivity and related phenomena in superconductor-ferromagnet structures, *Rev. Mod. Phys.* **77**, 1321 (2005).
 - [2] A. I. Buzdin, Proximity effects in superconductor-ferromagnet heterostructures, *Rev. Mod. Phys.* **77**, 935 (2005).
 - [3] M. Eschrig, Spin-polarized supercurrents for spintronics, *Physics Today* **64**, 43 (2011).
 - [4] J. Linder and J. W. Robinson, Superconducting spintronics, *Nat. Phys.* **11**, 307 (2015).
 - [5] M. Eschrig, Spin-polarized supercurrents for spintronics: a review of current progress, *Rep. Prog. Phys.* **78**, 104501 (2015).
 - [6] G. Yang, C. Ciccarelli, and J. W. Robinson, Boosting spintronics with superconductivity, *APL Materials* **9** (2021).
 - [7] A. Mel'nikov, S. V. Mironov, A. V. Samokhvalov, and A. I. Buzdin, Superconducting spintronics: state of the art and prospects, *Uspekhi Fiz. Nauk* **192**, 1339 (2022).
 - [8] R. Cai, I. Žutić, and W. Han, Superconductor/ferromagnet heterostructures: a platform for superconducting spintronics and quantum computation, *Advanced Quantum Technologies* **6**, 2200080 (2023).
 - [9] Y. Tanaka, M. Sato, and N. Nagaosa, Symmetry and topology in superconductors—odd-frequency pairing and edge states—, *J. Phys. Soc. Jpn.* **81**, 011013 (2011).
 - [10] M. Sato and S. Fujimoto, Majorana fermions and topology in superconductors, *J. Phys. Soc. Jpn.* **85**, 072001 (2016).
 - [11] M. Sato and Y. Ando, Topological superconductors: a review, *Reports on Progress in Physics* **80**, 076501 (2017).
 - [12] R. Aguado, Majorana quasiparticles in condensed matter, *Riv. Nuovo Cimento* **40**, 523 (2017).
 - [13] R. M. Lutchyn, E. P. Bakkers, L. P. Kouwenhoven, P. Krogstrup, C. M. Marcus, and Y. Oreg, Majorana zero modes in superconductor–semiconductor heterostructures, *Nat. Rev. Mater.* **3**, 52 (2018).
 - [14] S. M. Frolov, M. J. Manfra, and J. D. Sau, Topological superconductivity in hybrid devices, *Nat. Phys.* **16**, 718 (2020).
 - [15] J. Cayao, C. Triola, and A. M. Black-Schaffer, Odd-frequency superconducting pairing in one-dimensional systems, *The European Physical Journal Special Topics* **229**, 545 (2020).
 - [16] K. Flensberg, F. von Oppen, and A. Stern, Engineered platforms for topological superconductivity and Majorana zero modes, *Nat. Rev. Mater.* **6**, 944 (2021).
 - [17] Y. Tanaka, S. Tamura, and J. Cayao, Theory of majorana zero modes in unconventional superconductors, *Progress of Theoretical and Experimental Physics* **2024**, 08C105 (2024).
 - [18] S. D. Sarma, M. Freedman, and C. Nayak, Majorana zero modes and topological quantum computation, *npj Quantum Inf.* **1**, 15001 (2015).
 - [19] P. Krantz, M. Kjaergaard, F. Yan, T. P. Orlando, S. Gustavsson, and W. D. Oliver, A quantum engineer's guide to superconducting qubits, *Applied physics reviews* **6** (2019).
 - [20] G. Burkard, Hybrid superconductor-semiconductor systems for quantum technology, *Appl. Phys. Lett.* **116** (2020).
 - [21] R. Aguado and L. P. Kouwenhoven, Majorana qubits for topological quantum computing, *Physics Today* **73**, 44 (2020).
 - [22] C. W. J. Beenakker, Search for non-Abelian Majorana braiding statistics in superconductors, *SciPost Phys. Lect. Notes*, 15 (2020).
 - [23] M. Kjaergaard, M. E. Schwartz, J. Braumüller,

- P. Krantz, J. I.-J. Wang, S. Gustavsson, and W. D. Oliver, Superconducting qubits: Current state of play, *Annual Review of Condensed Matter Physics* **11**, 369 (2020).
- [24] P. Marra, Majorana nanowires for topological quantum computation, *Journal of Applied Physics* **132**, 231101 (2022).
- [25] A. I. Buzdin, M. Fauré, and M. Houzet, Superconductor-ferromagnet heterostructures, in *Nanoscale Devices-Fundamentals and Applications* (Springer, 2006) pp. 197–224.
- [26] K.-R. Jeon, B. K. Hazra, K. Cho, A. Chakraborty, J.-C. Jeon, H. Han, H. L. Meyerheim, T. Kontos, and S. S. Parkin, Long-range supercurrents through a chiral non-collinear antiferromagnet in lateral josephson junctions, *Nature materials* **20**, 1358 (2021).
- [27] G. A. Bobkov, V. M. Gordeeva, L. Johnsen Kamra, S. Chourasia, A. M. Bobkov, A. Kamra, and I. V. Bobkova, Superconducting spin valves based on antiferromagnet/superconductor/antiferromagnet heterostructures, *Phys. Rev. B* **109**, 184504 (2024).
- [28] I. Bobkova, G. Bobkov, V. Gordeeva, and A. Bobkov, Neel proximity effect in superconductor/antiferromagnet heterostructures, arXiv:2408.11883 (2024).
- [29] E. H. Fyhn, A. Brataas, A. Qaiumzadeh, and J. Linder, Superconducting proximity effect and long-ranged triplets in dirty metallic antiferromagnets, *Phys. Rev. Lett.* **131**, 076001 (2023).
- [30] G. A. Bobkov, I. V. Bobkova, and A. M. Bobkov, Proximity effect in superconductor/antiferromagnet hybrids: Néel triplets and impurity suppression of superconductivity, *Phys. Rev. B* **108**, 054510 (2023).
- [31] L. Néel, Some new results on antiferromagnetism and ferromagnetism, *Rev. Mod. Phys.* **25**, 58 (1953).
- [32] M. I. Kaganov and V. M. Tsukernik, *The nature of magnetism* (MIR, 1985).
- [33] W. Nolting and W. D. Brewer, *Fundamentals of many-body physics* (Springer, 2008).
- [34] W. Nolting and A. Ramakanth, *Quantum theory of magnetism* (Springer Science & Business Media, 2009).
- [35] A. Aharoni, *Introduction to the Theory of Ferromagnetism*, Vol. 109 (Clarendon Press, 2000).
- [36] Y. Tserkovnyak, A. Brataas, G. E. W. Bauer, and B. I. Halperin, Nonlocal magnetization dynamics in ferromagnetic heterostructures, *Rev. Mod. Phys.* **77**, 1375 (2005).
- [37] A. Manchon, J. Železný, I. M. Miron, T. Jungwirth, J. Sinova, A. Thiaville, K. Garello, and P. Gambardella, Current-induced spin-orbit torques in ferromagnetic and antiferromagnetic systems, *Rev. Mod. Phys.* **91**, 035004 (2019).
- [38] V. Baltz, A. Manchon, M. Tsoi, T. Moriyama, T. Ono, and Y. Tserkovnyak, Antiferromagnetic spintronics, *Rev. Mod. Phys.* **90**, 015005 (2018).
- [39] A. Hirohata, K. Yamada, Y. Nakatani, I.-L. Prejbeanu, B. Diény, P. Pirro, and B. Hillebrands, Review on spintronics: Principles and device applications, *Journal of Magnetism and Magnetic Materials* **509**, 166711 (2020).
- [40] Editorial, New horizons in spintronics, *Nat. Mater.* **21**, 1 (2022).
- [41] A. Dal Din, O. Amin, P. Wadley, and K. Edmonds, Antiferromagnetic spintronics and beyond, *npj Spintronics* **2**, 25 (2024).
- [42] T. Jungwirth, J. Sinova, A. Manchon, X. Marti, J. Wunderlich, and C. Felser, The multiple directions of antiferromagnetic spintronics, *Nature Physics* **14**, 200 (2018).
- [43] T. Jungwirth, X. Marti, P. Wadley, and J. Wunderlich, Antiferromagnetic spintronics, *Nature Nanotechnology* **11**, 231 (2016).
- [44] Y. Noda, K. Ohno, and S. Nakamura, Momentum-dependent band spin splitting in semiconducting mno 2: a density functional calculation, *Physical Chemistry Chemical Physics* **18**, 13294 (2016).
- [45] K.-H. Ahn, A. Hariki, K.-W. Lee, and J. Kuneš, Antiferromagnetism in ruo₂ as *d*-wave pomeranchuk instability, *Phys. Rev. B* **99**, 184432 (2019).
- [46] S. Hayami, Y. Yanagi, and H. Kusunose, Momentum-dependent spin splitting by collinear antiferromagnetic ordering, *J. Phys. Soc. Jpn.* **88**, 123702 (2019).
- [47] L.-D. Yuan, Z. Wang, J.-W. Luo, E. I. Rashba, and A. Zunger, Giant momentum-dependent spin splitting in centrosymmetric low-*z* antiferromagnets, *Phys. Rev. B* **102**, 014422 (2020).
- [48] L. Šmejkal, R. González-Hernández, T. Jungwirth, and J. Sinova, Crystal time-reversal symmetry breaking and spontaneous hall effect in collinear antiferromagnets, *Sci. Adv.* **6**, eaaz8809 (2020).
- [49] H.-Y. Ma, M. Hu, N. Li, J. Liu, W. Yao, J.-F. Jia, and J. Liu, Multifunctional antiferromagnetic materials with giant piezomagnetism and noncollinear spin current, *Nat. Commun.* **12**, 2846 (2021).
- [50] T. Jungwirth, R. M. Fernandes, J. Sinova, and L. Šmejkal, Altermagnets and beyond: Nodal magnetically-ordered phases, arXiv: 2409.10034 (2024).
- [51] T. Jungwirth, R. M. Fernandes, E. Fradkin, A. H. MacDonald, J. Sinova, and L. Šmejkal, From supefluid ³he to altermagnets, arXiv: 2411.00717 (2024).
- [52] L. Šmejkal, J. Sinova, and T. Jungwirth, Emerging research landscape of altermagnetism, *Phys. Rev. X* **12**, 040501 (2022).
- [53] L. Šmejkal, J. Sinova, and T. Jungwirth, Beyond conventional ferromagnetism and antiferromagnetism: A phase with nonrelativistic spin and crystal rotation symmetry, *Phys. Rev. X* **12**, 031042 (2022).
- [54] Y. B. Kudasov, Topological band structure due to modified kramers degeneracy for electrons in a helical magnetic field, *Phys. Rev. B* **109**, L140402 (2024).
- [55] A. B. Hellenes, T. Jungwirth, R. Jaeschke-Ubiergo, A. Chakraborty, J. Sinova, and L. Šmejkal, P-wave magnets, arXiv:2309.01607 (2024).
- [56] B. Brekke, P. Sukhachov, H. G. Giil, A. Brataas, and J. Linder, Minimal models and transport properties of unconventional *p*-wave magnets, *Phys. Rev. Lett.* **133**, 236703 (2024).
- [57] V. Galitski and I. B. Spielman, Spin-orbit coupling in quantum gases, *Nature* **494**, 49 (2013).
- [58] A. Manchon, H. C. Koo, J. Nitta, S. M. Frolov, and R. A. Duine, New perspectives for rashba spin-orbit coupling, *Nat. Mater.* **14**, 871 (2015).
- [59] I. Mazin, Editorial: Altermagnetism—a new punch line of fundamental magnetism, *Phys. Rev. X* **12**, 040002 (2022).
- [60] L. Bai, W. Feng, S. Liu, L. Smejkal, Y. Mokrousov, and Y. Yao, Altermagnetism: Exploring new frontiers in magnetism and spintronics, *Advanced Functional Materials* **34**, 10.1002/adfm.202409327 (2024).
- [61] R. Tamang, S. Gurung, D. P. Rai, S. Brahim, and

- S. Lounis, Newly discovered magnetic phase: A brief review on altermagnets, arXiv:2412.05377 (2024).
- [62] M. Sigrist and K. Ueda, Phenomenological theory of unconventional superconductivity, *Rev. Mod. Phys.* **63**, 239 (1991).
- [63] K. Maki, Introduction to d -wave superconductivity, *AIP Conference Proceedings* **438**, 83 (1998).
- [64] S.-W. Cheong and F.-T. Huang, Altermagnetism with non-collinear spins, *npj Quantum Materials* **9**, 13 (2024).
- [65] Y. Guo, H. Liu, O. Janson, I. C. Fulga, J. van den Brink, and J. I. Facio, Spin-split collinear antiferromagnets: A large-scale ab-initio study, *Materials Today Physics* **32**, 100991 (2023).
- [66] F. Zhang, X. Cheng, Z. Yin, C. Liu, L. Deng, Y. Qiao, Z. Shi, S. Zhang, J. Lin, Z. Liu, M. Ye, Y. Huang, X. Meng, C. Zhang, T. Okuda, K. Shimada, S. Cui, Y. Zhao, G.-H. Cao, S. Qiao, J. Liu, and C. Chen, Crystal-symmetry-paired spin-valley locking in a layered room-temperature antiferromagnet, arXiv:2407.19555 (2024).
- [67] B. Jiang, M. Hu, J. Bai, Z. Song, C. Mu, G. Qu, W. Li, W. Zhu, H. Pi, Z. Wei, Y. Sun, Y. Huang, X. Zheng, Y. Peng, L. He, S. Li, J. Luo, Z. Li, G. Chen, H. Li, H. Weng, and T. Qian, Discovery of a metallic room-temperature d -wave altermagnet $\text{Kv}_2\text{Se}_2\text{O}$, arXiv:2408.00320 (2024).
- [68] M. Hu, X. Cheng, Z. Huang, and J. Liu, Catalogue of c -paired spin-valley locking in antiferromagnetic systems, arxiv:2407.02319 (2024).
- [69] K.-H. Ahn, A. Hariki, K.-W. Lee, and J. Kuneš, Antiferromagnetism in RuO_2 as d -wave pomeranchuk instability, *Phys. Rev. B* **99**, 184432 (2019).
- [70] O. Fedchenko, J. Minár, A. Akashdeep, S. W. D'Souza, D. Vasilyev, O. Tkach, L. Odenbreit, Q. L. Nguyen, D. Kutnyakhov, N. Wind, L. Wenthous, M. Scholz, K. Rossnagel, M. Hoesch, M. Aeschlimann, B. Stadtmueller, M. Kläui, G. Schoenhense, G. Jakob, T. Jungwirth, L. Šmejkal, J. Sinova, and H. J. Elmers, Observation of time-reversal symmetry breaking in the band structure of altermagnetic RuO_2 , *Science Advances* **10**, eadj4883 (2024).
- [71] Z. Lin, D. Chen, W. Lu, X. Liang, S. Feng, K. Yamagami, J. Osiecki, M. Leandersson, B. Thiagarajan, J. Liu, C. Felser, and J. Ma, Observation of giant spin splitting and d -wave spin texture in room temperature altermagnet RuO_2 , arXiv:2402.04995 (2024).
- [72] H. Reichlová, R. L. Seeger, R. González-Hernández, I. Kounta, R. Schlitz, D. Kriegner, P. Ritzinger, M. Lammel, M. Leiviskä, V. Petříček, P. Doležal, E. Schmoranzzerová, A. Bad'ura, A. Thomas, V. Baltz, L. Michez, J. Sinova, S. T. B. Goennenwein, T. Jungwirth, and L. Šmejkal, Macroscopic time reversal symmetry breaking by staggered spin-momentum interaction, arXiv: 2012.15651 (2021).
- [73] L. Han, X. Fu, R. Peng, X. Cheng, J. Dai, L. Liu, Y. Li, Y. Zhang, W. Zhu, H. Bai, Y. Zhou, S. Liang, C. Chen, Q. Wang, X. Chen, L. Yang, Y. Zhang, C. Song, J. Liu, and F. Pan, Electrical 180 switching of néel vector in spin-splitting antiferromagnet, *Sci. Adv.* **10**, eadn0479 (2024).
- [74] S. López-Moreno, A. H. Romero, J. Mejía-López, and A. Muñoz, First-principles study of pressure-induced structural phase transitions in MnF_2 , *Phys. Chem. Chem. Phys.* **18**, 33250 (2016).
- [75] S. Lee, S. Lee, S. Jung, J. Jung, D. Kim, Y. Lee, B. Seok, J. Kim, B. G. Park, L. Šmejkal, C.-J. Kang, and C. Kim, Broken kramers degeneracy in altermagnetic MnTe , *Phys. Rev. Lett.* **132**, 036702 (2024).
- [76] T. Osumi, S. Souma, T. Aoyama, K. Yamauchi, A. Honma, K. Nakayama, T. Takahashi, K. Ohgushi, and T. Sato, Observation of a giant band splitting in altermagnetic MnTe , *Phys. Rev. B* **109**, 115102 (2024).
- [77] J. Krempaský, L. Šmejkal, S. W. D'Souza, M. Hajlaoui, G. Springholz, K. Uhlířová, F. Alarab, P. C. Constantinou, V. Strocov, D. Usanov, W. R. Pudelko, R. González-Hernández, A. Birk Hellenes, Z. Jansa, H. Reichlová, Z. Šobáň, R. D. Gonzalez Betancourt, P. Wadley, J. Sinova, D. Kriegner, J. Minár, J. H. Dil, and T. Jungwirth, Altermagnetic lifting of kramers spin degeneracy, *Nature* **626**, 517 (2024).
- [78] Y.-P. Zhu, X. Chen, X.-R. Liu, Y. Liu, P. Liu, H. Zha, G. Qu, C. Hong, J. Li, Z. Jiang, *et al.*, Observation of plaid-like spin splitting in a noncoplanar antiferromagnet, *Nature* **626**, 523 (2024).
- [79] S. Reimers, L. Odenbreit, L. Šmejkal, V. N. Strocov, P. Constantinou, A. B. Hellenes, R. Jaeschke Ubierno, W. H. Campos, V. K. Bharadwaj, A. Chakraborty, T. Denneulin, W. Shi, R. E. Durnin-Borkowski, S. Das, M. Kläui, J. Sinova, and M. Jourdan, Direct observation of altermagnetic band splitting in CrSb thin films, *Nature Communications* **15**, 2116 (2024).
- [80] W. Lu, S. Feng, Y. Wang, D. Chen, Z. Lin, X. Liang, S. Liu, W. Feng, K. Yamagami, J. Liu, C. Felser, Q. Wu, and J. Ma, Observation of surface fermi arcs in altermagnetic weyl semimetal CrSb , arXiv: 2407.13497 (2024).
- [81] Y. Liu, H. Bai, Y. Song, Z. Ji, S. Lou, Z. Zhang, C. Song, and Q. Jin, Inverse altermagnetic spin splitting effect-induced terahertz emission in RuO_2 , *Advanced Optical Materials* **11**, 2300177 (2023).
- [82] C.-T. Liao, Y.-C. Wang, Y.-C. Tien, S.-Y. Huang, and D. Qu, Separation of inverse altermagnetic spin-splitting effect from inverse spin hall effect in RuO_2 , *Phys. Rev. Lett.* **133**, 056701 (2024).
- [83] H. Chen, Z. Wang, P. Qin, Z. Meng, X. Zhou, X. Wang, L. Liu, G. Zhao, Z. Duan, T. Zhang, J. Liu, D. Shao, and Z. Liu, Altermagnetic spin-splitting magnetoresistance, arXiv: 2412.18220 (2024).
- [84] N. J. Ghimire, A. Botana, J. Jiang, J. Zhang, Y.-S. Chen, and J. Mitchell, Large anomalous hall effect in the chiral-lattice antiferromagnet CoNb_3S_6 , *Nature Communications* **9**, 3280 (2018).
- [85] Z. Feng, X. Zhou, L. Šmejkal, L. Wu, Z. Zhu, H. Guo, R. González-Hernández, X. Wang, H. Yan, P. Qin, X. Zhang, H. Wu, H. Chen, Z. Meng, L. Liu, Z. Xia, J. Sinova, T. Jungwirth, and Z. Liu, An anomalous hall effect in altermagnetic ruthenium dioxide, *Nature Electronics* **5**, 735–743 (2022).
- [86] T. Tschirner, P. Keßler, R. D. Gonzalez Betancourt, T. Kotte, D. Kriegner, B. Büchner, J. Dufouleur, M. Kamp, V. Jovic, L. Šmejkal, J. Sinova, R. Claessen, T. Jungwirth, S. Moser, H. Reichlova, and L. Veyrat, Saturation of the anomalous hall effect at high magnetic fields in altermagnetic RuO_2 , *APL Materials* **11** (2023).
- [87] M. Wang, K. Tanaka, S. Sakai, Z. Wang, K. Deng, Y. Lyu, C. Li, D. Tian, S. Shen, N. Ogawa, *et al.*, Emergent zero-field anomalous hall effect in a reconstructed

- rutile antiferromagnetic metal, *Nat. Commun.* **14**, 8240 (2023).
- [88] X. Zhou, W. Feng, R.-W. Zhang, L. Šmejkal, J. Sinova, Y. Mokrousov, and Y. Yao, Crystal thermal transport in altermagnetic ruo_2 , *Phys. Rev. Lett.* **132**, 056701 (2024).
- [89] M. Leiviskä, J. Rial, A. Bad'ura, R. L. Seeger, I. Kounta, S. Beckert, D. Kriegner, I. Joumard, E. Schmoranzarová, J. Sinova, O. Gomonay, A. Thomas, S. T. B. Goennenwein, H. Reichlová, L. Šmejkal, L. Michez, T. Jungwirth, and V. Baltz, Anisotropy of the anomalous hall effect in thin films of the altermagnet candidate mn_5si_3 , *Phys. Rev. B* **109**, 224430 (2024).
- [90] D.-F. Shao, S.-H. Zhang, M. Li, C.-B. Eom, and E. Y. Tsymbal, Spin-neutral currents for spintronics, *Nature Communications* **12**, 7061 (2021).
- [91] R. González-Hernández, L. Šmejkal, K. Výborný, Y. Yahagi, J. Sinova, T. c. v. Jungwirth, and J. Železný, Efficient electrical spin splitter based on nonrelativistic collinear antiferromagnetism, *Phys. Rev. Lett.* **126**, 127701 (2021).
- [92] H. Bai, L. Han, X. Y. Feng, Y. J. Zhou, R. X. Su, Q. Wang, L. Y. Liao, W. X. Zhu, X. Z. Chen, F. Pan, X. L. Fan, and C. Song, Observation of spin splitting torque in a collinear antiferromagnet ruo_2 , *Phys. Rev. Lett.* **128**, 197202 (2022).
- [93] A. Bose, N. J. Schreiber, R. Jain, D.-F. Shao, H. P. Nair, J. Sun, X. S. Zhang, D. A. Muller, E. Y. Tsymbal, D. G. Schlom, and D. C. Ralph, Tilted spin current generated by the collinear antiferromagnet ruthenium dioxide, *Nature Electronics* **5**, 267–274 (2022).
- [94] S. Karube, T. Tanaka, D. Sugawara, N. Kadoguchi, M. Kohda, and J. Nitta, Observation of spin-splitter torque in collinear antiferromagnetic ruo_2 , *Phys. Rev. Lett.* **129**, 137201 (2022).
- [95] H. Bai, Y. C. Zhang, Y. J. Zhou, P. Chen, C. H. Wan, L. Han, W. X. Zhu, S. X. Liang, Y. C. Su, X. F. Han, F. Pan, and C. Song, Efficient spin-to-charge conversion via altermagnetic spin splitting effect in antiferromagnet ruo_2 , *Phys. Rev. Lett.* **130**, 216701 (2023).
- [96] Q. Cui, Y. Zhu, X. Yao, P. Cui, and H. Yang, Giant spin-hall and tunneling magnetoresistance effects based on a two-dimensional nonrelativistic antiferromagnetic metal, *Phys. Rev. B* **108**, 024410 (2023).
- [97] Z. Li, Z. Zhang, X. Lu, and Y. Xu, Spin splitting in altermagnetic ruo_2 enables field-free spin-orbit torque switching via dominant out-of-plane spin polarization, *arXiv: 2407.07447* (2024).
- [98] C. Pan, S. Hu, F. Yang, D. Yang, W. Fan, Z. Shi, L. Pan, S. Zhou, and X. Qiu, Unveiling the nonrelativistic spin current polarization in an altermagnet, *arXiv:2412.18937* (2024).
- [99] X. Zhou, W. Feng, X. Yang, G.-Y. Guo, and Y. Yao, Crystal chirality magneto-optical effects in collinear antiferromagnets, *Phys. Rev. B* **104**, 024401 (2021).
- [100] N. Wang, J. Chen, N. Ding, H. Zhang, S. Dong, and S.-S. Wang, Magneto-optical kerr effect and magnetoelasticity in a weakly ferromagnetic ruf_4 monolayer, *Phys. Rev. B* **106**, 064435 (2022).
- [101] I. Gray, Q. Deng, Q. Tian, M. Chilcote, J. S. Dodge, M. Brahlek, and L. Wu, Time-resolved magneto-optical effects in the altermagnet candidate mnte , *arXiv: 2404.05020* (2024).
- [102] A. Hariki, A. Dal Din, O. J. Amin, T. Yamaguchi, A. Badura, D. Kriegner, K. W. Edmonds, R. P. Campion, P. Wadley, D. Backes, L. S. I. Veiga, S. S. Dhesi, G. Springholz, L. Šmejkal, K. Výborný, T. Jungwirth, and J. Kuneš, X-ray magnetic circular dichroism in altermagnetic $\alpha\text{-mnte}$, *Phys. Rev. Lett.* **132**, 176701 (2024).
- [103] A. Hariki, Y. Takahashi, and J. Kuneš, X-ray magnetic circular dichroism in ruo_2 , *Phys. Rev. B* **109**, 094413 (2024).
- [104] A. Kimel, T. Rasing, and B. Ivanov, Optical read-out and control of antiferromagnetic néel vector in altermagnets and beyond, *J.f Magn. Magn. Mater.* **598**, 172039 (2024).
- [105] M. Naka, S. Hayami, H. Kusunose, Y. Yanagi, Y. Motome, and H. Seo, Anomalous hall effect in κ -type organic antiferromagnets, *Phys. Rev. B* **102**, 075112 (2020).
- [106] M. Naka, Y. Motome, and H. Seo, Anomalous hall effect in antiferromagnetic perovskites, *Phys. Rev. B* **106**, 195149 (2022).
- [107] T. P. T. Nguyen and K. Yamauchi, Ab initio prediction of anomalous hall effect in antiferromagnetic cacro_3 , *Phys. Rev. B* **107**, 155126 (2023).
- [108] X.-Y. Hou, H.-C. Yang, Z.-X. Liu, P.-J. Guo, and Z.-Y. Lu, Large intrinsic anomalous hall effect in both nb_2feb_2 and ta_2feb_2 with collinear antiferromagnetism, *Phys. Rev. B* **107**, L161109 (2023).
- [109] A. Fakhredine, R. M. Sattigeri, G. Cuono, and C. Autieri, Interplay between altermagnetism and nonsymorphic symmetries generating large anomalous hall conductivity by semi-dirac points induced anticrossings, *Phys. Rev. B* **108**, 115138 (2023).
- [110] M. Naka, S. Hayami, H. Kusunose, Y. Yanagi, Y. Motome, and H. Seo, Spin current generation in organic antiferromagnets, *Nat. Commun.* **10**, 4305 (2019).
- [111] M. Naka, Y. Motome, and H. Seo, Perovskite as a spin current generator, *Phys. Rev. B* **103**, 125114 (2021).
- [112] Q. Cui, B. Zeng, P. Cui, T. Yu, and H. Yang, Efficient spin seebeck and spin nernst effects of magnons in altermagnets, *Phys. Rev. B* **108**, L180401 (2023).
- [113] C. Sun and J. Linder, Spin pumping from a ferromagnetic insulator into an altermagnet, *Phys. Rev. B* **108**, L140408 (2023).
- [114] E. W. Hodt and J. Linder, Spin pumping in an altermagnet/normal-metal bilayer, *Phys. Rev. B* **109**, 174438 (2024).
- [115] E. W. Hodt, P. Sukhachov, and J. Linder, Interface-induced magnetization in altermagnets and antiferromagnets, *Phys. Rev. B* **110**, 054446 (2024).
- [116] M. Ezawa, Third-order and fifth-order nonlinear spin-current generation in g -wave and i -wave altermagnets and perfect spin-current diode based on f -wave magnets, *arXiv:2411.16036* (2024).
- [117] H.-J. Lin, S.-B. Zhang, H.-Z. Lu, and X. C. Xie, Coulomb drag in altermagnets, *arXiv: 2412.13927* (2024).
- [118] Y. Chen, X. Liu, H.-Z. Lu, and X. C. Xie, Electrical switching of altermagnetism, *arXiv: 2412.20938* (2024).
- [119] X.-J. Yi, Y. Mao, X. Lu, and Q.-F. Sun, Spin splitting nernst effect in altermagnets, *Phys. Rev. B* **111**, 035423 (2025).
- [120] P. A. McClarty and J. G. Rau, Landau theory of altermagnetism, *Phys. Rev. Lett.* **132**, 176702 (2024).
- [121] M. Roig, A. Kreisel, Y. Yu, B. M. Andersen, and D. F.

- Agterberg, Minimal models for altermagnetism, *Phys. Rev. B* **110**, 144412 (2024).
- [122] Y.-X. Li, Y. Liu, and C.-C. Liu, Creation and manipulation of higher-order topological states by altermagnets, *Phys. Rev. B* **109**, L201109 (2024).
- [123] R. Hoyer, R. Jaeschke-Ubiergo, K.-H. Ahn, L. Šmejkal, and A. Mook, Spontaneous crystal thermal hall effect in insulating altermagnets, *Phys. Rev. B* **111**, L020412 (2025).
- [124] L. V. Pupim and M. S. Scheurer, Adatom engineering magnetic order in superconductors: Applications to altermagnetic superconductivity (2024), arXiv:2411.02489.
- [125] A. Chakraborty, A. B. Hellenes, R. Jaeschke-Ubiergo, T. Jungwirth, L. Šmejkal, and J. Sinova, Highly efficient non-relativistic edelstein effect in p -wave magnets, arXiv: 2411.16378 (2025).
- [126] P. Sukhachov and J. Linder, Impurity-induced friedel oscillations in altermagnets and p -wave magnets, *Phys. Rev. B* **110**, 205114 (2024).
- [127] M. Ezawa, Purely electrical detection of the néel vector of p -wave magnets based on linear and nonlinear conductivities, arXiv:2410.21854 (2024).
- [128] I. I. Mazin, Notes on altermagnetism and superconductivity, arXiv: 2203.05000 (2022).
- [129] S. Sumita, M. Naka, and H. Seo, Fulde-ferrell-larkin-ovchinnikov state induced by antiferromagnetic order in κ -type organic conductors, *Phys. Rev. Res.* **5**, 043171 (2023).
- [130] D. Chakraborty and A. M. Black-Schaffer, Zero-field finite-momentum and field-induced superconductivity in altermagnets, *Phys. Rev. B* **110**, L060508 (2024).
- [131] A. Bose, S. Vadnais, and A. Paramakanti, Altermagnetism and superconductivity in a multiorbital $t - j$ model, *Phys. Rev. B* **110**, 205120 (2024).
- [132] G. Sim and J. Knolle, Pair density waves and supercurrent diode effect in altermagnets, arXiv: 2407.01513 (2024).
- [133] S. Hong, M. J. Park, and K.-M. Kim, Unconventional p -wave and finite-momentum superconductivity induced by altermagnetism through the formation of bogoliubov fermi surface, arXiv: 2407.02059 (2024).
- [134] K. Mukasa and Y. Masaki, Finite-momentum superconductivity in two-dimensional altermagnets with a rashba-type spin-orbit coupling, arXiv: 2409.08972 (2024).
- [135] M. Uchida, T. Nomoto, M. Musashi, R. Arita, and M. Kawasaki, Superconductivity in uniquely strained RuO_2 films, *Phys. Rev. Lett.* **125**, 147001 (2020).
- [136] J. P. Ruf, H. Paik, N. J. Schreiber, H. P. Nair, L. Miao, J. K. Kawasaki, J. N. Nelson, B. D. Faeth, Y. Lee, B. H. Goodge, *et al.*, Strain-stabilized superconductivity, *Nature Communications* **12**, 59 (2021).
- [137] C. A. Occhialini, L. G. P. Martins, S. Fan, V. Bisogni, T. Yasunami, M. Musashi, M. Kawasaki, M. Uchida, R. Comin, and J. Pellicciari, Strain-modulated anisotropic electronic structure in superconducting RuO_2 films, *Phys. Rev. Mater.* **6**, 084802 (2022).
- [138] I. Mazin, R. González-Hernández, and L. Šmejkal, Induced monolayer altermagnetism in $\text{mmp}(s,se)_3$ and fese , arXiv: 2309.02355 (2023).
- [139] R. Soto-Garrido and E. Fradkin, Pair-density-wave superconducting states and electronic liquid-crystal phases, *Phys. Rev. B* **89**, 165126 (2014).
- [140] H. O. Jeschke, M. Shimizu, and I. I. Mazin, Highly unusual, doubly-strongly-correlated, altermagnetic, 3d analogue of parent compounds of high- t_c cuprates, arXiv:2403.02201 (2024).
- [141] M. Domański, Z. Mazej, and W. Grochala, A unique two-dimensional silver (ii) antiferromagnet Cu [Ag(SO₄)₂] and perspectives for its further modifications, *Chemistry—A European Journal* **29**, e202302042 (2023).
- [142] D. Zhu, Z.-Y. Zhuang, Z. Wu, and Z. Yan, Topological superconductivity in two-dimensional altermagnetic metals, *Phys. Rev. B* **108**, 184505 (2023).
- [143] B. Brekke, A. Brataas, and A. Sudbø, Two-dimensional altermagnets: Superconductivity in a minimal microscopic model, *Phys. Rev. B* **108**, 224421 (2023).
- [144] C. Autieri, G. Cuono, D. Chakraborty, P. Gentile, and A. M. Black-Schaffer, Conditions for orbital-selective altermagnetism in SrRuO_4 : tight-binding model, similarities with cuprates, and implications for superconductivity, 2501.14378 (2025).
- [145] K. Maeda, Y. Fukaya, K. Yada, B. Lu, Y. Tanaka, and J. Cayao, Classification of pair symmetries in superconductors with unconventional magnetism, arXiv: 2501.08646 (2025).
- [146] Y. Fukaya, K. Maeda, K. Yada, J. Cayao, Y. Tanaka, and B. Lu, Josephson effect and odd-frequency pairing in superconducting junctions with unconventional magnets, *Phys. Rev. B* **111**, 064502 (2025).
- [147] D. Chakraborty and A. M. Black-Schaffer, Constraints on superconducting pairing in altermagnets, arXiv: 2408.03999 (2024).
- [148] P. Sukhachov, H. G. Giil, B. Brekke, and J. Linder, Coexistence of p -wave magnetism and superconductivity, arXiv: 2412.14245 (2025).
- [149] P. Chatterjee and V. Juričić, Interplay between altermagnetism and topological superconductivity in an unconventional superconducting platform, arXiv: 2501.05451 (2025).
- [150] C. Sun, A. Brataas, and J. Linder, Andreev reflection in altermagnets, *Phys. Rev. B* **108**, 054511 (2023).
- [151] M. Papaj, Andreev reflection at the altermagnet-superconductor interface, *Phys. Rev. B* **108**, L060508 (2023).
- [152] K. Maeda, B. Lu, K. Yada, and Y. Tanaka, Theory of tunneling spectroscopy in unconventional p -wave magnet-superconductor hybrid structures, *J. Phys. Soc. Jpn* **93**, 114703 (2024).
- [153] Y. Nagae, A. P. Schnyder, and S. Ikegaya, Spin-polarized specular andreev reflections in altermagnets, arXiv:2403.07117 (2024).
- [154] Z. P. Niu and Z. Yang, Orientation-dependent andreev reflection in an altermagnet/altermagnet/superconductor junction, *J. Phys. D: Appl. Phys.* **57**, 395301 (2024).
- [155] M. Wei, L. Xiang, F. Xu, L. Zhang, G. Tang, and J. Wang, Gapless superconducting state and mirage gap in altermagnets, *Phys. Rev. B* **109**, L201404 (2024).
- [156] W. Zhao, Y. Fukaya, P. Buset, J. Cayao, Y. Tanaka, and B. Lu, Orientation-dependent transport property with an altermagnetic interlayer in proximity to a d -wave superconductor, arXiv:2501.12141 (2025).
- [157] S. Das and A. Soori, Crossed andreev reflection in altermagnets, *Phys. Rev. B* **109**, 245424 (2024).
- [158] Z. P. Niu and Y. M. Zhang, Electrically controlled crossed andreev reflection in altermag-

- net/superconductor/altersmagnet junctions, *Supercond. Sci. Technol.* **37**, 055012 (2024).
- [159] D. Kazmin, V. Esin, Y. Barash, A. Timonina, N. Kolesnikov, and E. Deviatov, Andreev reflection for mnte altersmagnet candidate, *Physica B: Condensed Matter* **696**, 416602 (2025).
- [160] T. M. Klapwijk, Proximity effect from an andreev perspective, *Journal of superconductivity* **17**, 593 (2004).
- [161] A. Maiani and R. S. Souto, Impurity states in altersmagnetic superconductors, arXiv: 2409.01008 (2024).
- [162] B. D. Josephson, Possible new effects in superconductive tunnelling, *Phys. Lett.* **1**, 251 (1962).
- [163] K. K. Likharev, Superconducting weak links, *Rev. Mod. Phys.* **51**, 101 (1979).
- [164] S. Kashiwaya and Y. Tanaka, Tunnelling effects on surface bound states in unconventional superconductors, *Reports on Progress in Physics* **63**, 1641 (2000).
- [165] A. A. Golubov, M. Y. Kupriyanov, and E. Il'ichev, The current-phase relation in Josephson junctions, *Rev. Mod. Phys.* **76**, 411 (2004).
- [166] C. Beenakker, Three "universal" mesoscopic Josephson effects, in *Transport phenomena in mesoscopic systems: Proceedings of the 14th Taniguchi symposium, Shima, Japan, November 10-14, 1991*, Vol. 109 (Springer-Verlag, 1992) p. 235.
- [167] J. Cayao, *Hybrid superconductor-semiconductor nanowire junctions as useful platforms to study Majorana bound states*, Phd thesis, Autonomous University of Madrid (UAM), Madrid, Spain (2016), see Chapter.
- [168] J. Sauls, Andreev bound states and their signatures, *Philos. Trans. Royal Soc. A* **376**, 20180140 (2018).
- [169] M. Eschrig, Theory of andreev bound states in sfs junctions and sf proximity devices, *Philosophical Transactions of the Royal Society A: Mathematical, Physical and Engineering Sciences* **376**, 20150149 (2018).
- [170] T. Mizushima and K. Machida, Multifaceted properties of andreev bound states: interplay of symmetry and topology, *Philos. Trans. Royal Soc. A* **376**, 20150355 (2018).
- [171] V. Ambegaokar and A. Baratoff, Tunneling between superconductors, *Phys. Rev. Lett.* **10**, 486 (1963).
- [172] I. Kulik and A. Omel'Yanchuk, Contribution to the microscopic theory of the Josephson effect in superconducting bridges, *JETP Lett.* **21**, 216 (1975).
- [173] I. Kulik and A. Omel'Yanchuk, Josephson effect in superconductive bridges: microscopic theory, *Soviet Journal of Low Temperature Physics* **4**, 142 (1978).
- [174] A. Furusaki and M. Tsukada, Current-carrying states in josephson junctions, *Phys. Rev. B* **43**, 10164 (1991).
- [175] A. Furusaki and M. Tsukada, Dc Josephson effect and Andreev reflection, *Solid State Commun.* **78**, 299 (1991).
- [176] A. Furusaki, H. Takayanagi, and M. Tsukada, Josephson effect of the superconducting quantum point contact, *Phys. Rev. B* **45**, 10563 (1992).
- [177] A. Furusaki, Josephson current carried by Andreev levels in superconducting quantum point contacts, *Superlattices and Microstructures* **25**, 809 (1999).
- [178] Y. Asano, Direct-current Josephson effect in SNS junctions of anisotropic superconductors, *Phys. Rev. B* **64**, 224515 (2001).
- [179] Y. Asano, Y. Tanaka, and S. Kashiwaya, Anomalous Josephson effect in p -wave dirty junctions, *Phys. Rev. Lett.* **96**, 097007 (2006).
- [180] J. Cayao, A. M. Black-Schaffer, E. Prada, and R. Aguado, Andreev spectrum and supercurrents in nanowire-based SNS junctions containing Majorana bound states, *Beilstein J. Nanotechnol.* **9**, 1339 (2018).
- [181] J. A. Ouassou, A. Brataas, and J. Linder, dc josephson effect in altersmagets, *Phys. Rev. Lett.* **131**, 076003 (2023).
- [182] C. W. J. Beenakker and T. Vakhtel, Phase-shifted andreev levels in an altersmagnet josephson junction, *Phys. Rev. B* **108**, 075425 (2023).
- [183] S.-B. Zhang, L.-H. Hu, and T. Neupert, Finite-momentum Cooper pairing in proximitized altersmagets, *Nat. Commun.* **15**, 1801 (2024).
- [184] B. Lu, K. Maeda, H. Ito, K. Yada, and Y. Tanaka, φ josephson junction induced by altersmagnetism, *Phys. Rev. Lett.* **133**, 226002 (2024).
- [185] H.-P. Sun, S.-B. Zhang, C.-A. Li, and B. Trauzettel, Tunable second-order josephson response in altersmagets, arXiv: 2407.19413 (2024).
- [186] Q. Cheng and Q.-F. Sun, Orientation-dependent josephson effect in spin-singlet superconductor/altersmagnet/spin-triplet superconductor junctions, *Phys. Rev. B* **109**, 024517 (2024).
- [187] Y. Tanaka and S. Kashiwaya, Theory of the josephson effect in d -wave superconductors, *Phys. Rev. B* **53**, R11957 (1996).
- [188] Y. Tanaka and S. Kashiwaya, Theory of josephson effects in anisotropic superconductors, *Phys. Rev. B* **56**, 892 (1997).
- [189] A. Buzdin and A. E. Koshelev, Periodic alternating 0- and π -junction structures as realization of φ -josephson junctions, *Phys. Rev. B* **67**, 220504 (2003).
- [190] E. Goldobin, D. Koelle, R. Kleiner, and A. Buzdin, Josephson junctions with second harmonic in the current-phase relation: Properties of φ junctions, *Phys. Rev. B* **76**, 224523 (2007).
- [191] Y.-X. Li, Realizing tunable higher-order topological superconductors with altersmagets, *Phys. Rev. B* **109**, 224502 (2024).
- [192] S. A. A. Ghorashi, T. L. Hughes, and J. Cano, Altersmagnetic routes to majorana modes in zero net magnetization, *Phys. Rev. Lett.* **133**, 106601 (2024).
- [193] Y.-X. Li and C.-C. Liu, Majorana corner modes and tunable patterns in an altersmagnet heterostructure, *Phys. Rev. B* **108**, 205410 (2023).
- [194] Z.-T. Sun, X. Feng, Y.-M. Xie, B. T. Zhou, J.-X. Hu, and K. T. Law, Pseudo-ising superconductivity induced by p -wave magnetism, arXiv: 2501.10960 (2025).
- [195] Y. Nagae, L. Katayama, and S. Ikegaya, Majorana flat bands and anomalous proximity effects in p -wave magnet-superconductor hybrid systems, arXiv: 2502.02053 (2025).
- [196] D. Mondal, A. Pal, A. Saha, and T. Nag, Distinguishing between topological majorana and trivial zero modes via transport and shot noise study in an altersmagnet heterostructure, arXiv: 2409.08009 (2024).
- [197] O. A. Awoga, J. Cayao, and A. M. Black-Schaffer, Supercurrent detection of topologically trivial zero-energy states in nanowire junctions, *Phys. Rev. Lett.* **123**, 117001 (2019).
- [198] J. Cayao and A. M. Black-Schaffer, Distinguishing trivial and topological zero-energy states in long nanowire junctions, *Phys. Rev. B* **104**, L020501 (2021).
- [199] L. Baldo, L. G. D. Da Silva, A. M. Black-Schaffer, and

- J. Cayao, Zero-frequency supercurrent susceptibility signatures of trivial and topological zero-energy states in nanowire junctions, *Supercond. Sci. Technol.* **36**, 034003 (2023).
- [200] B. i. e. i. f. m. c. Pekerten, J. D. Pakizer, B. Hawn, and A. Matos-Abiague, Anisotropic topological superconductivity in Josephson junctions, *Phys. Rev. B* **105**, 054504 (2022).
- [201] E. Prada, P. San-Jose, M. W. de Moor, A. Geresdi, E. J. Lee, J. Klinovaja, D. Loss, J. Nygård, R. Aguado, and L. P. Kouwenhoven, From andreev to majorana bound states in hybrid superconductor–semiconductor nanowires, *Nat. Rev. Phys.* **2**, 575 (2020).
- [202] D. Bagrets and A. Altland, Class *D* spectral peak in Majorana quantum wires, *Phys. Rev. Lett.* **109**, 227005 (2012).
- [203] D. I. Pikulin, J. P. Dahlhaus, M. Wimmer, H. Schomerus, and C. W. J. Beenakker, A zero-voltage conductance peak from weak antilocalization in a Majorana nanowire, *New J. Phys.* **14**, 125011 (2012).
- [204] G. Kells, D. Meidan, and P. W. Brouwer, Near-zero-energy end states in topologically trivial spin-orbit coupled superconducting nanowires with a smooth confinement, *Phys. Rev. B* **86**, 100503 (2012).
- [205] J. Cayao, E. Prada, P. San-Jose, and R. Aguado, SNS junctions in nanowires with spin-orbit coupling: Role of confinement and helicity on the subgap spectrum, *Phys. Rev. B* **91**, 024514 (2015).
- [206] E. Prada, P. San-Jose, and R. Aguado, Transport spectroscopy of *ns* nanowire junctions with Majorana fermions, *Phys. Rev. B* **86**, 180503 (2012).
- [207] C. Reeg, O. Dmytruk, D. Chevallier, D. Loss, and J. Klinovaja, Zero-energy andreev bound states from quantum dots in proximitized rashba nanowires, *Phys. Rev. B* **98**, 245407 (2018).
- [208] F. Domínguez, J. Cayao, P. San-Jose, R. Aguado, A. L. Yeyati, and E. Prada, Zero-energy pinning from interactions in Majorana nanowires, *npj Quantum Mater.* **2**, 13 (2017).
- [209] O. Dmytruk, D. Loss, and J. Klinovaja, Pinning of Andreev bound states to zero energy in two-dimensional superconductor–semiconductor rashba heterostructures, *Phys. Rev. B* **102**, 245431 (2020).
- [210] S. Das Sarma and H. Pan, Disorder-induced zero-bias peaks in Majorana nanowires, *Phys. Rev. B* **103**, 195158 (2021).
- [211] O. A. Awoga, J. Cayao, and A. M. Black-Schaffer, Robust topological superconductivity in weakly coupled nanowire–superconductor hybrid structures, *Phys. Rev. B* **105**, 144509 (2022).
- [212] J. Cayao and P. Buset, Confinement-induced zero-bias peaks in conventional superconductor hybrids, *Phys. Rev. B* **104**, 134507 (2021).
- [213] P. Marra and A. Nigro, Majorana/andreev crossover and the fate of the topological phase transition in inhomogeneous nanowires, *Journal of Physics: Condensed Matter* **34**, 124001 (2022).
- [214] B. S. de Mendonça, A. L. R. Manesco, N. Sandler, and L. G. G. V. Dias da Silva, Near zero energy Caroli–de Gennes–Matricon vortex states in the presence of impurities, *Phys. Rev. B* **107**, 184509 (2023).
- [215] O. A. Awoga, M. Leijnse, A. M. Black-Schaffer, and J. Cayao, Mitigating disorder-induced zero-energy states in weakly coupled superconductor–semiconductor hybrid systems, *Phys. Rev. B* **107**, 184519 (2023).
- [216] O. A. Awoga and J. Cayao, Identifying trivial and majorana zero-energy modes using the majorana polarization, *Phys. Rev. B* **110**, 165404 (2024).
- [217] J. Cayao, Non-hermitian zero-energy pinning of andreev and majorana bound states in superconductor–semiconductor systems, *Phys. Rev. B* **110**, 085414 (2024).
- [218] V. K. Vimal and J. Cayao, Entanglement measures of majorana bound states, *Phys. Rev. B* **110**, 224510 (2024).
- [219] E. Ahmed, S. Tamura, Y. Tanaka, and J. Cayao, Odd-frequency pairing due to majorana and trivial andreev bound states, arXiv: 2412.14439 (2024).
- [220] S. Banerjee and M. S. Scheurer, Altermagnetic superconducting diode effect, *Phys. Rev. B* **110**, 024503 (2024).
- [221] Q. Cheng, Y. Mao, and Q.-F. Sun, Field-free Josephson diode effect in altermagnet/normal metal/altermagnet junctions, *Phys. Rev. B* **110**, 014518 (2024).
- [222] D. Chakraborty and A. M. Black-Schaffer, Perfect superconducting diode effect in altermagnets, arXiv:2408.07747 (2024).
- [223] J. Cayao, N. Nagaosa, and Y. Tanaka, Enhancing the Josephson diode effect with majorana bound states, *Phys. Rev. B* **109**, L081405 (2024).
- [224] Y. Tanaka, B. Lu, and N. Nagaosa, Theory of giant diode effect in *d*-wave superconductor junctions on the surface of a topological insulator, *Phys. Rev. B* **106**, 214524 (2022).
- [225] B. Lu, S. Ikegaya, P. Buset, Y. Tanaka, and N. Nagaosa, Tunable Josephson diode effect on the surface of topological insulators, *Phys. Rev. Lett.* **131**, 096001 (2023).
- [226] P.-H. Fu, Y. Xu, C. H. Lee, S. A. Yang, Y. S. Ang, and J.-F. Liu, Field-effect Josephson diode via asymmetric spin-momentum locking states, arXiv:2212.01980 (2023).
- [227] F. Ando, Y. Miyasaka, T. Li, J. Ishizuka, T. Arakawa, Y. Shiota, T. Moriyama, Y. Yanase, and T. Ono, Observation of superconducting diode effect, *Nature* **584**, 373 (2020).
- [228] K. Misaki and N. Nagaosa, Theory of the nonreciprocal Josephson effect, *Phys. Rev. B* **103**, 245302 (2021).
- [229] M. Davydova, S. Prembabu, and L. Fu, Universal Josephson diode effect, *Sci. Adv.* **8**, eabo0309 (2022).
- [230] A. Daido, Y. Ikeda, and Y. Yanase, Intrinsic superconducting diode effect, *Phys. Rev. Lett.* **128**, 037001 (2022).
- [231] J. J. He, Y. Tanaka, and N. Nagaosa, A phenomenological theory of superconductor diodes, *New J. Phys.* **24**, 053014 (2022).
- [232] B. Pal, A. Chakraborty, P. K. Sivakumar, M. Davydova, A. K. Gopi, A. K. Pandeya, J. A. Krieger, Y. Zhang, M. Date, S. Ju, *et al.*, Josephson diode effect from Cooper pair momentum in a topological semimetal, *Nat. Phys.* **18**, 1228 (2022).
- [233] G. P. Mazur, N. van Loo, D. van Driel, J. Y. Wang, G. Badawy, S. Gazibegovic, E. P. A. M. Bakkers, and L. P. Kouwenhoven, The gate-tunable Josephson diode, arXiv:2211.14283 (2022).
- [234] M. Trahms, L. Melischek, J. F. Steiner, B. Mahendru, I. Tamir, N. Bogdanoff, O. Peters, G. Reecht, C. B. Winkelmann, F. von Oppen, and K. J. Franke, Diode ef-

- fect in Josephson junctions with a single magnetic atom, *Nature* **615**, 628 (2023).
- [235] J.-X. Hu, Z.-T. Sun, Y.-M. Xie, and K. T. Law, Josephson diode effect induced by valley polarization in twisted bilayer graphene, *Phys. Rev. Lett.* **130**, 266003 (2023).
- [236] A. Costa, J. Fabian, and D. Kochan, Microscopic study of the Josephson supercurrent diode effect in Josephson junctions based on two-dimensional electron gas, *Phys. Rev. B* **108**, 054522 (2023).
- [237] M. Nadeem, M. S. Fuhrer, and X. Wang, The superconducting diode effect, *Nat. Rev. Phys.* **5**, 558 (2023).
- [238] P.-H. Fu, S. Mondal, J.-F. Liu, Y. Tanaka, and J. Cayao, Floquet engineering spin-triplet Cooper pairs in unconventional magnets, In preparation (2025).
- [239] A. A. Zyuzin, Magnetoelectric effect in superconductors with d -wave magnetization, *Phys. Rev. B* **109**, L220505 (2024).
- [240] J.-X. Hu, O. Matsyshyn, and J. C. W. Song, Nonlinear superconducting magnetoelectric effect, *Phys. Rev. Lett.* **134**, 026001 (2025).
- [241] L. Šmejkal, A. H. MacDonald, J. Sinova, S. Nakatsuji, and T. Jungwirth, Anomalous Hall antiferromagnets, arXiv: 2107.03321 (2021).
- [242] S. Fukami, V. O. Lorenz, and O. Gomonay, Antiferromagnetic spintronics, *Journal of Applied Physics* **128**, 070401 (2020).
- [243] A. Kurenkov, S. Fukami, and H. Ohno, Neuromorphic computing with antiferromagnetic spintronics, *Journal of Applied Physics* **128**, 010902 (2020).
- [244] S. Wolf, D. Awschalom, R. Buhrman, J. Daughton, v. S. von Molnár, M. Roukes, A. Y. Chtchelkanova, and D. Treger, Spintronics: a spin-based electronics vision for the future, *science* **294**, 1488 (2001).
- [245] I. Žutić, J. Fabian, and S. Das Sarma, Spintronics: Fundamentals and applications, *Rev. Mod. Phys.* **76**, 323 (2004).
- [246] C. Chappert, A. Fert, and F. N. Van Dau, The emergence of spin electronics in data storage, *Nature Materials* **6**, 813 (2007).
- [247] S. D. Bader and S. S. P. Parkin, Spintronics, *Annu. Rev. Condens. Matter Phys.* **1**, 71 (2010).
- [248] H. Zhang, D. E. Liu, M. Wimmer, and L. P. Kouwenhoven, Next steps of quantum transport in majorana nanowire devices, *Nat. Commun.* **10**, 5128 (2019).
- [249] S. Hayami, Y. Yanagi, and H. Kusunose, Bottom-up design of spin-split and reshaped electronic band structures in antiferromagnets without spin-orbit coupling: Procedure on the basis of augmented multipoles, *Phys. Rev. B* **102**, 144441 (2020).
- [250] I. I. Mazin, K. Koepernik, M. D. Johannes, R. González-Hernández, and L. Šmejkal, Prediction of unconventional magnetism in doped FeSb₂, *Proc. Natl. Acad. Sci. U.S.A.* **118**, e2108924118 (2021).
- [251] S. Bhowal and N. A. Spaldin, Ferroically ordered magnetic octupoles in d -wave altermagnets, *Phys. Rev. X* **14**, 011019 (2024).
- [252] L. Šmejkal, A. Marmodoro, K.-H. Ahn, R. González-Hernández, I. Turek, S. Mankovsky, H. Ebert, S. W. D'Souza, O. c. v. Šipr, J. Sinova, and T. c. v. Jungwirth, Chiral magnons in altermagnetic RuO₂, *Phys. Rev. Lett.* **131**, 256703 (2023).
- [253] V. Baltz, A. Hoffmann, S. Emori, D.-F. Shao, and T. Jungwirth, Emerging materials in antiferromagnetic spintronics, *APL Materials* **12**, 030401 (2024).
- [254] M. Weber, K. Leckron, L. Haag, R. Jaeschke-Ubiergo, L. Šmejkal, J. Sinova, and H. C. Schneider, Ultrafast electron dynamics in altermagnetic materials, 2411.08160 (2024).
- [255] L. Šmejkal, A. B. Hellènes, R. González-Hernández, J. Sinova, and T. Jungwirth, Giant and tunneling magnetoresistance in unconventional collinear antiferromagnets with nonrelativistic spin-momentum coupling, *Phys. Rev. X* **12**, 011028 (2022).
- [256] Z. Jin, Z. Zeng, Y. Cao, and P. Yan, Skyrmion Hall effect in altermagnets, arXiv: 2407.03959 (2024).
- [257] P. Werner, M. Lysne, and Y. Murakami, High harmonic generation in altermagnets (2024), arXiv:2407.07752 [cond-mat.mes-hall].
- [258] K. D. Belashchenko, Giant strain-induced spin splitting effect in mntc, a g -wave altermagnetic semiconductor, arXiv: 2407.20440 (2024).
- [259] D. Zhu, D. Liu, Z.-Y. Zhuang, Z. Wu, and Z. Yan, Field-sensitive dislocation bound states in two-dimensional d -wave altermagnets, arXiv: 2406.08563 (2024).
- [260] Y.-H. Wan and Q.-F. Sun, Altermagnetism-induced parity anomaly in weak topological insulators, *Phys. Rev. B* **111**, 045407 (2025).
- [261] S. Zeng and Y.-J. Zhao, Bilayer stacking a -type altermagnet: A general approach to generating two-dimensional altermagnetism, *Physical Review B* **110** (2024).
- [262] M. Zhao, W.-W. Yang, X. Guo, H.-G. Luo, and Y. Zhong, Altermagnetism in heavy fermion systems, arXiv: 2407.05220 (2024).
- [263] S. Rooj, S. Saxena, and N. Ganguli, Altermagnetism in the orthorhombic $pnma$ structure through group theory and dft calculations, *Phys. Rev. B* **111**, 014434 (2025).
- [264] Q. N. Meier, A. Carta, C. Ederer, and A. Cano, (anti-)altermagnetism from orbital ordering in the ruddlesden-popper chromates $\text{Sr}_{n+1}\text{Cr}_n\text{O}_{3n+1}$, arXiv: 2502.01515 (2025).
- [265] G. Yang, Z. Li, S. Yang, J. Li, H. Zheng, W. Zhu, Z. Pan, Y. Xu, S. Cao, W. Zhao, *et al.*, Three-dimensional mapping of the altermagnetic spin splitting in CrSb, *Nat. Commun.* **16**, 1442 (2025).
- [266] A. A. Hedayati and M. Salehi, Transverse spin current at normal-metal p -wave magnet junctions, *Phys. Rev. B* **111**, 035404 (2025).
- [267] A. Chakraborty, A. B. Hellènes, R. Jaeschke-Ubiergo, T. Jungwirth, L. Šmejkal, and J. Sinova, Highly efficient non-relativistic Edelstein effect in p -wave magnets, arXiv: 2411.16378 (2024).
- [268] B. A. Bernevig, J. Orenstein, and S.-C. Zhang, Exact $su(2)$ symmetry and persistent spin helix in a spin-orbit coupled system, *Phys. Rev. Lett.* **97**, 236601 (2006).
- [269] S. H. Jacobsen, J. A. Ouassou, and J. Linder, Critical temperature and tunneling spectroscopy of superconductor-ferromagnet hybrids with intrinsic Rashba-Dresselhaus spin-orbit coupling, *Phys. Rev. B* **92**, 024510 (2015).
- [270] F. Yang and M. W. Wu, Gapped superconductivity with all symmetries in InSb (110) quantum wells in proximity to s -wave superconductor in Fulde-Ferrell-Larkin-Ovchinnikov phase or with a supercurrent, *Phys. Rev. B* **95**, 075304 (2017).
- [271] M. Alidoust, Critical supercurrent and φ_0 state for probing a persistent spin helix, *Phys. Rev. B* **101**, 155123 (2020).

- [272] M. Alidoust, C. Shen, and I. Žutić, Cubic spin-orbit coupling and anomalous josephson effect in planar junctions, *Phys. Rev. B* **103**, L060503 (2021).
- [273] J. Lee, S. Ikegaya, and Y. Asano, Odd-parity pairing correlations in a d -wave superconductor, *Phys. Rev. B* **103**, 104509 (2021).
- [274] S. Ikegaya, J. Lee, A. P. Schnyder, and Y. Asano, Strong anomalous proximity effect from spin-singlet superconductors, *Phys. Rev. B* **104**, L020502 (2021).
- [275] M.-H. Liu, K.-W. Chen, S.-H. Chen, and C.-R. Chang, Persistent spin helix in rashba-dresselhaus two-dimensional electron systems, *Phys. Rev. B* **74**, 235322 (2006).
- [276] J. Schliemann, Colloquium: Persistent spin textures in semiconductor nanostructures, *Rev. Mod. Phys.* **89**, 011001 (2017).
- [277] M. Kohda and G. Salis, Physics and application of persistent spin helix state in semiconductor heterostructures, *Semicond. Sci. Technol.* **32**, 073002 (2017).
- [278] A. J. Wu, B. Z. Zhang, C. J. Liu, and D. X. Shao, Magnetic quadratic nodal line with spin-orbital coupling in crsb, *Applied Physics Letters* **123**, 052407 (2023).
- [279] D. S. Antonenko, R. M. Fernandes, and J. W. F. Venderbos, Mirror chern bands and weyl nodal loops in altermagnets, arXiv:2402.10201 (2024).
- [280] K. Parshukov, R. Wiedmann, and A. P. Schnyder, Topological responses from gapped weyl points in 2d altermagnets, arXiv: 2403.09520 (2024).
- [281] S. K. Das and B. Roy, From local spin nematicity to altermagnets: Footprints of band topology, arXiv: 2403.14620 (2024).
- [282] Y. Zhao, Y. Jiang, H. Bae, K. Das, Y. Li, C.-X. Liu, and B. Yan, Hybrid-order topology in unconventional magnets of eu-based zintl compounds with surface-dependent quantum geometry, *Phys. Rev. B* **110**, 205111 (2024).
- [283] R. M. Fernandes, V. S. de Carvalho, T. Birol, and R. G. Pereira, Topological transition from nodal to nodeless zeeman splitting in altermagnets, *Phys. Rev. B* **109**, 024404 (2024).
- [284] C. Li, M. Hu, Z. Li, Y. Wang, W. Chen, B. Thiragarajan, M. Leandersson, C. Polley, T. Kim, H. Liu, C. Fulga, M. G. Vergniory, O. Janson, O. Tjernberg, and J. van den Brink, Topological weyl altermagnetism in crsb, arXiv: 2405.14777 (2024).
- [285] H.-Y. Ma and J.-F. Jia, Altermagnetic topological insulator and the selection rules, *Phys. Rev. B* **110**, 064426 (2024).
- [286] P. Rao, A. Mook, and J. Knolle, Tunable band topology and optical conductivity in altermagnets, *Phys. Rev. B* **110**, 024425 (2024).
- [287] R. D. Gonzalez Betancourt, J. Zubáč, R. Gonzalez-Hernandez, K. Geishendorf, Z. Šobán, G. Springholz, K. Olejník, L. Šmejkal, J. Sinova, T. Jungwirth, S. T. B. Goennenwein, A. Thomas, H. Reichlová, J. Železný, and D. Kriegner, Spontaneous anomalous hall effect arising from an unconventional compensated magnetic phase in a semiconductor, *Phys. Rev. Lett.* **130**, 036702 (2023).
- [288] Y. Fang, J. Cano, and S. A. A. Ghorashi, Quantum geometry induced nonlinear transport in altermagnets, *Phys. Rev. Lett.* **133**, 106701 (2024).
- [289] J. Yu, B. A. Bernevig, R. Queiroz, E. Rossi, P. Törmä, and B.-J. Yang, Quantum geometry in quantum materials, arXiv: 2501.00098 (2024).
- [290] M. Ezawa, Topological insulators and superconductors based on p -wave magnets: Electrical control and detection of a domain wall, *Phys. Rev. B* **110**, 165429 (2024).
- [291] K. Mæland, B. Brekke, and A. Sudbø, Many-body effects on superconductivity mediated by double-magnon processes in altermagnets, *Phys. Rev. B* **109**, 134515 (2024).
- [292] V. S. de Carvalho and H. Freire, Unconventional superconductivity in altermagnets with spin-orbit coupling, *Phys. Rev. B* **110**, L220503 (2024).
- [293] S. Chourasia, A. Svetogorov, A. Kamra, and W. Belzig, Thermodynamic properties of a superconductor interfaced with an altermagnet, arXiv: 2403.10456 (2024).
- [294] P. O. Sukhachov, E. W. Hoft, and J. Linder, Thermoelectric effect in altermagnet-superconductor junctions, *Phys. Rev. B* **110**, 094508 (2024).
- [295] H. G. Giil, B. Brekke, J. Linder, and A. Brataas, Quasi-classical theory of superconducting spin-splitter effects and spin-filtering via altermagnets, *Phys. Rev. B* **110**, L140506 (2024).
- [296] T. Kokkeler, I. Tokatly, and F. S. Bergeret, Quantum transport theory for unconventional magnets; interplay of altermagnetism and p -wave magnetism with superconductivity, arXiv: 2412.10236 (2024).
- [297] A. Zagoskin, *Quantum Theory of Many-Body Systems: Techniques and Applications* (Springer, 2014).
- [298] Y. Tanaka, *Physics of Superconducting junctions* (Nagoya University Press, 2021).
- [299] B. A. Bernevig, *Topological insulators and topological superconductors* (Princeton university press, 2013).
- [300] Y. Tanaka and S. Kashiwaya, Theory of tunneling spectroscopy of d -wave superconductors, *Phys. Rev. Lett.* **74**, 3451 (1995).
- [301] S. Kashiwaya, Y. Tanaka, M. Koyanagi, and K. Kajimura, Theory for tunneling spectroscopy of anisotropic superconductors, *Phys. Rev. B* **53**, 2667 (1996).
- [302] T. Löfwander, V. S. Shumeiko, and G. Wendin, Andreev bound states in high- t_c superconducting junctions, *Superconductor Science and Technology* **14**, R53 (2001).
- [303] Y. A. Bychkov and É. I. Rashba, Properties of a 2d electron gas with lifted spectral degeneracy, *JETP Lett* **39**, 78 (1984).
- [304] G. Eliashberg, Interactions between electrons and lattice vibrations in a superconductor, *Sov. Phys. JETP* **11**, 696 (1960).
- [305] G. Eliashberg, Temperature green's functions of electrons in a superconductor, *Zh. Eksp. Teor. Fiz.* **39**, 1437 (1960), [*Sov. JETP* **12**, 1000 (1961)].
- [306] K. Leraand, K. Mæland, and A. Sudbø, Phonon-mediated spin-polarized superconductivity in altermagnets, arXiv: 2502.08704 (2025).
- [307] J. Linder and A. V. Balatsky, Odd-frequency superconductivity, *Rev. Mod. Phys.* **91**, 045005 (2019).
- [308] C. Triola, J. Cayao, and A. M. Black-Schaffer, The role of odd-frequency pairing in multiband superconductors, *Ann. Phys.* **532**, 1900298 (2020).
- [309] M. Eschrig, T. Löfwander, T. Champel, J. C. Cuevas, J. Kopu, and G. Schön, Symmetries of pairing correlations in superconductor-ferromagnet nanostructures, *Journal of Low Temperature Physics* **147**, 457 (2007).
- [310] V. L. Berezinskii, New model of the anisotropic phase of superfluid ^3He , *JETP Lett.* **20**, 287 (1974).
- [311] T. R. Kirkpatrick and D. Belitz, Disorder-induced triplet superconductivity, *Phys. Rev. Lett.* **66**, 1533

- (1991).
- [312] D. Belitz and T. R. Kirkpatrick, Properties of spin-triplet, even-parity superconductors, *Phys. Rev. B* **60**, 3485 (1999).
- [313] Y. Tanaka and A. A. Golubov, Theory of the proximity effect in junctions with unconventional superconductors, *Phys. Rev. Lett.* **98**, 037003 (2007).
- [314] Y. Tanaka, Y. Tanuma, and A. A. Golubov, Odd-frequency pairing in normal-metal/superconductor junctions, *Phys. Rev. B* **76**, 054522 (2007).
- [315] Y. Asano and Y. Tanaka, Majorana fermions and odd-frequency cooper pairs in a normal-metal nanowire proximity-coupled to a topological superconductor, *Phys. Rev. B* **87**, 104513 (2013).
- [316] B. Sothmann, S. Weiss, M. Governale, and J. König, Unconventional superconductivity in double quantum dots, *Phys. Rev. B* **90**, 220501 (2014).
- [317] Y. V. Fominov, Y. Tanaka, Y. Asano, and M. Eschrig, Odd-frequency superconducting states with different types of meissner response: Problem of coexistence, *Phys. Rev. B* **91**, 144514 (2015).
- [318] P. Burset, B. Lu, G. Tkachov, Y. Tanaka, E. M. Hankiewicz, and B. Trauzettel, Superconducting proximity effect in three-dimensional topological insulators in the presence of a magnetic field, *Phys. Rev. B* **92**, 205424 (2015).
- [319] O. Kashuba, B. Sothmann, P. Burset, and B. Trauzettel, Majorana stm as a perfect detector of odd-frequency superconductivity, *Phys. Rev. B* **95**, 174516 (2017).
- [320] J. Cayao and A. M. Black-Schaffer, Odd-frequency superconducting pairing and subgap density of states at the edge of a two-dimensional topological insulator without magnetism, *Phys. Rev. B* **96**, 155426 (2017).
- [321] Y. Tanaka and S. Tamura, Surface andreev bound states and odd-frequency pairing in topological superconductor junctions, *Journal of Low Temperature Physics* **191**, 61 (2018).
- [322] C. Fleckenstein, N. T. Ziani, and B. Trauzettel, Conductance signatures of odd-frequency superconductivity in quantum spin hall systems using a quantum point contact, *Phys. Rev. B* **97**, 134523 (2018).
- [323] S.-Y. Hwang, P. Burset, and B. Sothmann, Odd-frequency superconductivity revealed by thermopower, *Phys. Rev. B* **98**, 161408 (2018).
- [324] S. Tamura and Y. Tanaka, Theory of the proximity effect in two-dimensional unconventional superconductors with rashba spin-orbit interaction, *Phys. Rev. B* **99**, 184501 (2019).
- [325] S. Tamura, S. Hoshino, and Y. Tanaka, Odd-frequency pairs in chiral symmetric systems: Spectral bulk-boundary correspondence and topological criticality, *Phys. Rev. B* **99**, 184512 (2019).
- [326] A. Tsintzis, A. M. Black-Schaffer, and J. Cayao, Odd-frequency superconducting pairing in kitaev-based junctions, *Phys. Rev. B* **100**, 115433 (2019).
- [327] S. Tamura, S. Nakosai, A. M. Black-Schaffer, Y. Tanaka, and J. Cayao, Bulk odd-frequency pairing in the superconducting su-schrieffer-heeger model, *Phys. Rev. B* **101**, 214507 (2020).
- [328] D. Takagi, S. Tamura, and Y. Tanaka, Odd-frequency pairing and proximity effect in kitaev chain systems including a topological critical point, *Phys. Rev. B* **101**, 024509 (2020).
- [329] D. Takagi, M. T. Mercaldo, Y. Tanaka, and M. Cuoco, Odd-frequency pairing in a nonunitary p -wave superconductor with multiple majorana fermions, *Phys. Rev. B* **105**, 224506 (2022).
- [330] J. Cayao, P. Dutta, P. Burset, and A. M. Black-Schaffer, Phase-tunable electron transport assisted by odd-frequency cooper pairs in topological josephson junctions, *Phys. Rev. B* **106**, L100502 (2022).
- [331] F. Keidel, S.-Y. Hwang, B. Trauzettel, B. Sothmann, and P. Burset, On-demand thermoelectric generation of equal-spin cooper pairs, *Phys. Rev. Res.* **2**, 022019 (2020).
- [332] J. Cayao, Emergent pair symmetries in systems with poor man's majorana modes, *Phys. Rev. B* **110**, 125408 (2024).
- [333] M. Vojta and E. Dagotto, Indications of unconventional superconductivity in doped and undoped triangular antiferromagnets, *Phys. Rev. B* **59**, R713 (1999).
- [334] K. Shigeta, S. Onari, K. Yada, and Y. Tanaka, Theory of odd-frequency pairings on a quasi-one-dimensional lattice in the hubbard model, *Phys. Rev. B* **79**, 174507 (2009).
- [335] K. Shigeta, S. Onari, and Y. Tanaka, Symmetry of superconducting pairing state in a staggered field, *Phys. Rev. B* **85**, 224509 (2012).
- [336] K. Shigeta, Y. Tanaka, K. Kuroki, S. Onari, and H. Aizawa, Competition of pairing symmetries and a mechanism for berezinskii pairing in quasi-one-dimensional systems, *Phys. Rev. B* **83**, 140509 (2011).
- [337] Y. Fuseya, H. Kohno, and K. Miyake, Realization of odd-frequency p -wave spin-singlet superconductivity coexisting with antiferromagnetic order near quantum critical point, *Journal of the Physical Society of Japan* **72**, 2914 (2003).
- [338] H. Kusunose, Y. Fuseya, and K. Miyake, Possible odd-frequency superconductivity in strong-coupling electron-phonon systems, *Journal of the Physical Society of Japan* **80**, 044711 (2011).
- [339] A. Aperis, P. Maldonado, and P. M. Oppeneer, Ab initio theory of magnetic-field-induced odd-frequency two-band superconductivity in mgb_2 , *Phys. Rev. B* **92**, 054516 (2015).
- [340] F. Schrodi, A. Aperis, and P. M. Oppeneer, Induced odd-frequency superconducting state in vertex-corrected eliashberg theory, *Phys. Rev. B* **104**, 174518 (2021).
- [341] J. Cayao and A. M. Black-Schaffer, Odd-frequency superconducting pairing in junctions with Rashba spin-orbit coupling, *Phys. Rev. B* **98**, 075425 (2018).
- [342] Y. Asano, *Andreev reflection in superconducting junctions* (Springer, 2021).
- [343] P. Dutta, J. Cayao, A. M. Black-Schaffer, and P. Burset, Nonlocality of majorana bound states revealed by electron waiting times in a topological andreev interferometer, *Phys. Rev. Res.* **6**, L012062 (2024).
- [344] G. D. Mahan, *Many-particle physics* (Springer Science & Business Media, 2013).
- [345] S. Datta, *Electronic transport in mesoscopic systems* (Cambridge university press, 1997).
- [346] J. C. Cuevas, A. Martín-Rodero, and A. L. Yeyati, Hamiltonian approach to the transport properties of superconducting quantum point contacts, *Phys. Rev. B* **54**, 7366 (1996).
- [347] A. Andreev, The thermal conductivity of the intermediate state in superconductors, *JETP* **46**, 1823 (1964).

- [348] A. Andreev *et al.*, Thermal conductivity of the intermediate state of superconductors ii, *Sov. Phys. JETP* **20**, 1490 (1965).
- [349] G. E. Blonder, M. Tinkham, and T. M. Klapwijk, Transition from metallic to tunneling regimes in superconducting microconstrictions: Excess current, charge imbalance, and supercurrent conversion, *Phys. Rev. B* **25**, 4515 (1982).
- [350] M. J. M. de Jong and C. W. J. Beenakker, Andreev reflection in ferromagnet-superconductor junctions, *Phys. Rev. Lett.* **74**, 1657 (1995).
- [351] C. R. Reeg and D. L. Maslov, Proximity-induced triplet superconductivity in rashba materials, *Phys. Rev. B* **92**, 134512 (2015).
- [352] S. Kashiwaya, Y. Tanaka, N. Yoshida, and M. R. Beasley, Spin current in ferromagnet-insulator-superconductor junctions, *Phys. Rev. B* **60**, 3572 (1999).
- [353] C. W. J. Beenakker, Specular andreev reflection in graphene, *Phys. Rev. Lett.* **97**, 067007 (2006).
- [354] A. Soori, Crossed andreev reflection in collinear p -wave magnet-triplet superconductor junctions, arXiv: 2501.13783 (2025).
- [355] N. M. Chtchelkatchev and Y. V. Nazarov, Andreev quantum dots for spin manipulation, *Phys. Rev. Lett.* **90**, 226806 (2003).
- [356] M. Tanhayi Ahari and Y. Tserkovnyak, Proposal for a nonadiabatic geometric gate with an andreev spin qubit, *Phys. Rev. A* **109**, 032601 (2024).
- [357] Y. Chen and Y. V. Nazarov, Spin weyl quantum unit: A theoretical proposal, *Phys. Rev. B* **103**, 045410 (2021).
- [358] Y. Fukaya, B. Lu, K. Yada, Y. Tanaka, and J. Cayao, Proximity and inverse proximity effect in superconducting junctions with unconventional magnets, In preparation (2025).
- [359] Y. Tanaka and S. Kashiwaya, Local density of states of quasiparticles near the interface of nonuniform d -wave superconductors, *Phys. Rev. B* **53**, 9371 (1996).
- [360] B. Lu and Y. Tanaka, Study on green's function on topological insulator surface, *Phil. Trans. R. Soc. A* **376**, 20150246 (2018).
- [361] F. S. Bergeret, A. F. Volkov, and K. B. Efetov, Induced ferromagnetism due to superconductivity in superconductor-ferromagnet structures, *Phys. Rev. B* **69**, 174504 (2004).
- [362] L. Covaci and F. Marsiglio, Proximity effect and josephson current in clean strong/weak/strong superconducting trilayers, *Phys. Rev. B* **73**, 014503 (2006).
- [363] A. Golubov and M. Y. Kupriyanov, Theoretical investigation of josephson tunnel junctions with spatially inhomogeneous superconducting electrodes, *Journal of low temperature physics* **70**, 83 (1988).
- [364] T. Tokuyasu, J. A. Sauls, and D. Rainer, Proximity effect of a ferromagnetic insulator in contact with a superconductor, *Phys. Rev. B* **38**, 8823 (1988).
- [365] S. Tollis, M. Daumens, and A. Buzdin, Inversion of the proximity effect in atomic-scale ferromagnet/superconductor/ferromagnet trilayers, *Phys. Rev. B* **71**, 024510 (2005).
- [366] F. S. Bergeret, A. L. Yeyati, and A. Martín-Rodero, Inverse proximity effect in superconductor-ferromagnet structures: From the ballistic to the diffusive limit, *Phys. Rev. B* **72**, 064524 (2005).
- [367] S.-I. Suzuki, T. Hirai, M. Eschrig, and Y. Tanaka, Anomalous inverse proximity effect in unconventional superconductor junctions, *Phys. Rev. Res.* **3**, 043148 (2021).
- [368] T. Löthman, C. Triola, J. Cayao, and A. M. Black-Schaffer, Disorder-robust p -wave pairing with odd-frequency dependence in normal metal-conventional superconductor junctions, *Phys. Rev. B* **104**, 094503 (2021).
- [369] T. Löthman, C. Triola, J. Cayao, and A. M. Black-Schaffer, Efficient numerical method for evaluating normal and anomalous time-domain equilibrium green's functions in inhomogeneous systems, *Phys. Rev. B* **104**, 125405 (2021).
- [370] A. M. Black-Schaffer and A. V. Balatsky, Odd-frequency superconducting pairing in multiband superconductors, *Phys. Rev. B* **88**, 104514 (2013).
- [371] P. Burset, B. Lu, H. Ebisu, Y. Asano, and Y. Tanaka, All-electrical generation and control of odd-frequency s -wave cooper pairs in double quantum dots, *Phys. Rev. B* **93**, 201402 (2016).
- [372] J. Cayao, P. Burset, and Y. Tanaka, Controllable odd-frequency cooper pairs in multisuperconductor josephson junctions, *Phys. Rev. B* **109**, 205406 (2024).
- [373] H. Ohldag, Hidden in not-so-plain sight: altermagnets, *npj Spintronics* **2**, 57 (2024).
- [374] Y. Tanaka and S. Kashiwaya, Anomalous charge transport in triplet superconductor junctions, *Phys. Rev. B* **70**, 012507 (2004).
- [375] Y. Tanaka, S. Kashiwaya, and T. Yokoyama, Theory of enhanced proximity effect by midgap andreev resonant state in diffusive normal-metal/triplet superconductor junctions, *Phys. Rev. B* **71**, 094513 (2005).
- [376] Y. Tanaka, Y. Asano, A. A. Golubov, and S. Kashiwaya, Anomalous features of the proximity effect in triplet superconductors, *Phys. Rev. B* **72**, 140503 (2005).
- [377] S. Ikegaya, S.-I. Suzuki, Y. Tanaka, and Y. Asano, Quantization of conductance minimum and index theorem, *Phys. Rev. B* **94**, 054512 (2016).
- [378] Y. Hou, F. Nichele, H. Chi, A. Lodesani, Y. Wu, M. F. Ritter, D. Z. Haxell, M. Davydova, S. Ilić, O. Glezakou-Elbert, A. Varambally, F. S. Bergeret, A. Kamra, L. Fu, P. A. Lee, and J. S. Moodera, Ubiquitous superconducting diode effect in superconductor thin films, *Phys. Rev. Lett.* **131**, 027001 (2023).
- [379] F. Liu, Y. M. Itahashi, S. Aoki, Y. Dong, Z. Wang, N. Ogawa, T. Ideue, and Y. Iwasa, Superconducting diode effect under time-reversal symmetry, *Science Advances* **10**, eado1502 (2024).
- [380] S. Li, Y. Deng, D. Hu, C. Zhu, Z. Yang, W. Tian, X. Wang, M. Yue, Q. Wu, Z. Liu, *et al.*, Field-free superconducting diode effect and magnetochiral anisotropy in $\text{fete}_0.7\text{se}_0.3$ junctions with the inherent asymmetric barrier, *ACS nano* **18**, 31076 (2024).
- [381] S. Qi, J. Ge, C. Ji, Y. Ai, G. Ma, Z. Wang, Z. Cui, Y. Liu, Z. Wang, and J. Wang, High-temperature field-free superconducting diode effect in high- t_c cuprates, *Nature Communications* **16**, 531 (2025).
- [382] L. A. Coldren, S. W. Corzine, and M. L. Mashanovitch, *Diode Lasers and Photonic Integrated Circuits* (John Wiley & Sons, 2012).
- [383] I. Mehdi, J. V. Siles, C. Lee, and E. Schlecht, THz diode technology: Status, prospects, and applications, *Proceedings of the IEEE* **105**, 990 (2017).
- [384] J. Semple, D. G. Georgiadou, G. Wyatt-Moon,

- G. Gelinck, and T. D. Anthopoulos, Flexible diodes for radio frequency (RF) electronics: A materials perspective, *Semicond. Sci. Technol.* **32**, 123002 (2017).
- [385] Y. Tokura and N. Nagaosa, Nonreciprocal responses from non-centrosymmetric quantum materials, *Nat. Commun.* **9**, 3740 (2018).
- [386] M. Kim, E. Pallecchi, R. Ge, X. Wu, G. Ducournau, J. C. Lee, H. Happy, and D. Akinwande, Analogue switches made from boron nitride monolayers for application in 5G and terahertz communication systems, *Nat. Electron.* **3**, 479 (2020).
- [387] K. Loganathan, H. Faber, E. Yengel, A. Seitkhan, A. Bakytbekov, E. Yarali, B. Adilbekova, A. AlBatati, Y. Lin, Z. Felemban, *et al.*, Rapid and up-scalable manufacturing of gigahertz nanogap diodes, *Nat. Commun.* **13**, 3260 (2022).
- [388] F. Braun, Ueber die stromleitung durch schwefelmetalle, *Ann. Phys.* **229**, 556 (1875).
- [389] S. M. Sze and M.-K. Lee, *Semiconductor Devices: Physics and Technology* (Wiley, Hoboken, NJ, 2016).
- [390] N. Nagaosa and Y. Yanase, Nonreciprocal transport and optical phenomena in quantum materials, *Annual Review of Condensed Matter Physics* **15**, 63 (2024).
- [391] N. F. Q. Yuan and L. Fu, Supercurrent diode effect and finite-momentum superconductors, *Proc. Natl. Acad. Sci.* **119**, e2119548119 (2022).
- [392] H. F. Legg, D. Loss, and J. Klinovaja, Superconducting diode effect due to magnetochiral anisotropy in topological insulators and Rashba nanowires, *Phys. Rev. B* **106**, 104501 (2022).
- [393] J.-X. Lin, P. Siriviboon, H. D. Scammell, S. Liu, D. Rhodes, K. Watanabe, T. Taniguchi, J. Hone, M. S. Scheurer, and J. Li, Zero-field superconducting diode effect in small-twist-angle trilayer graphene, *Nat. Phys.* **18**, 1221 (2022).
- [394] H. D. Scammell, J. Li, and M. S. Scheurer, Theory of zero-field superconducting diode effect in twisted trilayer graphene, *2D Mater.* **9**, 025027 (2022).
- [395] S. Banerjee and M. S. Scheurer, Enhanced superconducting diode effect due to coexisting phases, *Phys. Rev. Lett.* **132**, 046003 (2024).
- [396] J. J. He, Y. Tanaka, and N. Nagaosa, A phenomenological theory of superconductor diodes, *New Journal of Physics* **24**, 053014 (2022).
- [397] V. M. Edelstein, Magnetoelectric effect in polar superconductors, *Phys. Rev. Lett.* **75**, 2004 (1995).
- [398] S. Fujimoto, Magnetoelectric effects in heavy-fermion superconductors without inversion symmetry, *Phys. Rev. B* **72**, 024515 (2005).
- [399] V. M. Edelstein, Magnetoelectric effect in dirty superconductors with broken mirror symmetry, *Phys. Rev. B* **72**, 172501 (2005).
- [400] J. J. He, K. Hiroki, K. Hamamoto, and N. Nagaosa, Spin supercurrent in two-dimensional superconductors with rashba spin-orbit interaction, *Communications Physics* **2**, 128 (2019).
- [401] G. Tkachov, Magnetoelectric andreev effect due to proximity-induced nonunitary triplet superconductivity in helical metals, *Phys. Rev. Lett.* **118**, 016802 (2017).
- [402] W.-Y. He and K. T. Law, Magnetoelectric effects in gyrotropic superconductors, *Phys. Rev. Res.* **2**, 012073 (2020).
- [403] Y. Ikeda and Y. Yanase, Giant surface edelstein effect in *d*-wave superconductors, *Phys. Rev. B* **102**, 214510 (2020).
- [404] W.-Y. He and K. T. Law, Superconducting orbital magnetoelectric effect and its evolution across the superconductor-normal metal phase transition, *Phys. Rev. Res.* **3**, L032012 (2021).
- [405] L. Chirolli, M. T. Mercaldo, C. Guarcello, F. Giazzotto, and M. Cuoco, Colossal orbital edelstein effect in noncentrosymmetric superconductors, *Phys. Rev. Lett.* **128**, 217703 (2022).
- [406] S. Yip, Noncentrosymmetric superconductors, *Annu. Rev. Condens. Matter Phys.* **5**, 15 (2014).
- [407] C. A. Domenicali, Irreversible thermodynamics of thermoelectricity, *Rev. Mod. Phys.* **26**, 237 (1954).
- [408] I. Galperin, V. Gurevich, and V. Kozub, Thermoelectric effects in superconductors, *Zh. Eksp. Teor. Fiz.* **66**, 1387 (1974).
- [409] V. L. Ginzburg and G. F. Zharkov, Thermoelectric effects in superconductors, *Soviet Physics Uspekhi* **21**, 381 (1978).
- [410] D. K. C. MacDonald, *Thermoelectricity: an introduction to the principles* (Courier Corporation, 2006).
- [411] C. M. Falco and J. C. Garland, Thermoelectric effects in superconductors, in *Nonequilibrium Superconductivity, Phonons, and Kapitza Boundaries* (Springer, 1981) pp. 521–540.
- [412] D. J. Van Harlingen, Thermoelectric effects in the superconducting state, *Physica B+ C* **109**, 1710 (1982).
- [413] N. R. Claughton and C. J. Lambert, Thermoelectric properties of mesoscopic superconductors, *Phys. Rev. B* **53**, 6605 (1996).
- [414] Y. M. Galperin, V. L. Gurevich, V. I. Kozub, and A. L. Shelankov, Theory of thermoelectric phenomena in superconductors, *Phys. Rev. B* **65**, 064531 (2002).
- [415] A. Majumdar, Thermoelectricity in semiconductor nanostructures, *Science* **303**, 777 (2004).
- [416] B. Sothmann, R. Sánchez, and A. N. Jordan, Thermoelectric energy harvesting with quantum dots, *Nanotechnology* **26**, 032001 (2014).
- [417] M. Kamp and B. Sothmann, Phase-dependent heat and charge transport through superconductor–quantum dot hybrids, *Phys. Rev. B* **99**, 045428 (2019).
- [418] G. Yang, L. Sang, C. Zhang, N. Ye, A. Hamilton, M. S. Fuhrer, and X. Wang, The role of spin in thermoelectricity, *Nature Reviews Physics* **5**, 466 (2023).
- [419] C. Artini, G. Pennelli, P. Graziosi, Z. Li, N. Neophytou, C. Melis, L. Colombo, E. Isotta, K. Lohani, P. Scardi, *et al.*, Roadmap on thermoelectricity, *Nanotechnology* **34**, 292001 (2023).
- [420] S. Liu, M. Chen, C. Fu, and T. Zhu, The interplay of magnetism and thermoelectricity: A review, *Advanced Physics Research* **2**, 2300015 (2023).
- [421] J. Linder and M. E. Bathen, Spin caloritronics with superconductors: Enhanced thermoelectric effects, generalized onsager response-matrix, and thermal spin currents, *Phys. Rev. B* **93**, 224509 (2016).
- [422] A. Ozaeta, P. Virtanen, F. S. Bergeret, and T. T. Heikkilä, Predicted very large thermoelectric effect in ferromagnet-superconductor junctions in the presence of a spin-splitting magnetic field, *Phys. Rev. Lett.* **112**, 057001 (2014).
- [423] I. F. Lyuksyutov and V. Pokrovsky, Magnetization controlled superconductivity in a film with magnetic dots, *Phys. Rev. Lett.* **81**, 2344 (1998).
- [424] Z. Yang, M. Lange, A. Volodin, R. Szymczak, and

- V. V. Moshchalkov, Domain-wall superconductivity in superconductor–ferromagnet hybrids, *Nat. Mater.* **3**, 793 (2004).
- [425] J. Fritzsche, V. V. Moshchalkov, H. Eitel, D. Koelle, R. Kleiner, and R. Szymczak, Local observation of reverse-domain superconductivity in a superconductor-ferromagnet hybrid, *Phys. Rev. Lett.* **96**, 247003 (2006).
- [426] J. E. Villegas, C.-P. Li, and I. K. Schuller, Bistability in a superconducting thin film induced by arrays of ferromagnetic vortices, *Phys. Rev. Lett.* **99**, 227001 (2007).
- [427] V. Rouco, R. Córdoba, J. De Teresa, L. A. Rodríguez, C. Navau, N. Del-Valle, G. Via, A. Sánchez, C. Monton, F. Kronast, *et al.*, Competition between superconductor–ferromagnetic stray magnetic fields in $\text{YBa}_2\text{Cu}_3\text{O}_{7-x}$ films pierced with Co nano-rods, *Sci. Rep.* **7**, 5663 (2017).
- [428] Y. Liu, S. Vaitiekėnas, S. Martí-Sánchez, C. Koch, S. Hart, Z. Cui, T. Kanne, S. A. Khan, R. Tanta, S. Upadhyay, *et al.*, Semiconductor–ferromagnetic insulator–superconductor nanowires: Stray field and exchange field, *Nano Letters* **20**, 456 (2019).
- [429] A. Paschoa, J. L. Gonzalez, V. P. Nascimento, and E. C. Passamani, The role of the stray field on superconducting properties of hybrid ferromagnetic/superconducting heterostructures, *Journal of Applied Physics* **128**, 043902 (2020).
- [430] M. J. Martínez-Pérez, P. Solinas, and F. Giazotto, Coherent caloritronics in Josephson-based nanocircuits, *Journal of Low Temperature Physics* **175**, 813–837 (2014).
- [431] A. Fornieri and F. Giazotto, Towards phase-coherent caloritronics in superconducting circuits, *Nat. Nanotech.* **12**, 944 (2017).
- [432] S.-Y. Hwang and B. Sothmann, Phase-coherent caloritronics with ordinary and topological Josephson junctions, *The European Physical Journal Special Topics* **229**, 683 (2020).
- [433] I. O. Kulik, Macroscopic quantization and the proximity effect in SNS junctions, *Soviet Journal of Experimental and Theoretical Physics* **30**, 944 (1969).
- [434] C. Ishii, Josephson currents through junctions with normal metal barriers, *Progress of Theoretical Physics* **44**, 1525 (1970).
- [435] C. Ishii, Thermodynamical properties of Josephson junction with a normal metal barrier, *Progress of Theoretical Physics* **47**, 1464 (1972).
- [436] J. Bardeen and J. L. Johnson, Josephson current flow in pure superconducting-normal-superconducting junctions, *Physical Review B* **5**, 72 (1972).
- [437] A. Svidzinsky, T. Antsygina, and E. Bratus', Concerning the theory of the Josephson effect in pure SNS junctions, *Journal of Low Temperature Physics* **10**, 131 (1973).
- [438] A. Furusaki and M. Tsukada, A unified theory of clean Josephson junctions, *Physica B: Condensed Matter* **165**, 967 (1990).
- [439] C. W. J. Beenakker and H. van Houten, Josephson current through a superconducting quantum point contact shorter than the coherence length, *Phys. Rev. Lett.* **66**, 3056 (1991).
- [440] B. D. Josephson, *Phys. Lett.* **1**, 251 (1962).
- [441] R. Seoane Souto and R. Aguado, Subgap states in semiconductor-superconductor devices for quantum technologies: Andreev qubits and minimal Majorana chains, in *New Trends and Platforms for Quantum Technologies* (Springer, 2024) pp. 133–223.
- [442] M. H. Devoret and J. M. Martinis, Implementing qubits with superconducting integrated circuits, *Experimental aspects of quantum computing*, 163 (2005).
- [443] A. Acín, I. Bloch, H. Buhrman, T. Calarco, C. Eichler, J. Eisert, D. Esteve, N. Gisin, S. J. Glaser, F. Jelezko, *et al.*, The quantum technologies roadmap: a European community view, *New J. Phys.* **20**, 080201 (2018).
- [444] R. Aguado, A perspective on semiconductor-based superconducting qubits, *Appl. Phys. Lett.* **117** (2020).
- [445] M. Kjaergaard, M. E. Schwartz, J. Braumüller, P. Krantz, J. L.-J. Wang, S. Gustavsson, and W. D. Oliver, Superconducting qubits: Current state of play, *Annu. Rev. Condens. Matter Phys.* **11**, 369 (2020).
- [446] S. Rasmussen, K. Christensen, S. Pedersen, L. Kristensen, T. Bækgaard, N. Loft, and N. Zinner, Superconducting circuit companion—an introduction with worked examples, *PRX Quantum* **2**, 040204 (2021).
- [447] I. Siddiqi, Engineering high-coherence superconducting qubits, *Nat. Rev. Mater.* **6**, 875 (2021).
- [448] B. Altshuler and B. Spivak, Mesoscopic fluctuations in a superconductor–normal metal–superconductor junction, *Zh. Eksp. Teor. Fiz.* **92**, 607 (1987).
- [449] A. Furusaki, H. Takayanagi, and M. Tsukada, Theory of quantum conduction of supercurrent through a constriction, *Phys. Rev. Lett.* **67**, 132 (1991).
- [450] V. V. Schmidt, *The physics of superconductors: Introduction to fundamentals and applications* (Springer Science & Business Media, 2013).
- [451] M. Tinkham, *Introduction to superconductivity*, Vol. 1 (Courier Corporation, 2004).
- [452] W. L. McMillan, Theory of superconductor–normal metal interfaces, *Phys. Rev.* **175**, 559 (1968).
- [453] C. W. J. Beenakker, Random-matrix theory of quantum transport, *Rev. Mod. Phys.* **69**, 731 (1997).
- [454] J. Cayao and A. M. Black-Schaffer, Exceptional odd-frequency pairing in non-hermitian superconducting systems, *Phys. Rev. B* **105**, 094502 (2022).
- [455] K. Kawai, K. Yada, Y. Tanaka, Y. Asano, A. A. Golubov, and S. Kashiwaya, Josephson effect in a multi-orbital model for Sr_2RuO_4 , *Phys. Rev. B* **95**, 174518 (2017).
- [456] Y. Fukaya, K. Yada, Y. Tanaka, P. Gentile, and M. Cuoco, Orbital tunable $0 - \pi$ transitions in Josephson junctions with noncentrosymmetric topological superconductors, *Phys. Rev. B* **102**, 144512 (2020).
- [457] Y. Fukaya, Y. Tanaka, P. Gentile, K. Yada, and M. Cuoco, Anomalous Josephson coupling and high-harmonics in non-centrosymmetric superconductors with *s*-wave spin-triplet pairing, *npj Quantum Mater* **7**, 99 (2022).
- [458] Y.-J. Wei and J. Wang, Anomalous Josephson effect in altermagnet, *Europhysics Letters* **148**, 56003 (2024).
- [459] V. Ambegaokar and A. Baratoff, *Phys. Rev. Lett.* **10**, 486 (1963).
- [460] I. O. Kulik and A. N. Omelyanchuk, *Sov. J. Low Temp. Phys.* **4**, 142 (1978).
- [461] J. Cayao, P. San-Jose, A. M. Black-Schaffer, R. Aguado, and E. Prada, Majorana splitting from critical currents in Josephson junctions, *Phys. Rev. B* **96**, 205425 (2017).
- [462] J. Cayao and A. M. Black-Schaffer, Finite length effect on supercurrents between trivial and topological superconductors, *The European Physical Journal Special*

- Topics **227**, 1387 (2018).
- [463] N. G. Pugach, E. Goldobin, R. Kleiner, and D. Koelle, Method for reliable realization of a φ Josephson junction, *Phys. Rev. B* **81**, 104513 (2010).
- [464] Y. Tanaka and S. Kashiwaya, Phase dependent energy levels of bound states and d.c. Josephson current in unconventional superconductor / ferromagnetic insulator / unconventional superconductor junctions, *Journal of the Physical Society of Japan* **69**, 1152 (2000).
- [465] J. Hu, C. Wu, and X. Dai, Proposed design of a Josephson diode, *Phys. Rev. Lett.* **99**, 067004 (2007).
- [466] K. Misaki and N. Nagaosa, Theory of the nonreciprocal Josephson effect, *Phys. Rev. B* **103**, 245302 (2021).
- [467] Y. Zhang, Y. Gu, P. Li, J. Hu, and K. Jiang, General theory of Josephson diodes, *Phys. Rev. X* **12**, 041013 (2022).
- [468] R. S. Souto, M. Leijnse, and C. Schrade, Josephson diode effect in supercurrent interferometers, *Phys. Rev. Lett.* **129**, 267702 (2022).
- [469] A. Maiani, K. Flensberg, M. Leijnse, C. Schrade, S. Vaitiekėnas, and R. Seoane Souto, Nonsinusoidal current-phase relations in semiconductor–superconductor–ferromagnetic insulator devices, *Phys. Rev. B* **107**, 245415 (2023).
- [470] H. Wu, Y. Wang, Y. Xu, P. K. Sivakumar, C. Pasco, U. Filippozzi, S. S. Parkin, Y.-J. Zeng, T. McQueen, and M. N. Ali, The field-free Josephson diode in a van der Waals heterostructure, *Nature* **604**, 653 (2022).
- [471] C. Baumgartner, L. Fuchs, A. Costa, S. Reinhardt, S. Gronin, G. C. Gardner, T. Lindemann, M. J. Manfra, P. E. Faria Junior, D. Kochan, J. Fabian, N. Paradiso, and C. Strunk, Supercurrent rectification and magnetochiral effects in symmetric Josephson junctions, *Nat. Nanotech.* **17**, 39 (2022).
- [472] B. Turini, S. Salimian, M. Carrega, A. Iorio, E. Strambini, F. Giazotto, V. Zannier, L. Sorba, and S. Heun, Josephson diode effect in high-mobility insb nanoflags, *Nano Letters* **22**, 8502 (2022).
- [473] Y. Zhu, H. Wang, Z. Wang, S. Hu, G. Gu, J. Zhu, D. Zhang, and Q.-K. Xue, Persistent Josephson tunneling between $\text{Bi}_2\text{Sr}_2\text{CaCu}_2\text{O}_{8+x}$ flakes twisted by 45° across the superconducting dome, *Phys. Rev. B* **108**, 174508 (2023).
- [474] M. Valentini, O. Sagi, L. Baghumyan, T. de Gijssel, J. Jung, S. Calcaterra, A. Ballabio, J. A. Servin, K. Aggarwal, M. Janik, T. Adletzberger, R. S. Souto, M. Leijnse, J. Danon, C. Schrade, E. Bakkers, D. Christina, G. Isella, and G. Katsaros, Parity-conserving Cooper-pair transport and ideal superconducting diode in planar germanium, arXiv:2306.07109 (2023).
- [475] T. Berlijn, P. C. Snijders, O. Delaire, H.-D. Zhou, T. A. Maier, H.-B. Cao, S.-X. Chi, M. Matsuda, Y. Wang, M. R. Koehler, P. R. C. Kent, and H. H. Weiering, Itinerant antiferromagnetism in RuO_2 , *Phys. Rev. Lett.* **118**, 077201 (2017).
- [476] Z. H. Zhu, J. Stremper, R. R. Rao, C. A. Occhialini, J. Pellicciari, Y. Choi, T. Kawaguchi, H. You, J. F. Mitchell, Y. Shao-Horn, and R. Comin, Anomalous antiferromagnetism in metallic RuO_2 determined by resonant x-ray scattering, *Phys. Rev. Lett.* **122**, 017202 (2019).
- [477] H. Reichlova, R. Lopes Seeger, R. González-Hernández, I. Kounta, R. Schlitz, D. Kriegner, P. Ritzinger, M. Lammel, M. Leiviskä, A. Birk Hellenes, *et al.*, Observation of a spontaneous anomalous Hall response in the mn_5Si_3 d-wave altermagnet candidate, *Nat. Commun.* **15**, 4961 (2024).
- [478] J. Liu, J. Zhan, T. Li, J. Liu, S. Cheng, Y. Shi, L. Deng, M. Zhang, C. Li, J. Ding, Q. Jiang, M. Ye, Z. Liu, Z. Jiang, S. Wang, Q. Li, Y. Xie, Y. Wang, S. Qiao, J. Wen, Y. Sun, and D. Shen, Absence of altermagnetic spin splitting character in rutile oxide RuO_2 , *Phys. Rev. Lett.* **133**, 176401 (2024).
- [479] M. Hiraishi, H. Okabe, A. Koda, R. Kadono, T. Muroi, D. Hirai, and Z. Hiroi, Nonmagnetic ground state in RuO_2 revealed by muon spin rotation, *Phys. Rev. Lett.* **132**, 166702 (2024).
- [480] P. Kekler, L. Garcia-Gassull, A. Suter, T. Prokscha, Z. Salman, D. Khalyavin, P. Manuel, F. Orlandi, I. I. Mazin, R. Valentí, *et al.*, Absence of magnetic order in RuO_2 : insights from μ sr spectroscopy and neutron diffraction, *npj Spintronics* **2**, 50 (2024).
- [481] A. Smolyanyuk, I. I. Mazin, L. Garcia-Gassull, and R. Valentí, Fragility of the magnetic order in the prototypical altermagnet RuO_2 , *Phys. Rev. B* **109**, 134424 (2024).
- [482] S. G. Jeong, I. H. Choi, S. Nair, L. Buiarelli, B. Pourbahari, J. Y. Oh, N. Bassim, A. Seo, W. S. Choi, R. M. Fernandes, T. Birol, L. Zhao, J. S. Lee, and B. Jalan, Altermagnetic polar metallic phase in ultra-thin epitaxially-strained RuO_2 films, arXiv:2405.05838 (2024).
- [483] X. Feng, H. Bai, X. Fan, M. Guo, Z. Zhang, G. Chai, T. Wang, D. Xue, C. Song, and X. Fan, Incommensurate spin density wave in antiferromagnetic RuO_2 evinced by abnormal spin splitting torque, *Phys. Rev. Lett.* **132**, 086701 (2024).
- [484] M. Weber, S. Wust, L. Haag, A. Akashdeep, K. Leckron, C. Schmitt, R. Ramos, T. Kikkawa, E. Saitoh, M. Kläui, L. Šmejkal, J. Sinova, M. Aeschlimann, G. Jakob, B. Stadtmüller, and H. C. Schneider, All optical excitation of spin polarization in d-wave altermagnets, arXiv:2408.05187 (2024).
- [485] K.-W. Kim, B.-G. Park, and K.-J. Lee, Spin current and spin-orbit torque induced by ferromagnets, *npj Spintronics* **2**, 8 (2024).
- [486] J. Sinova, S. O. Valenzuela, J. Wunderlich, C. H. Back, and T. Jungwirth, Spin hall effects, *Rev. Mod. Phys.* **87**, 1213 (2015).
- [487] H. Nakayama, M. Althammer, Y.-T. Chen, K. Uchida, Y. Kajiwara, D. Kikuchi, T. Ohtani, S. Geprägs, M. Opel, S. Takahashi, R. Gross, G. E. W. Bauer, S. T. B. Goennenwein, and E. Saitoh, Spin hall magnetoresistance induced by a nonequilibrium proximity effect, *Phys. Rev. Lett.* **110**, 206601 (2013).
- [488] N. Zaki, G. Gu, A. Tsvetik, C. Wu, and P. D. Johnson, Time-reversal symmetry breaking in the Fe-chalcogenide superconductors, *Proceedings of the National Academy of Sciences* **118**, e2007241118 (2021).
- [489] C. Farhang, N. Zaki, J. Wang, G. Gu, P. D. Johnson, and J. Xia, Revealing the origin of time-reversal symmetry breaking in Fe-chalcogenide superconductor $\text{FeTe}_{1-x}\text{Se}_x$, *Phys. Rev. Lett.* **130**, 046702 (2023).
- [490] G. Qiu, H.-Y. Yang, L. Hu, H. Zhang, C.-Y. Chen, Y. Lyu, C. Eckberg, P. Deng, S. Krylyuk, A. V. Davydov, R. Zhang, and K. L. Wang, Concurrent ferromagnetism and superconductivity in Fe(Te,Se) van der Waals Josephson junctions, arXiv:2303.00966 (2023).
- [491] N. N. Orlova, A. A. Avakyants, A. V. Timonina, N. N. Kolesnikov, and E. V. Deviatov, Crossover from rela-

- tivistic to non-relativistic net magnetization for mntel
altermagnet candidate, JETP Letters **120**, 360–366
(2024).
- [492] A. M. Toxen, Size effects in thin superconducting in-
dium films, Phys. Rev. **123**, 442 (1961).
- [493] J. Eisenstein, Superconducting elements, Rev. Mod.
Phys. **26**, 277 (1954).
- [494] B. T. Matthias, T. H. Geballe, and V. B. Compton,
Superconductivity, Rev. Mod. Phys. **35**, 1 (1963).
- [495] A. Kononov, S. V. Egorov, Z. D. Kvon, N. N. Mikhailov,
S. A. Dvoretzky, and E. V. Deviatov, Andreev reflection
at the edge of a two-dimensional semimetal, Phys. Rev.
B **93**, 041303 (2016).
- [496] A. Kononov, V. A. Kostarev, B. R. Semyagin, V. V.
Preobrazhenskii, M. A. Putyato, E. A. Emelyanov, and
E. V. Deviatov, Proximity-induced superconductivity
within the InAs/GaSb edge conducting state, Phys.
Rev. B **96**, 245304 (2017).
- [497] I. E. Batov, T. Schäpers, A. A. Golubov, and A. V.
Ustinov, Andreev reflection and enhanced subgap con-
ductance in NbN/Au/InGaAs-InP junctions, Journal of
Applied Physics **96**, 3366 (2004).